SOAR TECH

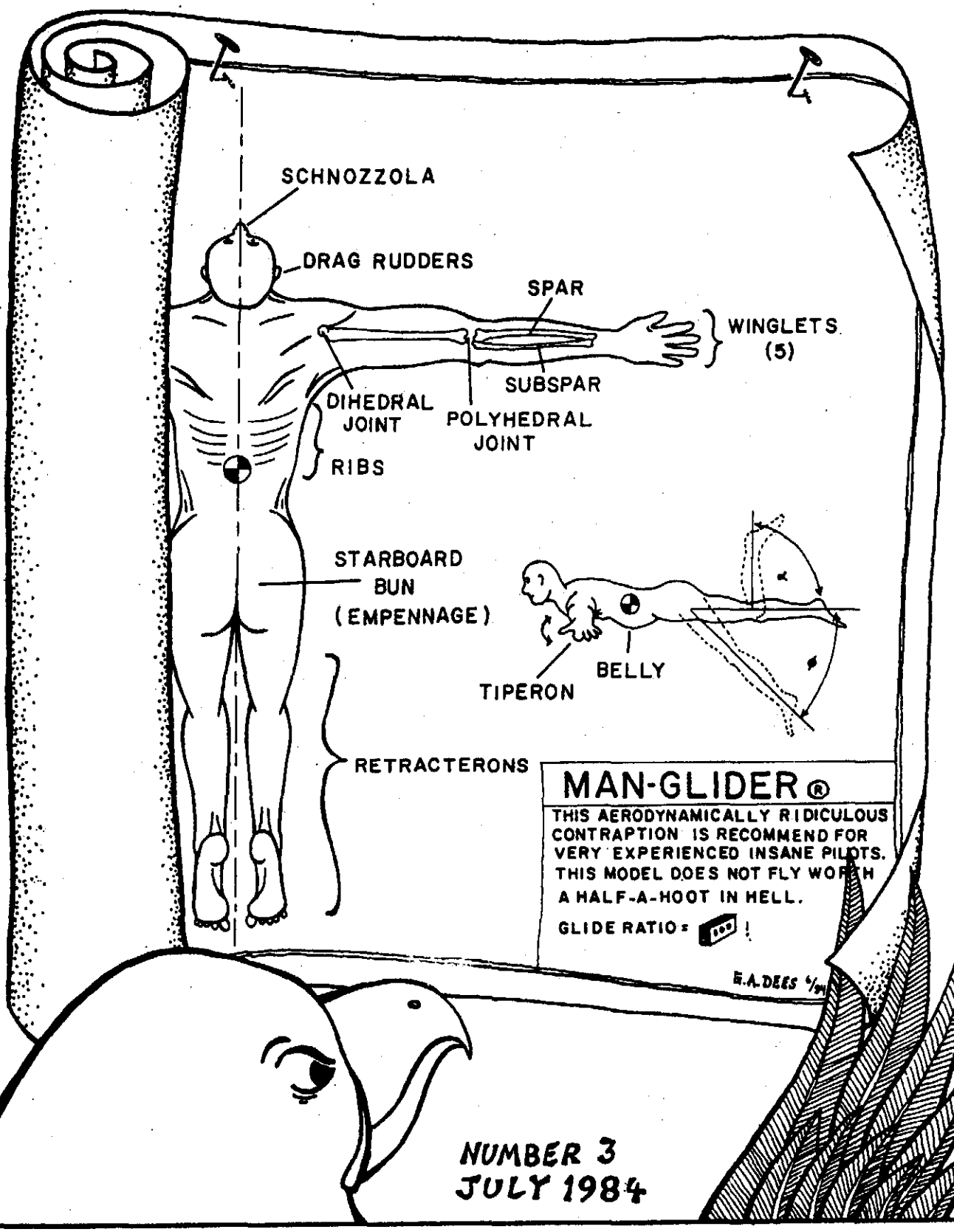

NUMBER 3
JULY 1984

THE DRAG OF SAILPLANES

Bob Said, the editor of "Soaring" explains the significance of this paper in his introductory comments. Its contents apply to model sailplanes as fully as they do to manned aircraft and it should tell us clearly, how drag reduction efforts will pay off in our design and building efforts. Oran W. Nicks is a noted researcher (Deputy Director of NASA's Langley Research Center at the time of his retirement), and an excellent sailplane pilot as well. He is now a member of the faculty of Texas A&M University, where he is continuing his aeronautical research.

This paper is published with the permission of Mr. Nicks and "Soaring" (the magazine of the Soaring Society of America).

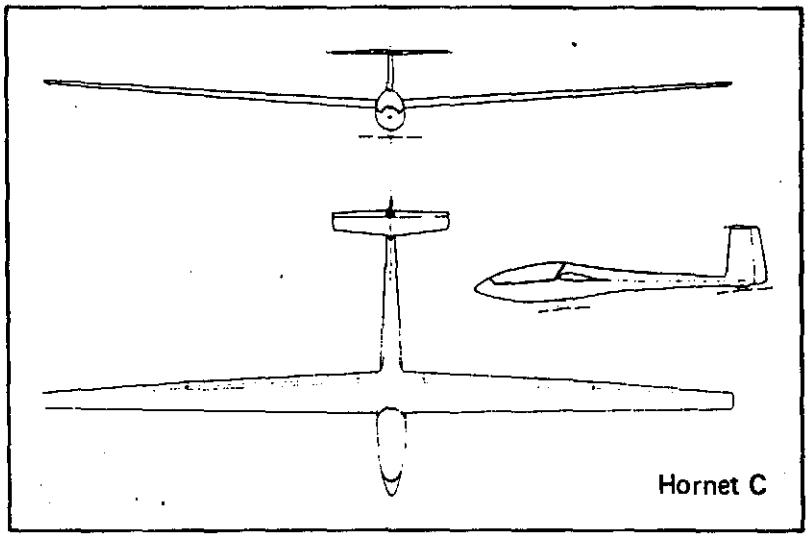

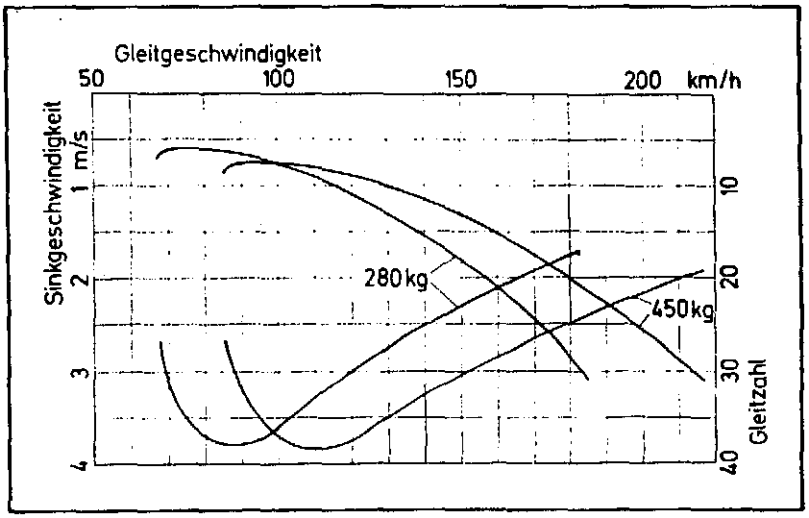

DRAG AWARENESS

In Simple English, The Lowdown on Slowdown

by ORAN W. NICKS

Two kinds of people talk about drag: those who don't know any more about it than you do, and those who know so much more that they can talk only in equations, coefficients, vector diagrams, Greek letters and other mystifying symbols. Here is an unusual discussion of drag by a man who knows a whole lot more about it than most of us, but who contrives to explain it in terms that even a glider pilot can understand. Want to know how many pounds of penalty drag is causing you, where and how, and what to do to cut it down? Read on. The author spent 12 years with North American and Chance Vought, 20 years with NASA (half of them as Deputy Director of the Langley Research Center) and the last four running the wind tunnel program at Texas A&M University. He is Chairman of the Technical Board of the SSA, and an active pilot of his own LS-1f. -Ed.

All soaring enthusiasts are aware of the importance of drag. Experts who make scientific studies of soaring speak of it in terms of coefficients, variations with Reynolds number, dynamic pressure and other expressions having vague or unknown meanings to most of us. Since drag needs to be understood by all who soar, there ought to be some way to relate its causes and effects in terms more easily understood.

The problem of learning to speak "Aerodynamics" before discussing drag with an aerodynamicist is somewhat like having to learn French before conversing with a Frenchman. Perhaps, if we are lucky, the Frenchman has already learned English and is able to communicate in that form. With that simile in mind, why, then, can't an aerodynamicist who also speaks English translate for us? At the risk of speaking "Aerodynamics" with a bad accent, I've decided to give it a try.

First, let's discuss the drag on a sailplane as a total force, measured in pounds, that is trying to hold us back. In a glide, we are always going "downhill", and like the kid on the skateboard, the steeper the hill the faster the speed. Of course, the less the drag, the faster we can go a given slope—the kid with bad bearings will have to find steeper hills to go as fast as he would like. Similarly, the more drag we have, the steeper our glide and the quicker the flight is over at the bottom of the "hill".

Figure 1

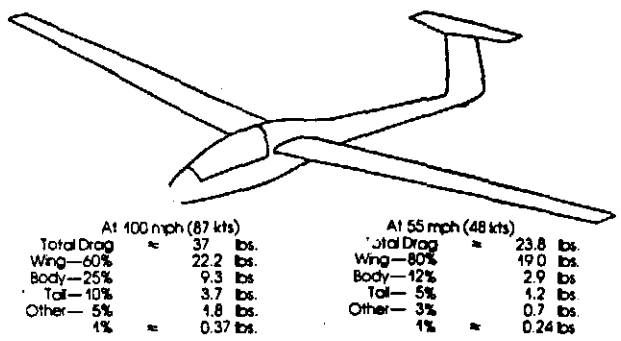

For the sake of illustration, the drag of a 15-meter sailplane is presented (Figure 1) at two conditions: 1) a cross-country or high-speed case and, 2) for maximum glide or a low-speed case. The total drag is about 37 pounds at 100 mph and is reduced to about 23.8 pounds at 55 mph. You probably expected it to be less at a lower speed, for after all, we are familiar with the change in resistance as we change speeds. It's very important when swimming in a fluid called water that our resistance is greater as we go faster, and believe it or not, air is a fluid that behaves in accord with the same laws as water at the speeds sailplanes fly.

Drag Breakdown By Component

Figure 1 shows the contributions of major components to the drag. In cruise flight the wing contributes 60% of the total drag or 22.2 pounds. Of course the wing provides the lift to make flight possible, and its size is determined by the

4

weight of the glider and the speeds to be flown. If we could always fly fast the wing could be smaller and its drag would be less, but we have to be able to fly slowly to thermal and to land safely, so the wing size is greater than required for cruise.

The body is just a streamlined fairing around the pilot and payload, but its cross-sectional area and its surface or "wetted" area are important parameters affecting drag. The supine seating in high performance sailplanes helps to reduce both the cross-section and the wetted areas.

Vertical and horizontal tails are necessary to meet the requirements for stability and control, which determine tail sizes and therefore tail drag. For optimum cruise conditions we could almost do without them, but alas, we must haul them around so that they will be available when we want to manuever, change speeds, change center of gravity or balance conditions, and deal with turbulence and gust disturbances. On most airplanes, the "tail group" contributes about 10% of the total drag during cruise. When the wing is doing a lot of lifting at low speeds, the tail drag percentage is less only because of the increase in wing drag.

When drag values for all major components are added together, they total somewhat less than the drag measured for the complete sailplane. Things like tail skids, total energy probes, air vents and such have to be included in a category called "other".

Figure 2

DRAG BREAKDOWN BY CAUSE—15 METER SPAN WINGS LEVEL

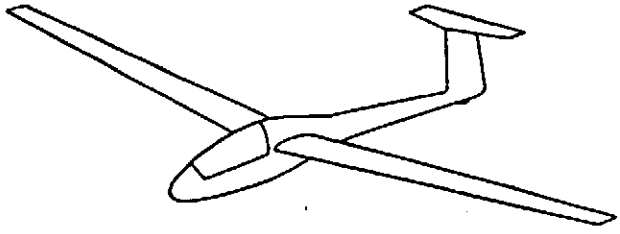

	At 100 mph (87 kts)		At 55 mph (48 kts)	
Friction	53%	19.6 lbs.	29%	6.8 lbs.
Pressure	32%	11.8 lbs.	9%	2.2 lbs.
Induced	10%	3.7 lbs.	57%	13.6 lbs.
Interference	5%	1.9 lbs.	5%	1.2 lbs.
TOTAL	100%	37.0 lbs.	100%	23.8 lbs.

The main point to be gained from this account is the obvious fact that as far as sailplane drag is concerned, "the wing's the thing!" As we will see later, in addition to the effect of area already mentioned, its airfoil profile, its planform, and its aspect ratio (span divided by chord) are especially important to drag.

Drag Breakdown by Cause

Now let us look at the drag account from another viewpoint—just what are the causes for drag and how much is each contributing? For now we will examine the drag causes for the entire sailplane (Figure 2) and afterward we will go into more detail about each.

At high speeds, friction is the big one at 53%, almost 20 pounds. This is a function of surface area, so the smaller the sailplane, the smaller friction drag would be. It is also very much affected by surface shape and smoothness.

Pressure drag is caused by the fact that the sailplane pushes air out of the way as it passes through, making the air turbulent, "stealing" energy from the moving object. If the object passing through air didn't cause flow turbulence or separation, pressure drag would be zero.

Induced drag is a term applied to the drag effects caused by lifting surfaces. Sometimes it is called "the drag due to lift." They say you can't get something for nothing; the drag that is caused by the production of lift is a price paid by a wing. Actually the induced drag is determined by how hard the wing is having to work to produce lift. If you water ski, you know how hard the rope pulls your arms when you're going very slowly. The drag is greater because the angle of the skis is greater in order to keep you from sinking. A wing has the same problem—it must be inclined at a greater angle of attack at low speeds to produce enough lift to balance the weight, which is the same at all speeds. This accounts for the almost four-fold increase in induced drag at 48 knots over that at 87 knots.

Where the wing joins the body and where tails join together, turbulence is created by interference, which causes additional drag. Its effects are usually more like pressure drag, but interference also affects friction drag when it triggers laminar flows and makes them transition to turbulent flows. Interference also can be manifested as induced drag. A classic case exists when the wing and tail are "lifting" in opposite directions. This is generally the case, for a requirement of stability is that the tail must push down for balance when the wing center of lift is anywhere aft of the center of gravity. The down-load on the tail forces the wing to provide even more lift, in order to offset the weight plus the tail down-load. Designers try to set wing and tail incidences to optimize balance for stability over a range of conditions, but this form of trim drag is hard to avoid entirely.

Perhaps your curiosity is now whetted enough to want to know more about why the things happen that we have just discussed. I remember an old saying that "The guy who knows how will always have a job, but he will always be working for the guy who knows why!" Perhaps knowing "why" will help you become a better pilot. I'll try to keep this part as simple as the accounting comments, but it will be tougher.

Friction Drag

If you were pulling a bobsled along snow and came to an icy place on the road, you would expect it to pull easier. If the snow had melted and you came to bare ground, you would expect more drag. Friction is at work! What if you could pull your sled onto a cushion of air; there would not seem to be any drag—but there would be. It would just be a good deal less.

Streamlined shapes seem to move so easily through air that we are fooled, but you may be sure that the fluid (air) scrubbing past the surfaces of a wing or body produces drag. If air were more viscous, like honey, you would believe it created friction; again I remind you that air *is* a fluid and at low speeds behaves according to the same basic laws as liquids.

Friction drag is affected by the density and viscosity of the air, as well as its speed along surfaces, but the three big things affecting the friction drag of sailplanes are:

1. The length of surface contact where scrubbing occurs.
2. The roughness of the surface that is being scrubbed by the air.
3. The waviness or local contours which may cause variations in the pressure field along the surfaces.

It has been determined experimentally that air flowing

along a perfectly smooth, flat plate will "transition" from laminar flow to turbulent flow after a finite distance. No matter how smooth the surface, there is friction and the air scrubbing the surface finally slows more and more along the length until it becomes turbulent and builds up on the surface. If the surface is roughened, this happens in a shorter distance. Slowing the air is the cause of drag, so naturally friction produces more drag the longer the air and surface are in contact.

Waviness effects simply tend to thicken the thin layer of air near the surface as the flow cannot follow the ups and downs. This thickening of the boundary layer at the surface encourages the earlier transition to turbulent flow, much like the effects of roughness.

Pressure Drag

Stirring iced tea with a spoon creates eddies and mixing because of the turbulence, and of course, creates drag on the spoon. An object moving through air tends to do the same. If you move the tea spoon very rapidly, the disturbance effects are obviously greater; thus pressure drag increases with speed. In fact, drag varies greatly with speed changes; for example, the drag is doubled when speed changes from 52 knots to 74 knots.

What is happening when the object is moved through the fluid is that the pressure builds up on the upstream side. If the flow around the body filled in immediately around it without turbulence, there would only be friction drag. But unless the shape is ideally streamlined and no friction exists, there will be some separation and eddying produced by the body. You know from experience that streamlining greatly reduces drag, but we hope to give you some quantitative feel for the significance of streamlining.

Ways of Reducing Friction and Pressure Drag

In the real world it is impossible to separate friction and pressure drag effects on a sailplane; two examples are offered to put them in better perspective. To do this I will first compare familiar shapes (**Figure 3**) and show experimental results of actual drag measurements.

(1) *Streamlining*:

For comparison I have taken one-foot lengths of three familiar shapes:

Figure 3

STREAMLINING REDUCES DRAG
These Sections Have Same Drag at 100 mph (87 kts)
0.32 lbs. Per Foot of Length

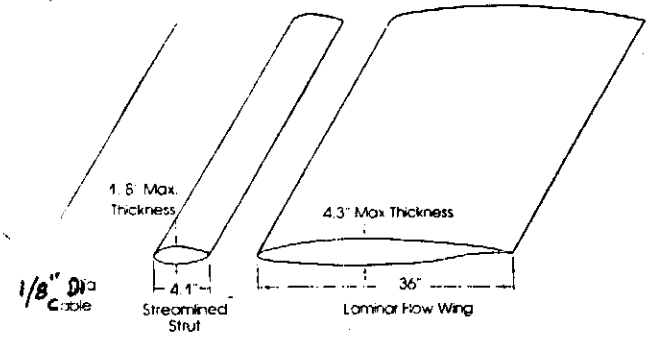

Figure 4

LAMINAR FLOW REDUCES DRAG
Wing Profile Drag at 100 mph (87 kts)
Combined Friction and Pressure Drag
12% Thick, 36 Inch Chord Section

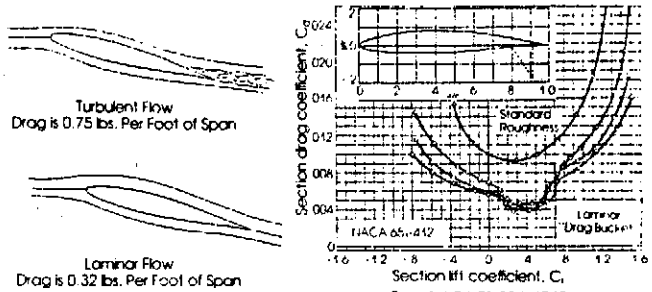

From NACA TR 824, 1945

1. A stranded cable
2. A streamlined strut
3. A laminar flow wing

From drag data obtained and verified over the years by many experimenters, we find that the same lengths of a 1/8 inch diameter stranded cable, a four-inch chord streamlined strut, and a three-foot-chord section of laminar flow wing have the very same drag at 100 mph or 87 knots. Using the experimentally obtained drag data shows that a foot of each produces about a third of a pound of drag at 100 mph, and lower but roughly equal amounts at lower speeds.

(2) Laminar Flow

In the case of the wing section, laminar flow is a big help in reducing drag. During the 1940's researchers at NACA Langley found an amazing effect they named a "drag bucket" while testing airfoil sections of different shapes in a wind tunnel (**Figure 4**). The facility had been carefully designed to produce almost undisturbed flows past their models, and aptly named "The Low Turbulence Pressure Tunnel." The term "drag bucket" was coined because the drag coefficient plotted against lift coefficient showed extremely low values over a certain range of lift values, making a plot that looked like it might hold water as shown in Figure 4. They also found that when they artificially roughened their models, the drag increased dramatically; in fact the "drag bucket" disappeared and drag more than doubled for some lift values. These new airfoil sections were named "laminar flow airfoils" because it was shown that the large extent of laminar flow was the cause for their drag reduction. While most sections used on gliders today are slightly different, they are descendants of the family of NACA-developed laminar flow shapes that have been tailored to sailplane conditions.

Induced Drag

As already mentioned, induced drag, the drag due to lift, is affected by such things as the span-to-chord ratio (aspect ratio) of the wing, the planform, the wing twist and the shape of the tips. All of these also influence the distribution of lift along the wing. The wing designer takes these factors into account, making tradeoffs between aerodynamic performance, weight, cost, and maneuverability. Most of the induced drag effects are evidenced as vortex flows around wing tips, so long slender wings with relatively small tips tend to cause less induced drag. Tip shape is also important

Figure 5

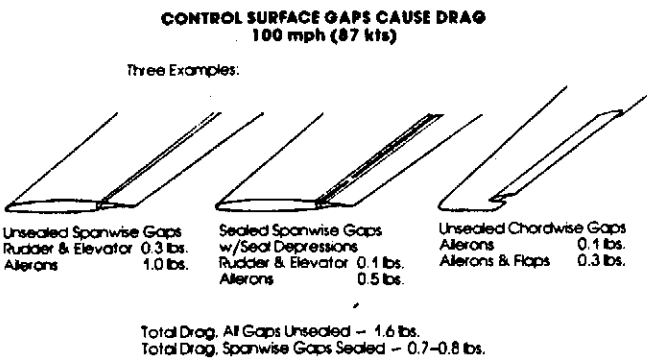

because it is high pressure air leaking from the lower surface to the upper surface which causes vortices to form. This "stirring" of the air by the wing tip transfers energy to the air which is dissipated—this loss is induced drag.

Interference Drag

In addition to the interactions between wing, body and tails, moveable control surfaces, spoilers, and air vent systems also cause drag. Some of these interferences are inherent in the design and some may be affected by the pilot. Control surface and flap gaps may create interference drag which can be reduced by sealing. Some sample data are provided in **Figure 5** to give an idea of the importance of these sources to sailplane drag.

One of the most insidious forms of drag in soaring is caused by air leaks. Because air is invisible, there are no obvious indications of flows into or out of sailplane canopy cracks, or around wing roots and spoilers, except for hissing sounds. Pilots must have cooling air inside their glass cages or they would melt, so some form of "controlled" leaks into and out of the cockpit is necessary. It is extremely difficult to quantify the drag due to all possible leaks, but a look at some of the classical cases may be informative. **Figure 6** illustrates these effects.

The cooling air system with the lowest drag would take in air at a place where the inlet would not disturb external flows, gradually diffuse and pass the air through the body at very low speeds, and exhaust it at the tail of the sailplane through a duct sized to bring the flow back to free stream velocity. This idealized system would still produce some drag, but not nearly as much as most cooling systems. The nose is a good place to take in air, although some designers have worried about disturbances the inlet might cause to laminar flow over the body and have located inlets aft under the wing.

Figure 7

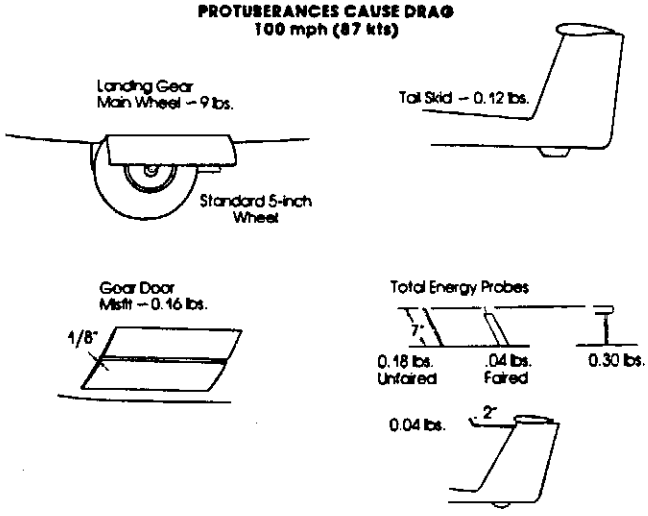

Figure 6

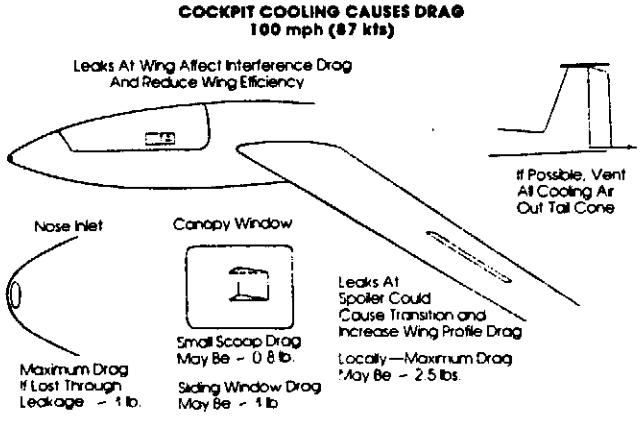

A more serious concern is cockpit sealing to prevent flows in or out of the sailplane at places other than specifically intended. Pressure variations along a fuselage, over a wing root or past a wheel well door can cause circulative flows into and out of the ship which interfere with the normal airflow along the surfaces. These create a momentum exchange drag and may also cause disturbances in the external flow field. For example, if the air taken in at the nose exhausted out the edges of the canopy through leaks, about one pound of drag would result. This does not even take into account interference effects caused by boundary layer disturbances. Leaks through the wing and exhausting around spoilers could be more devastating. They could cause boundary layer separation and turbulence over 10-15% of the wing span, seriously increasing drag locally, perhaps adding 2.5 pounds of drag.

It is common knowledge that protuberances like tail skids, landing gear, total energy probes, antennas and such cause drag; but from the number of these "drag items" seen on sailplanes, it is worth looking at the values for some of them. In **Figure 7** several typical items are shown, indicat-

ing the drag penalties that might be associated with them.

Finally, changes in the sailplane flight loading conditions should be mentioned for they can cause significant changes in drag. Increases in gross weight resulting from the addition of water or other ballast obviously change the lift requirements for the wing. Since induced drag is proportional to the square of the lift value, induced drag is increased significantly with an increased loading. For example, if the weight were to increase 10%, the induced drag at a given speed would increase 20%. Also important is the center of gravity position, as this affects the trim requirements and may result in larger tail down loads for balance. The drag variation caused by a shift from a forward CG to an aft CG may amount to about one pound at cruise conditions. This is approximately a three per cent variation in total drag, a number which may be highly significant to the racing pilot.

Maneuvering Drag

Another effect of significance in soaring is the drag caused by maneuvering, the most common maneuver being a simple turn. **Figure 8** summarizes the nature of these effects. Because of centrifugal forces, the wing has to provide lift in a turn greater than the weight of the sailplane, thus increasing the induced and control surface drags required to maintain the turning attitude. At a 45° bank angle, the lift must be increased to about 1.4 times the value required in a wings-level glide at the same speed; this causes the drag to increase to about 1.7 times what it would be for a wings-level glide at the same speed. The reasons are: 1) the induced drag is increased at greater lift values, 2) the trim drag is increased to maintain balance with the greater lift, 3) aileron and rudder misalignments are used to maintain attitude during the turn, and 4) there is a high probability of some slipping or skidding in a turn which increases drag. Serious pilots may want to do some experiments and simple calculations concerning the effects of turning on lift and drag.

Designers have reported that for design optimizations they assume that average bank angles of about 40 to 45 degrees are common. Since the sailplane drag at 48 knots in a wings-level glide is about 23.8 pounds and increases to 40.7 pounds in a 45 degree bank angle glide, it is obvious why pilots who are able to climb straight ahead do better than they would in circling flight.

Figure 8

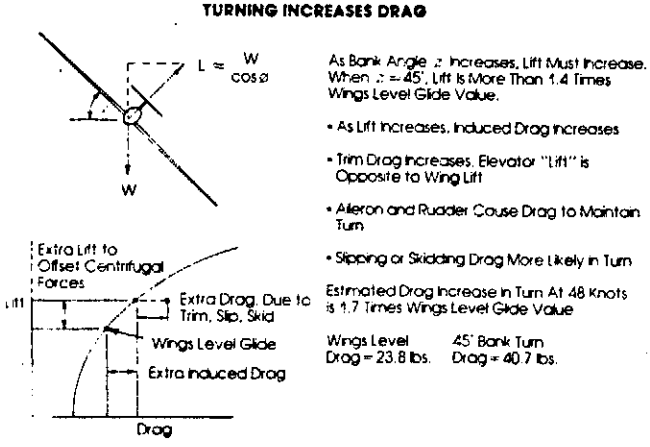

Summary

Drag is obviously "the enemy" in soaring flight. Not only are the design characteristics and the physical condition of the sailplane important, but the ways we prepare and operate the craft influence its drag. Of the major components, the wing is by far the largest contributor to drag, and its airfoil profile, aspect ratio and surface condition are critical to total sailplane drag. Streamlining is not only a matter of aesthetically pleasing shapes but also a product of sealing leaks, proper venting of air and treatment of interference regions. Air leaks are common causes of drag that can be reduced with owner attention. Finally we see that the way we fly can have a dramatic impact on drag. The most pronounced variation due to piloting is the effect of maneuvers on induced drag.

Yes, an awareness of the causes and effects of drag should be ever present in soaring. With a bit of study and with a reasonable application of TLC, we should all glide a little bit farther, faster or longer—and maybe all three!

REFERENCES

1. "Aerodynamic Drag," Sighord F. Hoerner: *Otterbein Press*, 1951.
2. "Summary of Airfoil Data," Ira H. Abbott, Albert E. VonDoenhoff and Louis S. Stivers, Jr.: *NACA Report No. 824*, 1945.
3. "Engineering Aerodynamics," Walter H. Diehl: *Roland Press*, 1942.
4. "Proceedings of the NASA/Industry/University General Aviation Drag Reduction Workshop": Jan Roskam, editor, 1975.
5. "Review of Drag Cleanup Tests in Langley Full Scale Tunnel," Paul L. Coe, Jr.: *NASA Technical Note D-8206*, 1975.
6. "Proceedings of the 1st International Symposium on The Technology and Science of Motorless Flight," James L. Nash-Webber, Editor: MIT, Cambridge USA, October 1972.
7. "Motorless Flight Research, 1972," James L. Nash-Webber, Editor: *NASA CR-2315*, 1973.
8. "Science and Technology of Low Speed and Motorless Flight," Perry W. Hansen, Compiler: *NASA Conference Publication 2085*, 1979.
9. "Influence of Systematic Variations on the Drag Polar of the Sailplane RJ-5," August Raspet: *Soaring*, September-October, 1951.

All of the numbers generated in this presentation were based on sound experimental and analytical data; however, in the process of generalizing and simplifying, the numbers necessarily become more qualitative than exact. Please consider them for the insight they provide—as "representative" only—and not as directly applicable to your specific sailplane. For those who wish to delve more deeply, a list of references is provided after the article.

—Oran W. Nicks

OPTIMIZING MODEL SAILPLANES

In the previous "Soartech" issues we published performance analysis and optimization studies that put into our hands the methods we need to zero-in on improved models. This paper, which takes on the popular two-meter class model sailplane, has a surprising conclusion. Martin Simons has thoroughly worked out the performance of the two-meter model and documented the whole process in detail. It puts the cap on his previous papers dealing with performance analysis. Taking on the two meter was a very good choice. It's hard to optimize the performance of models, because the range in which we fly them makes bigger models better. Any attempt to optimize without limits means that, basically, the biggest model has the best performance. Limiting span stops that process at a point, and by optimizing the rest of the dimensions, Martin Simons shows that we should do much better with lower aspect ratios.

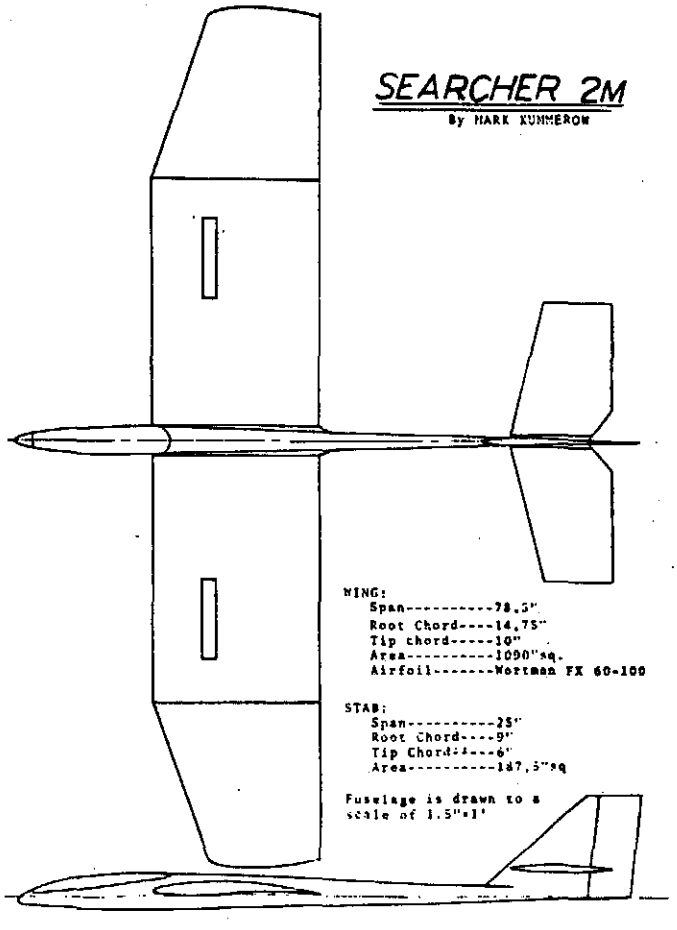

THE TWO METRE SAILPLANE

By Martin Simons

The Two Metre Sailplane

In Australia now the two metre span, radio controlled sailplane, seems to be recognised as a competition class and regulations have stabilised so that it is possible to do some theoretical work. Any future changes in the regulations will tend to invalidate the findings presented here.

Briefly, under the Australian rules, the two metre sailplane is to be controlled by rudder and elevator only or, if a V tail is used, by the usual 'ruddervators'. Ailerons, flaps, spoilers and radio-operated tow release hooks are disallowed. The standard methods of launching, hand towline or winch, are to be used with the usual limitations on line length, winch dimensions, etc.

Ballast is permitted but the contestant is not allowed to change the mass of the sailplane during a round. In other words, the two tasks, 'A' and 'B', constituting a round, have to be flown with the same ballast, but this may be changed between rounds. Anyone putting too much ballast in may thus suffer a disadvantage in task 'A' while gaining some benefit in task 'B', and vice versa if too little ballast is used. Task 'A' is the normal six minute duration task, with points deducted for times either less than or greater than six minutes. A spot landing may be added at the discretion of the contest organisers. Task 'B' is a speed task similar to that used for the FAI international F3B championships, four runs over a 150 metre course at right angles to two parallel sighting lines, line 'A' and line 'B'. The start is made by crossing line A, flying as fast as possible to cross and turn at line B, flying back to line A and turning again, to complete the task by flying again to B and turning back to cross line A. The task requires three high speed turns, which makes the exercise a good deal more interesting, from the theoretical point of view, than the former two lap, one turn speed course.

Whether or not a spot landing is required is of some importance in deciding what ballast to carry, because a heavier, faster-flying model without spoilers, is much harder to get down safely on the designated spot than a light, slower model. This is one of the factors the pilot must consider when making the decision, before a round, about ballast.

The ability to fly the turns efficiently in the speed task, is also of great importance. The direction of flight has to be reversed completely three times without the sailplane either slowing down too much or flying too far beyond the turning point. Without ailerons it is unlikely that pilots will be able to adopt the half roll and inverted 'pull through' diving technique used by some international champions. This method, if well judged, ensures that the sailplane accelerates, rather than slowing down, at each end of the lap. In the normal turn likely to be used in two metre competitions, a heavy load of ballast will tend to force the sailplane to turn on a large radius, adding distance to the task with some penalty showing on the timer's clock. The alternative is to steepen the turn to a large angle of bank, which reduces the radius of turn but causes a sharp increase of drag, especially wing tip vortex drag, which slows the aircraft down. The ability of the pilot to time the turns is most important and the theorist cannot help much here. Obviously the turn should begin before

reaching the mark, so that, ideally, the aircraft will cross the line only for an instant and start the return journey immediately. In some contests observed by the author (we shall say nothing about those in which he has actually flown), the winning times were achieved, not by those with the fastest sailplanes, but by those who judged the turns best. Some models spent more time turning outside the course than actually flying between the lines.

The combined effect of all the FAI general rules governing contest aircraft models, and the two metre span limitation, presents us with a flight 'envelope' of the type shown in Figure 1. The maximum total, projected, area of all wing and tail (or other similar) surfaces must not exceed 150 sq dm or 1.5 sq metres. Unless we build a tailless aircraft, the true effective wing area will always be less than the FAI area by an amount equal to the area of the tailplane or other stabilising surface. It is assumed for present purposes that the stabiliser will be 10% of the wing, so the maximum wing area in practice is 1.35 sq m. Small deviations caused by slightly larger or smaller tailplanes will make only marginal differences to the performance. They may have more important effects on the stability of the sailplane, but 10% is a fairly typical stabiliser area for a competition model. The FAI area limit determines the lower limits for the wing aspect ratio. This ratio is found by dividing the square of the span by the wing area, so for a two metre sailplane the lowest possible value of 'A' (aspect ratio) will be:

$$2 \times 2 - 1.35 = 2.963$$

Along the top edge of the diagram is a scale of aspect ratio. The corresponding wing areas and FAI total areas are also shown. There is no legal limit at the right hand side. We can build a model with as high an aspect ratio as we choose, but as the aspect ratio rises, the wing chord becomes narrower. As will be shown, there are grave disadvantages with a fixed, two metre span, if the wing chord is too small.

Down the left hand edge of the flight envelope is the FAI loading scale. Using the combined areas of wing and stabilising surfaces, the FAI confines contest models between the loadings of 12 and 75 grammes per sq dm. Allowing for the 10% tailplane area, these become effective wing loadings between 1.32 and 8.25 kg per sq m. (Full sized sailplanes commonly fly with wing loadings between 30 and 45 or 50 kg per sq m.) There is a further restriction of 5 kg on total all up mass, which appears in Figure 1 as a slanting line across the top left corner.

The modeller has a wide range of choices. The main variables are the wing aspect ratio, which controls area and chord, and the mass, which controls wing loading. Aspect ratio is a matter of design, and once the model is built, it cannot be changed much. To decide on this single figure is one of the chief preoccupations of the sailplane designer. The mass and hence flying weight of the model, can be varied to some extent on the field by adding or removing ballast, so although the designer can provide for ballast to be fitted, preferably in a way that adds strength to the wing as well as mass, the decision as to how much to carry has to be made by the pilot before each contest round. To use the ballast in such a way

that it adds strength and stiffness to the wing, can be done if the ballast itself is in the form of a steel rod or rods passing right through the fuselage and wing roots, adding greatly to the strength of the aircraft in this critical region. This method has been used with success by the Australian F3B team and should be applied also to the two metre sailplane. When all ballast has been removed, the structural weight of the sailplane will depend on its construction and the kind of radio gear used. By very careful weight control techniques and using ultra light radio equipment, a two metre sailplane could be made to have the FAI minimum wing loading. This, however, might create serious difficulties in practice. The stresses set up during a winch launch are quite severe and depend far more on the wing span and the strength of the line used on the winch, than on the other features of the sailplane. A delicate structure would also tend to break if the model landed badly when carrying ballast. These problems should not be overlooked when considering the theoretical arguments which follow. In the flight envelope of Figure 1, the lowest part of the unshaded area is more or less excluded for these structural and operational reasons.

The slanting, curved lines on Figure 1 indicate, very approximately, the Reynolds numbers at which models of this class fly when soaring. The Re number is one of the most important factors in all model aircraft design. Without going into detailed physical explanations, it expresses the relationship of the size and speed of the wing (or any other part of an aircraft) to the density and viscosity of the air. The larger and faster the aircraft, the larger the Re number. The wing tip of a full-sized sailplane near stalling speed, operates at Re about 400 000, and a model sailplane at its maximum velocity in a speed task, may reach this figure at the wing root. When the model is flying slowly, as it will be when soaring in thermals, the Re is much lower and since the speed, at this trim, is determined mainly by the wing area and flying weight, the Re is low for lightweight, high aspect ratio aircraft and somewhat higher for heavier, low aspect ratio types.

As the Re number falls, the effects of the air's viscosity become more pronounced and the drag of the wing profile increases in importance, relative to the size and weight of the aircraft. A crude way of expressing this is to say that the air becomes more 'treacly' to the smaller and slower wing. Ultra light aeroplanes and full-sized sailplanes suffer from this effect, but model aircraft much more so. With the kind of wing sections commonly used for radio controlled sailplanes, at Re numbers below about 60 000, there is often a very marked breakdown of the airflow, so that the wing stalls prematurely. It is very important to avoid any part of a wing reaching its 'critical' Re figure, and it must be remembered that the chord at a point on the span, is what counts. If a tapered wing has a Re number of 80 000 at the root, the tip, which is narrower, may be operating at less than 60 000, very close to or below the critical value. (The figure varies from one wing section to another.) In a turn, the inner wing tip will be moving slower through the air than the outer tip, so the Re number there will be lower again. Generally, therefore, a successful and legal two metre sailplane will lie in the unshaded area of the envelope, to the left of the sketched Re 60 000 line, and preferably should be flying at no less than Re 100 000 to

ensure a safe margin. In any case, the higher the Re, the more efficient the wing section will be.

(Free flight models often operate below Re 60 000. To achieve efficient flight, they require specialised aerofoil sections which are usually very thin, and may be fitted with turbulators and other devices to prevent the sub-critical flow breakdown. Such thin profiles are not really suitable for radio controlled sailplanes which have to fly speed tasks as well as soaring, and which require fairly deep spars to withstand the loads involved in launching and high speed turns.)

The Re depends on chord as well as flying speed, and chord depends on the aspect ratio. The lower the aspect ratio is, the more efficiently the wing profile will work. However, at low flying speeds, i.e., when soaring, the most important source of drag is not the wing profile but the wing tip vortex. Since there is a difference in pressure between the lower and upper surfaces of any lifting wing (or tail), the air tends to flow round the tip from lower to upper side. A strong, rotating vortex or 'swirlwind' forms behind and slightly inboard of each tip, and trails off, spiral fashion, downstream. Much energy is lost in this way, and at high angles of attack, as in slow speed trim, the drag resulting totals MORE THAN HALF the total drag of the entire sailplane. The most effective way of reducing these losses is to increase the aspect ratio. Tapering the wing in plan, preferably giving it a perfectly elliptical outline, can save a few percent more. The special wing tip vanes or 'winglets' seen on some modern aeroplanes may also be used to reduce the strength of the vortex and can save a little more drag at high angles of attack. These may prove useful for two metre models. If the winglet is vertical there is no increase in projected span. Their design and angular twist setting require a good deal of care. In any case, at high flight speeds vortex drag is much less significant than parasitic drag and the winglets which reduce drag in soaring become parasitic items at high speeds.

Against the benefits of low aspect ratio for the sake of lower profile drag, we have to set the benefits of high aspect ratio for lower vortex drag. Against the benefits of tapering the wing to reduce vortex drag, we have to set the dangers of a low Re at the tips. Against the advantages of winglets (which require very careful design and positioning), must be set their extra drag at high speeds. The final outcome has to be a compromise between all these factors and this is where some calculation can be of help.

The methods used in what follows are standard and have been described elsewhere. The work required is only simple arithmetic and can be done by anyone. A computer is used only to save time. In this case, the program is that devised some years ago for the full-sized 'Sigma' project, by Nick Goodhart. When the computed performance of some full-sized sailplanes was checked against their actual behaviour in flight, the Sigma program proved extremely accurate. The program has been adapted for models by Tom Nemeth. The great advantage of this program is that it allows the use of wind tunnel test results rather than relying entirely on theoretical aerofoil work. Perhaps the most important feature of the calculations is that wind tunnel data over a wide range of Reynolds numbers are

employed, rather than relying on a single test at one Re. A good many authors in the past, with all respect to their enthusiasm, have overlooked the point that a model wing operates at quite different Re as its flying speed varies. Performance estimates not allowing for this are very unreliable. The Goodhart program takes wind tunnel data at four different Re numbers and, having first worked out the flight speed of the sailplane at a given trim, and knowing the average wing chord, interpolates wing profile drag figures for the appropriate Reynolds number. A simplified version of this method has been described by the present writer in a previous article in Soartech 1. In other words, supposing always that the actual model wing is accurately made and smooth, the performance should be close to that predicted by the Sigma program. Wind tunnel models themselves are not quite perfect, so the practical modeller can at least aim to achieve similar results, whereas the mathematically perfect aerofoil curves coming from the computer but not proved in the wind tunnel, remain to be demonstrated in practice.

Figure 2 shows the effects of ballast. The performance of an example sailplane has been worked out and plotted in the usual way as a polar curve. This shows, at each trimmed flying speed, the rate of sink of the model through the air. For this diagram, the model is supposed to have an aspect ratio of 10 and the wing profile is the well known Eppler 193. This profile is used, not because it is necessarily the best available, but because it has been well tested in the Stuttgart wind tunnel and has also been amply proved in practical model flying. There has not been sufficient time to run the program with other wing profiles, although this may be done some day.

As the various different curves show, adding ballast to the model tends to shift the entire performance curve to the right, higher speed side of the chart, but also flattens the curve. There are no great surprises here. It will be noticed that the curve representing the lightest condition has some irregularities at the low speed end, and although this light model has a very low minimumn sinking speed, the curve is quite sharply peaked. These features of the polar are caused almost entirely by the low Reynolds number effects mentioned above. As indicated, the average Re of the wing, at this weight and trimmed for least sink, is only 68 000. The airflow is already beginning to separate on the upper surface of this wing, and in practice it is very doubtful if the model would ever achieve its 'peak' soaring performance. The peak is so narrow that a small piloting error or gust would move the model off it, either to the higher speed side of the curve, or to the stall. Increasing the weight to 1.3 kg brings the Re to a much safer average near 100 000, and while there is some penalty in both sinking speed and turn radius, the model would be much more tolerant.

Polar curves representing sailplanes of weights intermediate between those actually plotted, may be estimated fairly well by interpolating between the lines on the diagram. There are no anomalies or oddities arising.

Not only does ballast increase the rate of sink in straight flight, as shown on these polars, but it also increases the radius of turn at any given angle of bank. If a thermal is narrow, to remain within it the sailplane must turn on a small

radius. The light model can do this with a relatively gentle angle of bank, so the sinking speed in the turn is increased only slightly above that for the straight glide. A heavier sailplane can achieve the required small turn radius only by banking steeply, and the effect on sinking speed is quite serious. This may not matter if the thermal, once caught, is strong, but a narrow, weak thermal presents the pilot of a heavy model with real difficulties. The choice lies between circling with small angle of bank, which then probably takes the sailplane out of the thermal altogether, or circling tightly with large angle of bank, which will probably increase the sinking speed so much that the model will not climb. The only escape in such conditions, is for the pilot of the heavy model to use the good high speed performance of the aircraft to explore a larger area in search of a better thermal. There may not be one.

The advantage of the heavily ballasted sailplane for high speed flight, is probably clear enough. A rough measure of this is to note the flying speed at which each curve crosses the line representing a glide ratio of 1 : 10. Still, the effect of the additional mass, and speed, on the racing turns, mentioned above, must not be overlooked.

Figure 3 summarises in one chart, all these effects, so far as that can be done in a single diagram. The lowest line on this graph shows how additional mass causes the radius of turn, with a 30 degree angle of bank, to rise. The rate of sink in a turn increases, so the two central curves in the diagram show this effect, again based on a carefully flown, 30 degree banked turn. (Of course, every turn must be flown with the correct angle of bank. To try to turn 'flat' as some pilots do, is to cause considerable outward skidding in the turn, with consequent high drag and greater sink.) The uppermost curve shows how the speed at which the model flies when trimmed for minimum sink, rises with weight.

The question now arises as to whether the aspect ratio chosen for the example, 10, is the best compromise. The next diagram indicates that it is not. In Figure 4, polars have been plotted for three sailplanes all built and ballasted to the same flying weight, but with aspect ratios 4, 6, 10 and 14. Naturally the A = 10 curve is the same as that of the previous figures, and is included for comparison.

To the right appears the polar of a model weighing 1.3 kg with an aspect ratio of 14. Vortex drag has been cut, but at the cost of lower Re numbers. The curve shows a very sharp peak and the same sort of irregularity we have learned to associate with low Re conditions. Not only this, but the best rate of sink, even if the model could be trimmed accurately enough to achieve it, is less than that of the original A = 10 example. By increasing the aspect ratio we have made the model harder to trim, it will require a larger turn radius, and will not perform so well in Task A. The high aspect ratio curve improves relatively at high speeds, but more will be said about this later.

The polar curves for A = 4 and 6 are particularly interesting. Although such low aspect ratios imply high vortex drag, which is usually very bad for a soaring sailplane, the Re number for these wide chord wings is higher. The improvement

in profile drag counteracts the extra vortex drag. The minimum sinking speed is very similar to that for A = 10, at the same total weight. (The wing loading, of course, is less.) What is probably much more important is that this low sinking speed is reached at a low flying speed, and these polars are remarkably free from sharp peaks and irregularities. This means that the low A model will be tolerant of rough air, easier to trim, and capable of turning on small radii at shallow angles of bank. For soaring, these are very important features. It is also very encouraging to see that, because of the generally flat nature of the low A curves, the glide ratio does not deteriorate very rapidly as the forward speed increases. At velocities around 8 and 9 metres per second, the two low aspect ratio aircraft would 'penetrate' through sinking air, or make headway against the wind, just as well as the A = 10 sailplane. the A = 6 model maintains its superiority up to flying speeds of 11 m/sec. For general soaring and for exploring the air to find sources of lift, such a model would be excellent.

For the speed task, the light wing loading of the lower A model is against it to some extent. The polar curves cross over again as the velocity rises. The higher wing loadings of the high aspect ratio models, now at sufficient Re numbers for the narrow wings to be working well, gives them an apparent advantage.

It is therefore of some interest to compare low and high aspect ratio sailplanes at the same wing loadings. To achieve this, ballast would be added to the low A sailplanes and mass would have to be subtracted from the high A aircraft. The stalling speed, which depends mainly (not entirely, because of Re effects on lift coefficients) on the wing loading, should be very similar in all cases. The high aspect ratio wing, because of low vortex drag, should exhibit a better minimum rate of sink, so should have some advantage in the duration task. The low aspect ratio wing, because of its better Re numbers and because vortex drag is almost negligible at low angles of attack, might be expected to do better at high speed. Figure 5 shows what happens. The most interesting point about the curves here is that, while the A = 10 sailplane does indeed show better minimum sink, its superiority is confined to a very narrow range, close to the stall. The A = 14 polar has virtually collapsed. The reason is that, to get this wing to the same wing loading as the others, the flying weight has to be reduced. This brings the Re number down quite drastically to critical values. Such a model would be very unsatisfactory. The advantage of the lower aspect ratio at high speed is quite clear. The A = 6 sailplane is evidently a better compromise than A = 4, because its soaring performance and penetration remain excellent with very little given away to the lower A type at the highest velocities. It will occur to the reader that a low aspect ratio sailplane with intermediate ballast, to bring its wing loading up near but not equal to, the equivalent high A type, should be capable of both out-climbing and out racing, the high aspect ratio model. How much ballast to carry on a given occasion, remains for the pilot to decide on the day, or at the hour.

These facts are summarised in the next diagram, Figure 6, where the influence of mass and aspect ratio on the flying speeds at steep glide ratios, is shown. The speed task will probably be flown at a glide ratio of about 1 : 5. This

assumes a reasonably high start and efficient turning technique. The A = 14 model, at all weights, reaches this glide ratio at a higher flight speed than the lower aspect ratio aircraft. However, some of the models represented on this diagram would be disqualified because they fall outside the FAI limits. For instance, the A = 14 sailplane, would be loaded to the FAI maximum of 7.5 kg/sq m if it were flying at slightly over 2 kg all up. Its 1 : 5 glide speed would be surpassed by an A = 6 model loaded to about 3 kg, and this would be quite legal. Needless to say, to ballast any two metre model to this extent would prove a severe penalty in the duration task, but the point is probably sufficiently made.

It is also important to recognise some other advantages of the low aspect ratio. To taper the wings of a high A sailplane, with the two metre span restriction, brings the tips quickly into the critical Re zone and so it is unadvisable. Rectangular planforms are better for the two metre, high A, type. But if aspect ratio is reduced, the critical Re problem is avoided and the wing can safely be tapered. This helps, a little, to offset the high vortex drag. It also allows the wing roots to be both broader and deeper. The wing may then be built lightly, so the low aspect ratio model may, in weak conditions, truly be capable of soaring and winning task A when higher aspect ratio aircraft cannot stay up at all. Then although the speed task may have to be flown at a relatively slow speed, the final score may still be good enough to win. In the next round, when thermals pick up and a wind rises, the model may be able to carry ample ballast to win the speed task and still do well enough in task A. The final choice remains with the pilot, but the low aspect ratio sailplane seems to offer a greater range of possibilities. Figure 7 is equivalent to Figure 2, showing the polars for an A = 6 sailplane at the same flying weights. By tracing these curves and laying them one by one over the earlier figure, a fair comparison can be made.

In conclusion, it is emphasised again that this study has used only one aerofoil section and it remains to be found how a change of this important aspect of a design, affects the results. The author believes, from previous experience of similar studies, that the outcome will remain in favour of considerably lower aspect ratios than have been seen hitherto on two metre sailplanes. A further point worth making is that, throughout the above study, certain assumptions have been made about such things as parasitic drag, fuselage size, tailplane and vertical tail surface areas and drag coefficients and so on. Any and all of these may be in error to some extent, but the fact is, even if they are all removed from the calculations, the benefits of the lower aspect ratio still appear. The final diagram illustrates this. In computing sailplane performance, it is possible to work out the polar curve for the wing alone, and even to make unrealistic assumptions, such as, that the wing has the perfect, elliptical lift loading distribution giving minimum vortex drag. It is then fairly safe to assume that the best wing, fitted to a standard type of fuselage with a normal stabiliser and tail unit in proportion to the wing area, will produce the best sailplane. Figure 8 shows the results of such a theoretical exercise. It is obvious that all the polars improve a good deal, which is to be expected. Yet apart from a very narrow zone of flight, close to the stalling speed, the A = 6 wing

outperforms the others and gets better and better, relatively, as the velocity increases.

In practice the low aspect ratio sailplane offers some ways of reducing parasitic drag which have not been allowed for at all, yet. For instance, with a broad and deep wing root, some, if not all, the radio gear can be housed in the wing itself and the fuselage reduced to a very slender form, which will have less drag, especially at high speeds. This in its turn suggests the possibility of eliminating the fuselage altogether and attaching the elevators directly to the trailing edge of the mainplane. The resulting, apparently tailless, sailplane, would have a very light wing loading when unballasted, so the usual disadvantage of the tailless type, poor soaring ability, would be largely overcome. At high speeds, where parasitic drag becomes so important, the performance should be extremely good and, if control difficulties in the lateral sense can be overcome, the 'all wing' two metre model might prove to be a winner.

All this applies only to the two metre contest sailplane. There is no substitute for span, and larger aircraft will, other things being equal, always fly better than small ones. The two metre contest sailplane will become, under the influence of the Australian rules, highly specialised. Perhaps few people other than the keen competitors, will choose to fly such aircraft when allowed to employ something larger. What we have found is that a particular set of competition rules, is likely to lead to the development of sailplanes which will be efficient for their particular purposes, but which will still be outperformed by aircraft of larger dimensions and orthodox appearance.

Another point is, of course, to wonder whether this kind of sailplane is exactly what the rule makers had in mind when they searched for the ideal BEGINNERS' competition sailplane. What, we may ask, was wrong with the old 100 inch or 2.54 metre span, two control, so-called 'Standard Class"? The author of this article thinks there was nothing wrong with it at all, for beginners, and would like to see it back in the contest calendar.

Figure 1

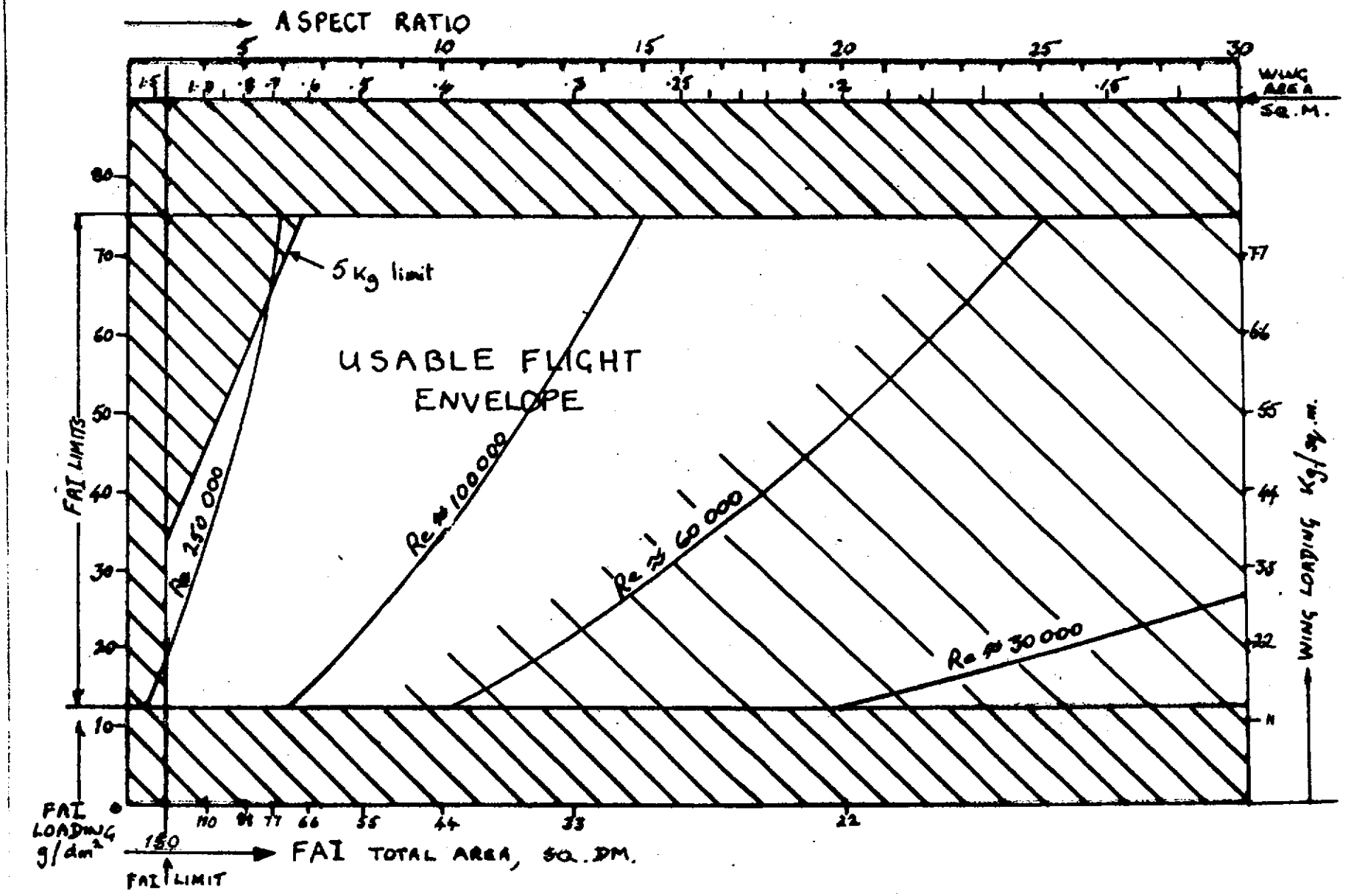
ASPECT RATIO
5
10
15
20
25
30
1·5
1·0
·9
·7
·6
·5
·4
·3
·25
·2
·15
WING AREA SQ.M.
80
70
60
50
40
30
20
10
5 kg limit
USABLE FLIGHT ENVELOPE
Re # 250 000
Re # 100 000
Re # 60 000
Re # 30 000
FAI LIMITS
77
66
55
44
33
22
11
WING LOADING Kg/sq.m.
FAI LOADING g/dm²
110
99
77
66
55
44
33
22
150
FAI TOTAL AREA, SQ.DM.
FAI LIMIT

Figure 2. The effects of ballast on a two metre sailplane with aspect ratio 10

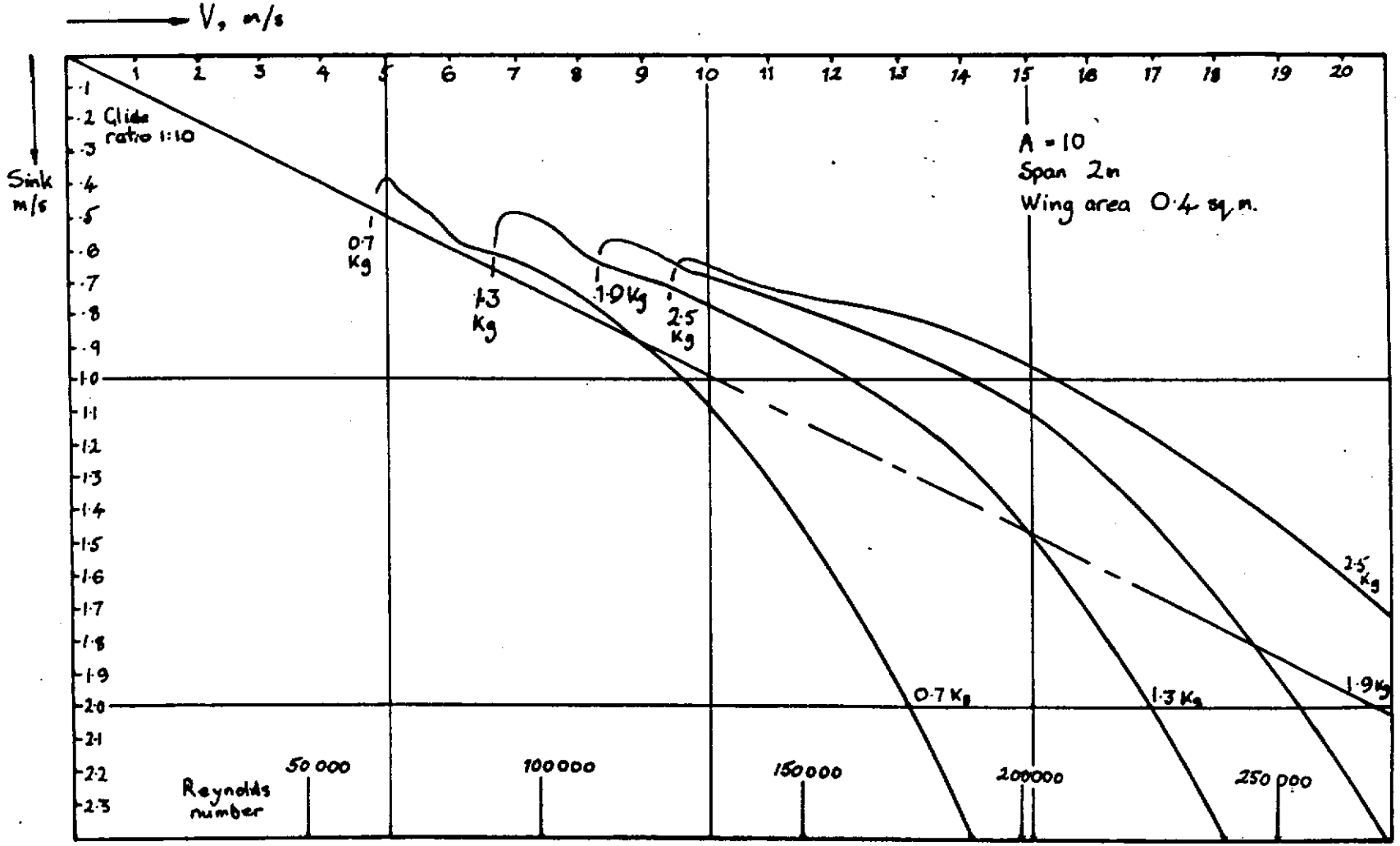

Figure 3
Summary diagram showing effects of ballast on turn radius and on sinking speed in turns

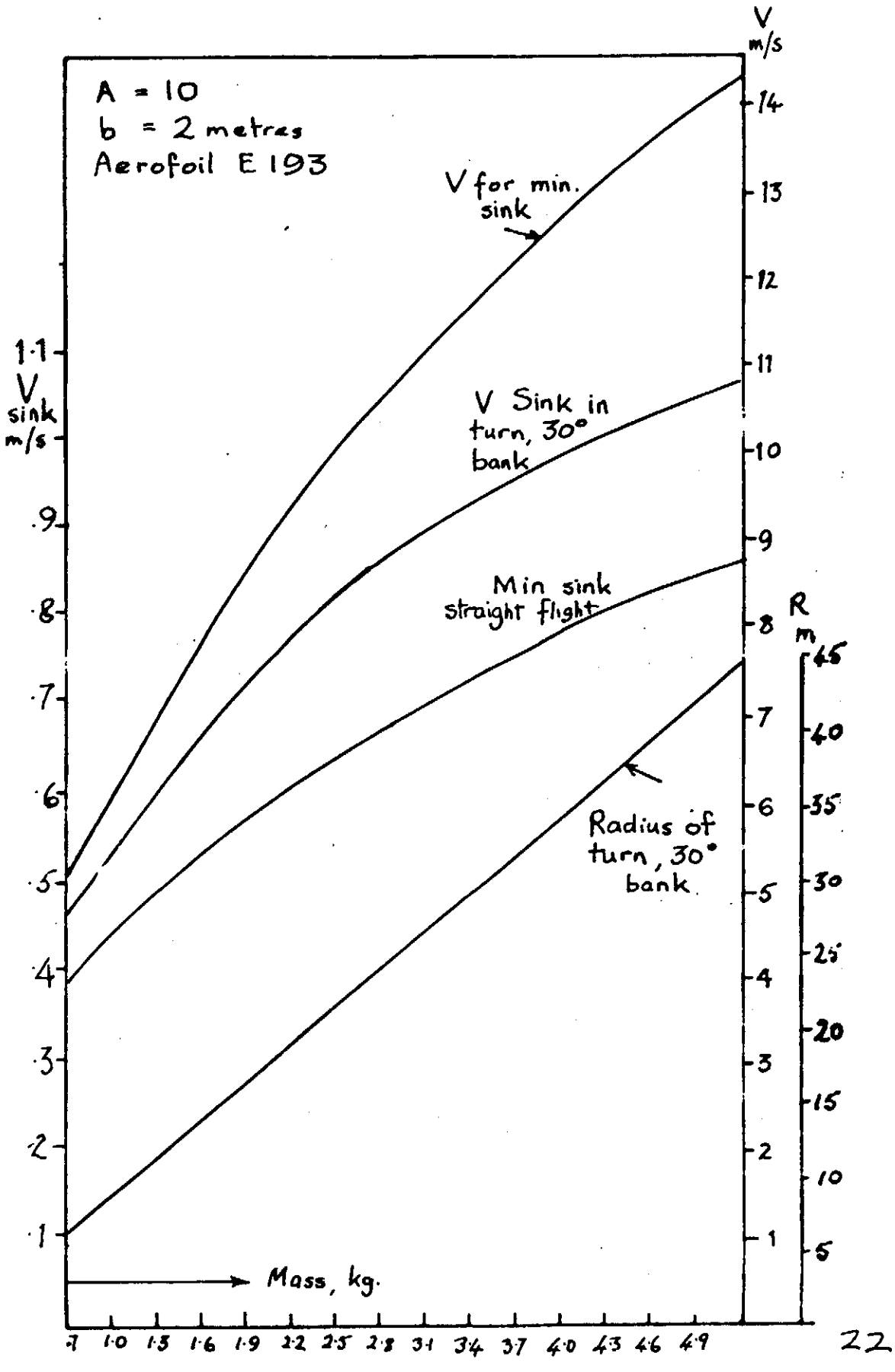

Figure 4. The effects of changing aspect ratio with two metre span sailplane of constant mass 1.3 kg.

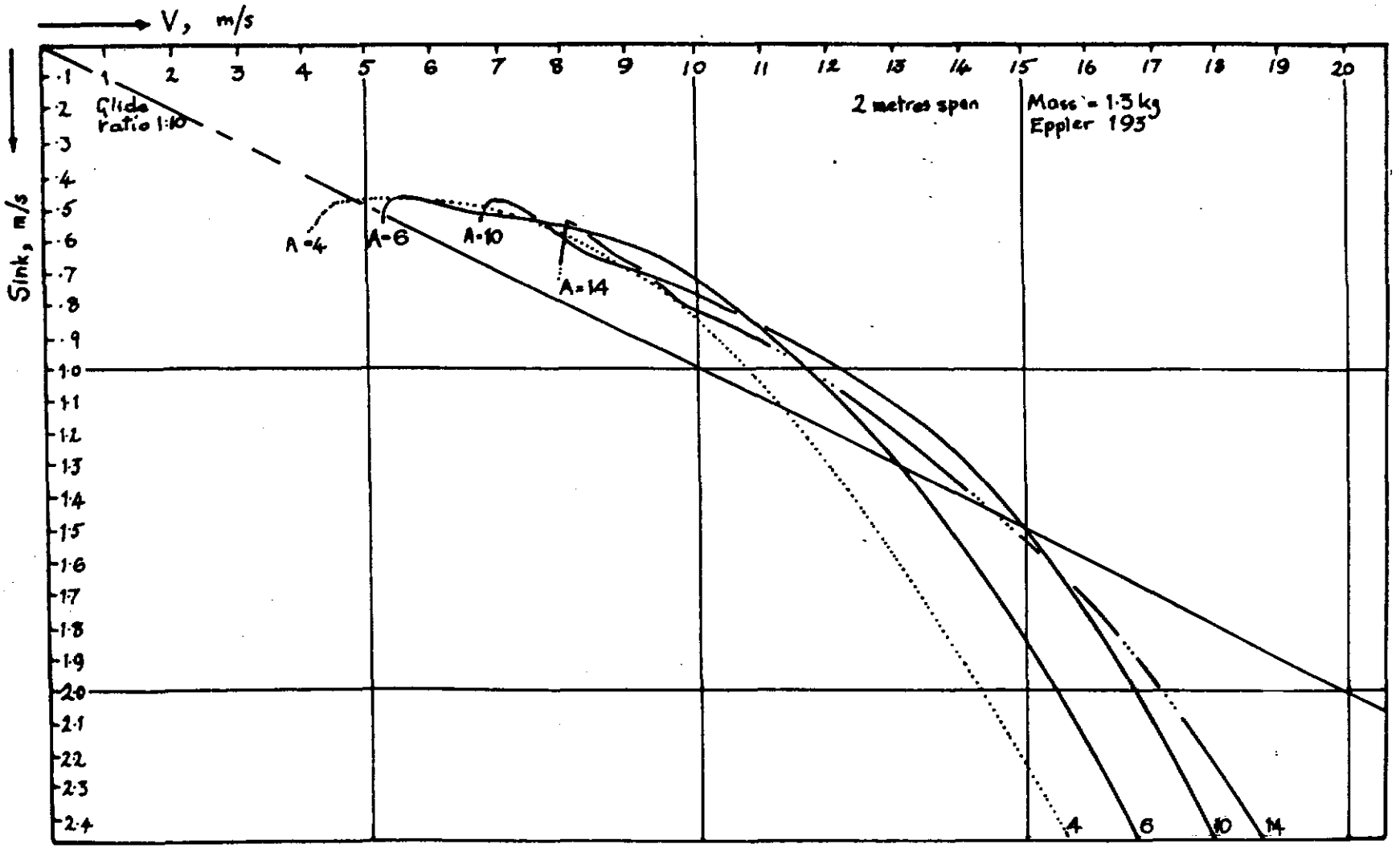

Figure 5 Changing the aspect ratio with ballast adjusted to keep wing loading constant

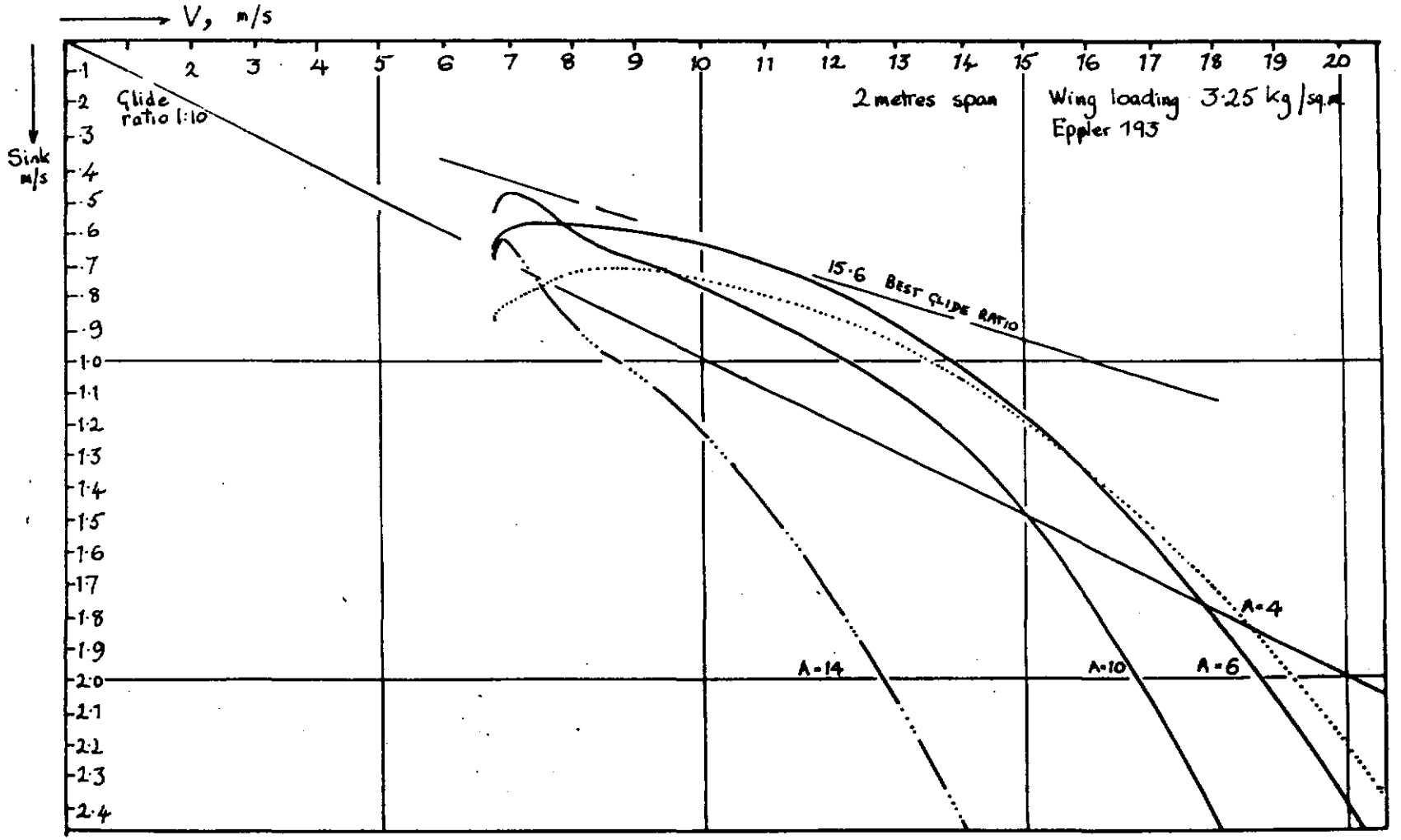

Figure 6. The effects of ballast and aspect ratio on high speed performance

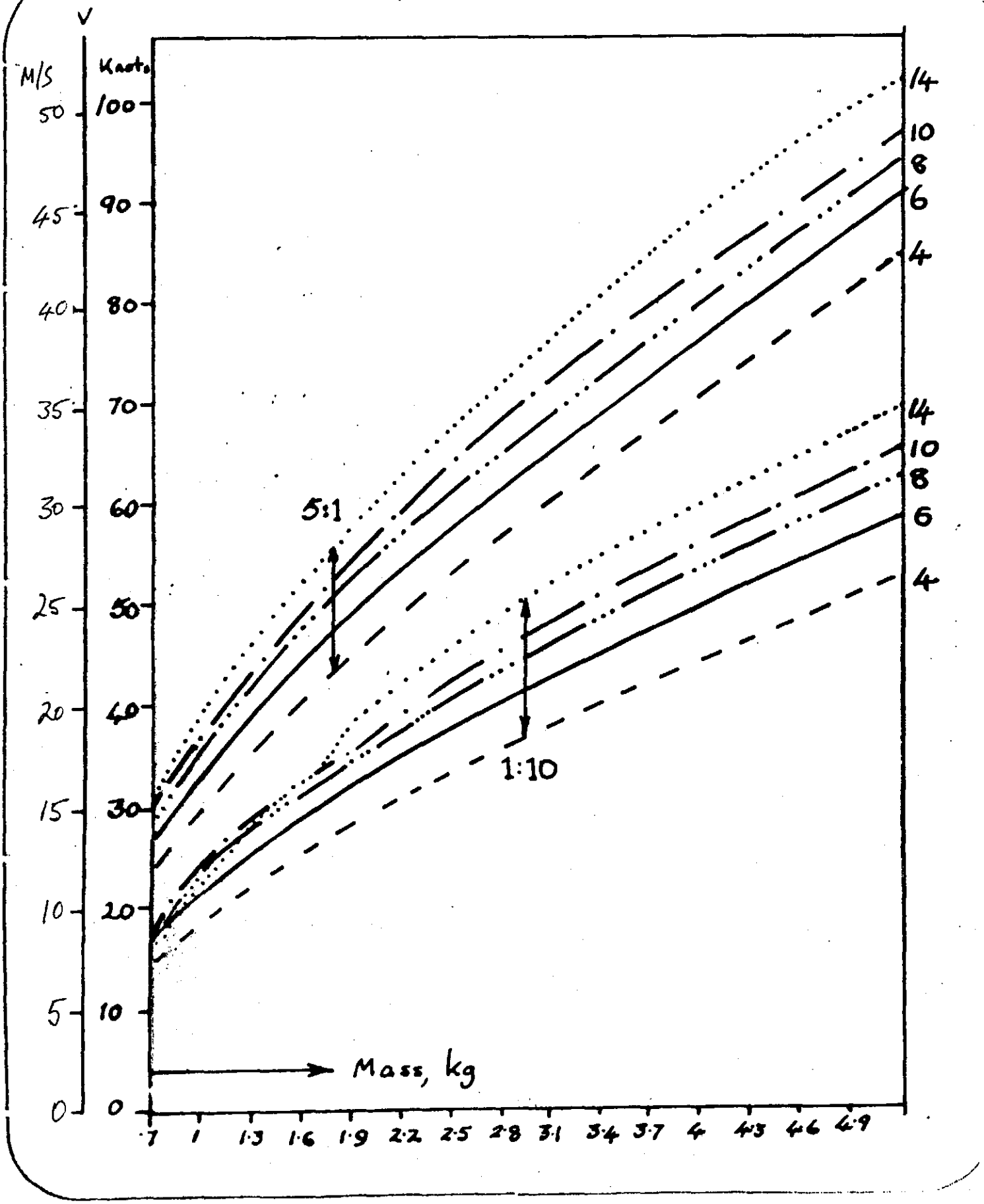

Figure 7. The polars of a two metre sailplane with aspect ratio 6, ballasted to various total flying weights. Compare with Figure 2.

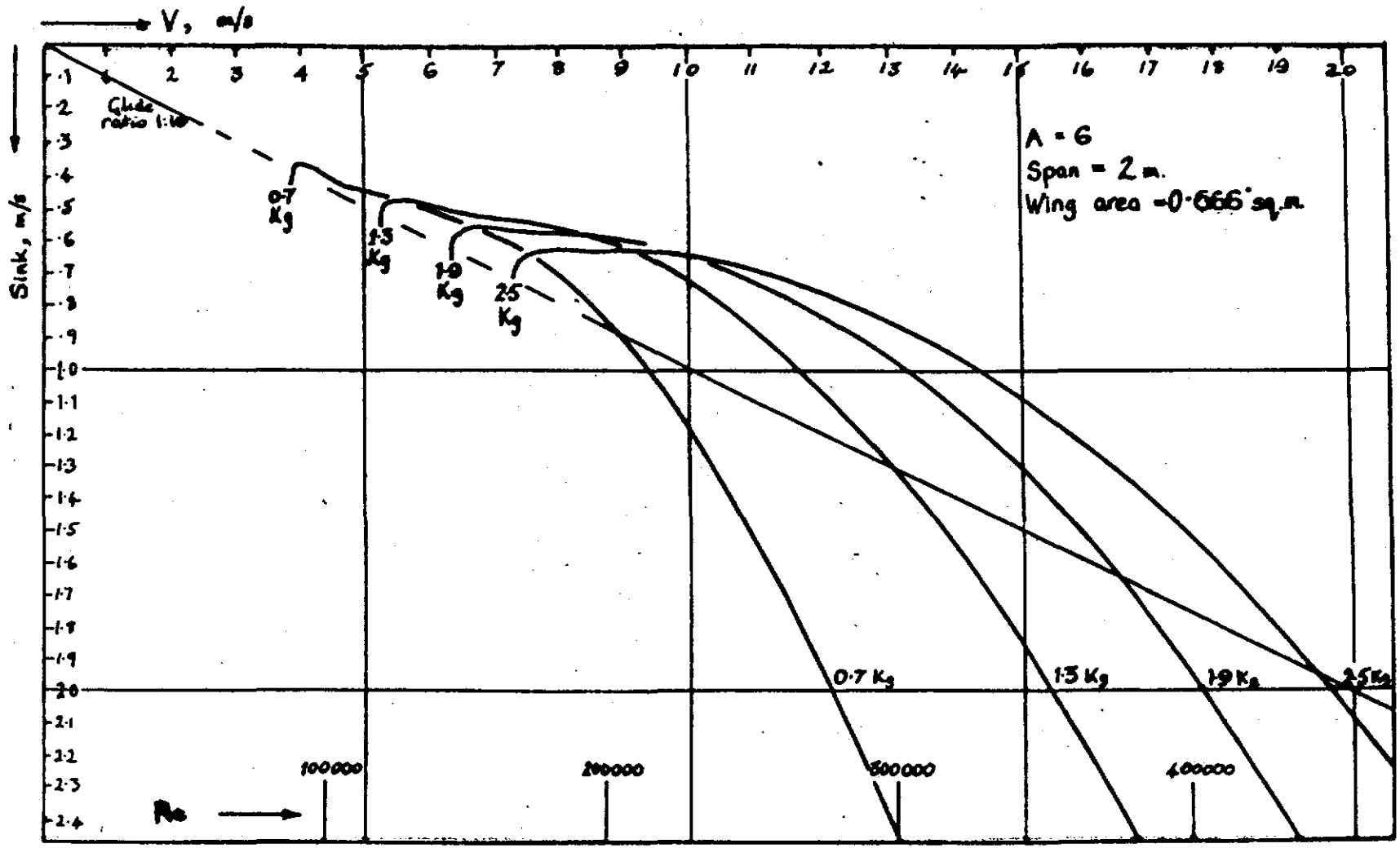

Figure 8. Polars for an idealised two metre wing without parasitic drag or other defects.

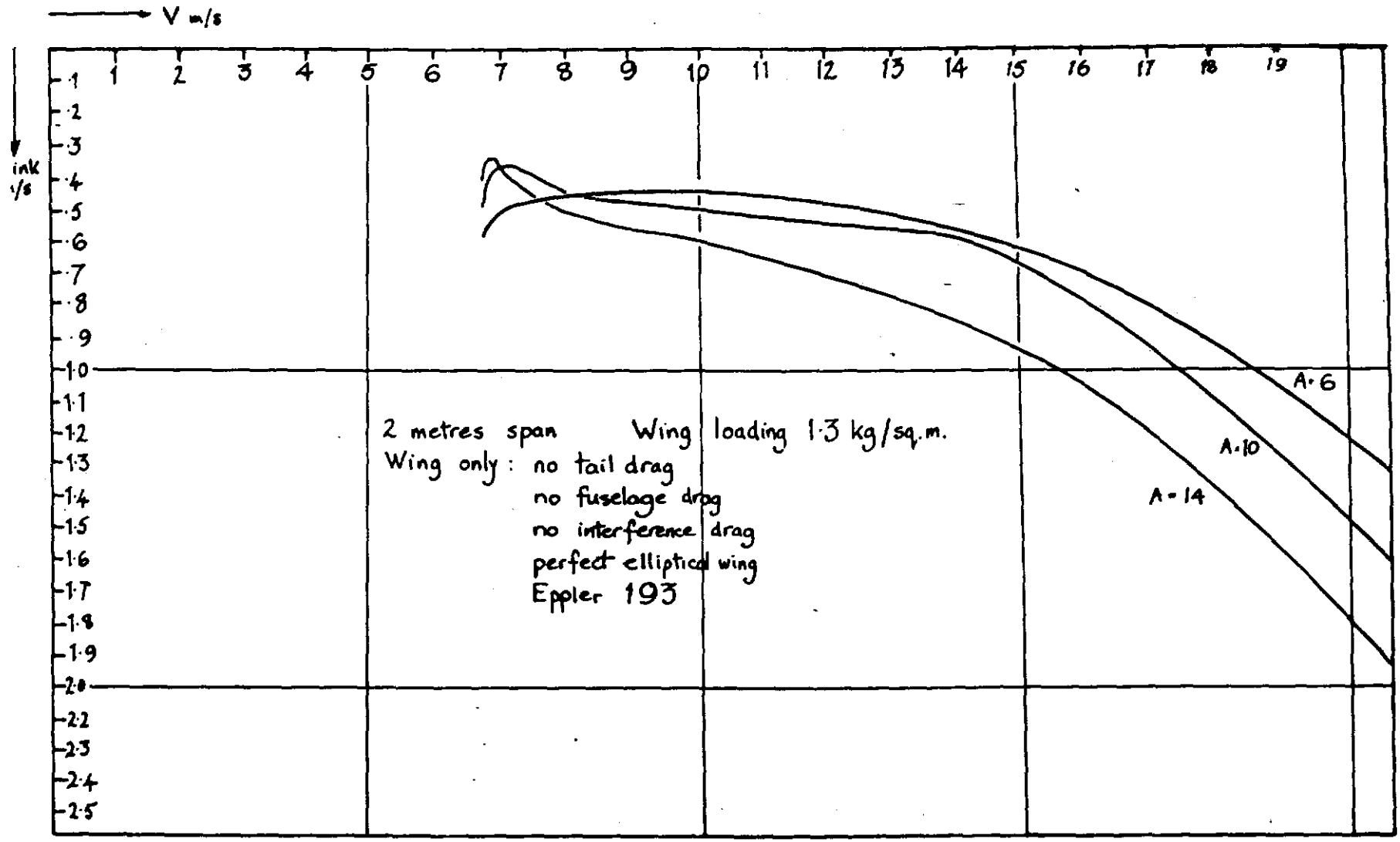

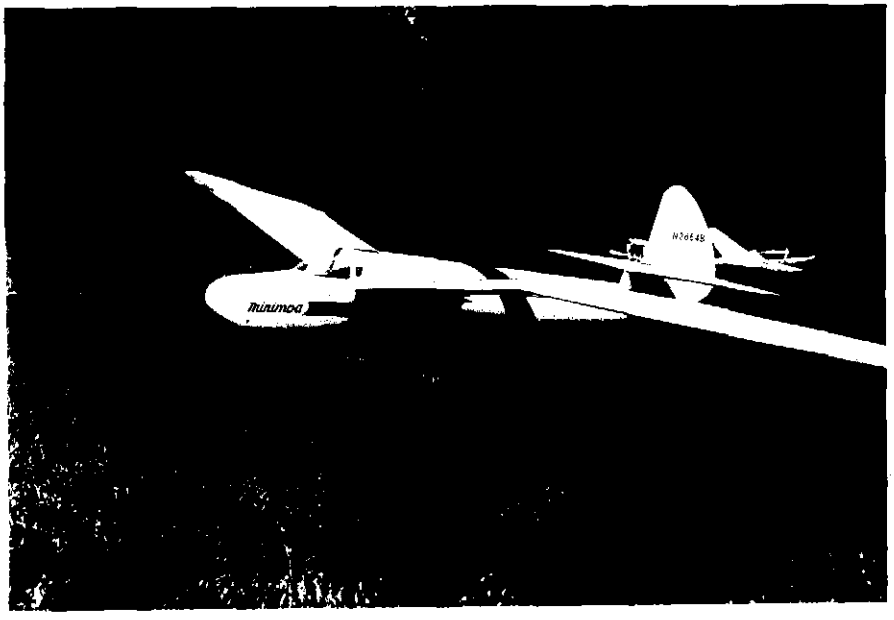
Minimoa

AIRFOIL DESIGN

This paper was entered by Michael Selig in a competition which was sponsored by the American Institute of Aeronautics and Astronautics. Although you might not think that a paper which referenced only model aircraft parameters was primary AIAA material, he won first place in the competition. Michael became skilled in using the Eppler airfoil design program during his undergraduate studies at the University of Illinois. Although a number of modelers have made use of the Eppler method to study and develop model airfoils, none that I am aware of, have gone to the depth that Michael explores in this paper. The conclusions that he has reached about the peculiarities of designing for models are important and unique. I hope that they point out useful directions for others who are studying airfoil development; and I'm sure that his designs and advice will help others to build superior sailplanes.

Michael is transferring his Aerospace studies to the graduate school at Princeton University this fall. He has been granted a position as a research assistant there where he will be working toward his Master's in Aerospace Engineering. He has also been sponsored by AIAA to present this paper at their national conference in Reno Nevada this fall.

THE DESIGN OF AIRFOILS AT LOW REYNOLDS NUMBERS

Presented at the 1984 AIAA Student Paper Conference

Sponsored by

Purdue University AIAA Student Chapter on March 23-24, 1984

By

MICHAEL S. SELIG

B. S. 1984
AERONAUTICAL AND ASTRONAUTICAL ENGINEERING
UNIVERSITY OF ILLINOIS AT URBANA-CHAMPAIGN

May 20, 1984

ABSTRACT

This report focuses on the design of airfoils at low Reynolds numbers ($100{,}000 < Re < 500{,}000$), specifically those applicable to radio-controlled model sailplanes. Two common types of airfoil lift and drag hysteresis are illustrated and explained in terms of the behavior of the upper-surface laminar separation bubble which is commonly present at these low Reynolds numbers. The theoretical section characteristics of several airfoils predicted by the Eppler computer program for the design and analysis of low-speed airfoils were compared with the recent data of Dieter Althaus. Good correlation was found between the type of hysteresis and the type of upper-surface pressure recovery. Also, the validity of the predicted section characteristics is discussed for this Reynolds number regime. From the comparisons, the desirable qualities of a low Reynolds number airfoil were determined. Based on these qualities, several airfoils for radio-controlled model sailplanes were subsequently designed and analyzed using the Eppler computer program.

INTRODUCTION

Increasing interest has been given to airfoils operating at chord Reynolds numbers (Rn) below 500,000. Radio-controlled (R/C) sailplanes, being the author's hobby and motivation for this study, fly in this Rn regime. Additional applications include the following: remotely piloted vehicles at low speeds or high altitudes, inboard sections of helicopter blades, human-powered aircraft, windmill blades, slats and flaps of high-lift, multi-element airfoils, struts on light aircraft, and turning vanes in air supply ducts.

This report focuses on the design of airfoils at low Reynolds numbers, specifically those applicable to R/C sailplanes. The approach taken in this report was to compare for several airfoils the theoretical section characteristics predicted by the Eppler computer program [1,2] with the experimental data of Althaus [3]. From these comparisons, the desirable qualities of a low Rn airfoil were determined. Based on these comparisons, several R/C sailplane airfoil were designed and analyzed using the Eppler computer program.

AIRFOILS AT LOW REYNOLDS NUMBERS

For airfoils at low Rn's, the phenomena of a laminar separation bubble and turbulent separation significantly increase the drag and decrease the lift which both contribute to low lift-to-drag ratios. Increasing the Rn will reduce the length of the laminar separation bubble and the extent of turbulent separation. Correspondingly, the lift-to-drag ratios increase. For the upper surface of the airfoil at

positive incidence, the boundary layer is laminar along the upper-forward surface of the airfoil. This laminar flow then separates upon entry into an adverse pressure gradient of sufficient magnitude, and then quickly undergoes transition to turbulent flow in the separated shear layer. Depending on the severity of the adverse pressure gradient, this separated turbulent boundary layer may or may not reattach to the airfoil's surface. The region of recirculating air enclosed by the laminar separation point and the turbulent reattachment point is called a laminar separation bubble. With reattachment, the turbulent boundary layer may then separate ahead of the trailing edge. For the lower surface at positive incidence, typically the boundary layer has little tendency to separate and commonly is entirely laminar. Figure 1 illustrates an airfoil with attached turbulent flow followed by turbulent separation on the upper surface and laminar flow on the lower surface.

If the Rn is low enough such that reattachment does not occur, increasing the Rn to some value, known as the critical Rn, causes reattachment of the turbulent boundary layer, which can be identified by a dramatic increase in the lift-to-drag ratio and a lift curve that is approximately linear with angle of attack, i.e. straight. Clearly, the possibility of both laminar and turbulent separation should be considered in the design of airfoils in this low Rn regime.

See Appendix I for a brief discussion of the Rn.

Hysteresis

As an airfoil is cycled through increasing angles of attack up to stall, the laminar separation point progresses forward. At some angle of attack, reattachment cannot occur, causing the laminar separation bubble to "burst." This bursting is manifested as a stall. Through decreasing angles of attack, the bubble, in general, does not behave in the same manner as for increasing angles of attack, thus accounting for the phenomenon of hysteresis shown in experimental lift and drag curves. Two common types of hysteresis will now be discussed.

Figure 2 illustrates the section characteristics of an airfoil that exhibits a common type of hysteresis which, for this discussion, will be called high-lift hysteresis. For this case, increasing the angle of attack causes the laminar separation point and turbulent reattachment point to both move forward toward the leading edge with the reattachment point moving forward at a slightly greater rate such that the bubble decreases in length. Eventually, a short bubble exists only on the leading edge of the airfoil. Further increasing the angle of attack causes this short leading edge bubble to "burst," resulting in a leading edge stall characterized by a sharp drop in lift. Upon decreasing the angle of attack, the leading edge bubble reattaches at an angle of attack lower than that of the stall for increasing angles of attack. The airfoil then behaves as it did for increasing angles of attack.

Figure 3 illustrates the section characteristics of an airfoil that exhibits another common type of hysteresis which, for this

discussion, will be called moderate-lift hysteresis. For this case, increasing the angle of attack causes the laminar separation point to progress forward, as it did for the case of high-lift hysteresis. In contrast to a airfoil with high-lift hysteresis the reattachment point moves backward toward the trailing edge forming a bubble of increasing length. As this happens, the lift curve begins to flatten out and the drag curve quickly increases. Up to this point, the process can be thought of as a soft trailing-edge stall. Increasing the angle of attack further unstalls the airfoil by causing the long bubble to collapse into a short bubble near the leading edge. This occurence can be identified by a sharp increase in the lift and a dramatic decrease in the drag. Increasing the angle of attack further causes the airfoil to fully stall. When decreasing the angle of attack, a sharp drop in lift is noted due to reformation of the long bubble at an angle of attack lower than that at which the sharp increase was noted with increasing angles of attack. For some airfoils, the contraction and reformation of the long bubble occur at the same angle of attack. Several popular Eppler airfoils exhibit this type of hysteresis as will be shown later.

Airfoils with moderate-lift hysteresis tend to show a high drag knee, that is, an increase in drag through the middle of the drag polar. Airfoils with high-lift hysteresis, on the other hand, do not exhibit a knee and generally have lower drag. Because of this, airfoils that exhibit high-lift hysteresis are favored for low Reynolds number applications.

INFLUENCING TRANSITION

The formation of the laminar separation bubble is due to the inability of the boundary layer to make a natural transition to turbulent flow before it attempts to negotiate an adverse pressure gradient of sufficient magnitude to cause laminar separation [4]. If it were possible at low Rn's for the boundary layer to make a transition before the adverse pressure gradient, the bubble and its drag could be eliminated. Several parameters which influence transition [5] are as follows:

1. Boundary-layer suction and blowing
2. Disturbances in the free-stream flow
3. Surface roughness
4. Pressure distribution (velocity distribution)

Although advantageous at low Rn's, boundary-layer suction and blowing [6] are of little practical value to the modeler because of the complexity of such a suction or blowing device and for this reason, will not be discussed here. Also, disturbances in the free-stream flow will not be discussed as they are not applicable in the case of R/C sailplanes.

Surface roughness has some application for low Rn airfoils. It is a common practice for free flight modelers to place a turbulator along the upper-forward surface. If effectively positioned, this turbulator artifically causes transition of the boundary layer to occur before the adverse pressure gradient and thereby eliminates the bubble and its drag.

4

The foremost disadvantage of the turbulator is its fixed position. While a turbulator may improve the overall performance of an airfoil at low Rn's, at higher values, the turbulator causes transition earlier than needed which results in more drag than necessary. Therefore, one can understand why this method of influencing transition is employed mostly on free-flight models that operate at very low Rn's about which there are minimal fluctuations.

The influence of the pressure distributions on transition will be discussed in a later section.

COMPARISONS OF THEORETICAL AND EXPERIMENTAL PERFORMANCE

The Eppler Computer Program

The theoretical section characteristics of several airfoils were computed using the Eppler computer program which has the following three capabilities: (1) potential flow design, (2) potential flow analysis, and (3) boundary-layer analysis. For the design method, the potential flow velocity distribution about an airfoil is specified. From this, the airfoil contour is determined by conformal mapping. In the analysis method, the velocity distribution for a given airfoil is determined by a panel method. To compute the section characteristics, the boundary-layer routines of the program incorporate an empirical transition criterion, and empirical skin friction, dissipation, and shape factor laws.

For Rn's greater than those considered in this report, the theoretical section characteristics compare favorably with experimental

measurements. As will be shown, however, the program does not accurately predict the section characteristics of airfoils at low Rn's since it makes the assumption that if the flow undergoes laminar separation before transition, the flow quickly reattaches as turbulent flow - the assumption of a short bubble. For higher Rn's, corresponding to those in the full-size sailplane regime, this quick reattachment is characteristic of the flow; but, for lower Rn's, this assumption is not valid since the bubble can extend over 20-30% of the upper surface of an airfoil. If the program predicts a laminar separation bubble longer than 0.03c, this is listed in the output summary as a warning that the theoretical section characteristics may not be indicative of the actual section characteristics. As one might expect, this warning commonly appears for airfoils analyzed at low Rn's.

The limitations of the program should be realized. Due to the incorporation of the short-bubble assumption, the present version of the program does not account for the additional $\hat{drag}$ bubble. If the program predicts turbulent separation, a small approximate drag penalty is added. Also, the program includes a correction for the pitching-moment and lift coefficients due to turbulent separation; however, it does not include a correction for a bubble. Despite this latter exclusion, the theoretical maximum lift coefficient is in most cases indicative of the experimental maximum lift coefficient. With these limitations in mind, the theoretical section characteristics should be cautiously interpreted in this low Rn regime. This interpretation is discussed in further detail in a later section.

6

Althaus' Experimental Work

Several problems are incountered in obtaining reliable experimental lift and drag measurements of an airfoil in the low Rn regime. First, the ambient turbulence, tunnel noise, model vibration, and model surface contaminations all cause transition to occur earlier on the test model than in actual use. This has profound consequences - namely, it produces a shorter bubble and hysteresis which is less pronounced than that found in actual use to such an extent that the airfoil appears better than it actually is. Second, accurately measuring the extremely small lift and drag forces presents many difficulties. These problems combined make it difficult to reliably conclude anything based on comparing the data of an airfoil tested in different wind tunnels.

In order that a self-consistent set of experimental data is considered, this paper will only examine data taken at a single facility. In particular, the author chose the data taken in 1980 by Althaus at the University of Stuttgart.

Comparisons

To represent a broad range of behavior, eleven airfoils were chosen for comparison of the theoretical and experimental section characteristics. For this report, however, only six of the eleven airfoils will be discussed. This is done without sacrafice to the clarity of the report or the conclusion which follow this section. These six airfoils may be grouped as follows:

1. Airfoils with high-lift hysteresis-
   FX63-137 and GOE801
2. Airfoils with moderate-lift hysteresis-
   E193 and E201
3. Airfoils without hysteresis-
   NACA0009 and FX60-100

The CLARK-Y, FX63-137, E392, GOE795, and FX60-100 were compared and are discussed in detail in reference [8].

For all airfoils compared, except those of Eppler, the original coordinates published in Althaus's book [3] had to be smoothed using a cubic spline smoothing program. This was done because the original coordinates caused irregularities or oscillations in the velocity distributions as shown in Figs. 4 and 5. The velocity distributions for the smoothed and unsmoothed FX60-100 are shown in Fig. 6. Since the boundary-layer routines are highly sensitive to such irregularities, the theoretical section characteristics computed from the original coordinates are meaningless. For most coordinates, the difference between the original and smoothed coordinates was less than 0.0004c. In the case of wind tunnel models, it is probably true that these coordinates are similarly smoothed in the construction of the models.

To compare the drag polars, each airfoil was analyzed at the test Rn's used by Althaus, at a Rn of 400,000, and in some cases at a Rn of 600,000. Analyzing each airfoil at a common Rn of 400,000 inables one to compare the theoretical data of one airfoil with another. In order to make comparisons of the lift vs. drag data, Althaus's experimental

data is co-plotted with the theoretical data. In some instances, Althaus's experimemtal data could not be co-plotted for a particular Rn because of the limits of the drag coefficient axis, this is indicated by the words "NOT SHOWN" on the graph. Commonly, due to a high drag knee at the lower test Rn's of Althaus ($60{,}000 < Rn < 100{,}000$), only a few experimental data points could be co-plotted at the high- and low-lift ends of the drag polar. In these cases, only those data points at the low-lift end were co-plotted. Also, Althaus' experimental lift curves are shown to illustrate the lift hysteresis of the airfoil. A theoretical lift curve is co-plotted with the experimental lift curves to show, in some cases, discrepencies which will be discussed in a later section.

The airfoil velocity distributions were plotted for angles of attack relative to the zero-lift line in increments of one or two degrees. The increment that was used can be distinguished by the relative differences in spacing between two adjacent velocity distributions.

A Theoretical Boundary-Layer Summary Table is presented that should be used as a guide when evaluating the theoretical section characteristics. When a "*" appears it indicates that the program predicts a laminar separation bubble longer than 0.03c. For these cases, the predicted drag is most likely too low since the program does not account for the additional bubble drag. When a "0" appears it indicates that the predicted bubble is shorter than 0.03c. In these cases, agreement between the theoretical and experimental section characteristics should be expected. If the predicted bubble is shorter

than 0.03c and transition occurs before 0.05c, a "●" indicates this. Agreement, for these cases, generally is good. When a "-" appears it indicates separation without reattachment - a stall. The symbol "+" has been placed beside the angles of attack relative to the zero-lift line which are within the low-drag range of the drag polar.

Discussed next is the agreement or lack thereof between the theoretical and experimental section characteristics. Following this several conclusion are drawn.

Symbols are defined in Appendix II.

1. Airfoils with high-lift hysteresis. Airfoils in this group are the FX63-137 and GOE801, shown in Figs. 7-8 and 9-10. Agreement between the theoretical and experimental drag at a Rn of 200,000 is relatively good for both airfoils. This suggests that at this Rn, the bubble is short. For the FX63-137 at Rn's greater than critical Rn near 85,000, the theoretical and experimental lift curves are in poor agreement. In contrast, for the GOE801 at Rn's greater than critical, the lift curves are in fairly good agreement. These two airfoils differ greatly in the amounts of aft loading with, the FX63-137 having the larger amount. For these airfoils at a Rn of 400,000, the program does not predict a laminar separation bubble at high angles of attack within the low-drag range of the drag polar. Notice that these airfoils have a have a convex velocity distribution recovery. This is in contrast to the next group of airfoils.

2. Airfoils with moderate-lift hysteresis. Airfoils in this group are the E193 and E201, shown in Figs. 11-12 and 13-14. Again,

agreement between the theoretical and experimental drag is good at a Rn of 200,000. At a Rn of 100,000 which is above the critical value of 60,000, these airfoils show a high drag knee between the lift coefficients of 0.5 and 1.0, which suggests the presence of an attached bubble of increasing length for increasing angles of attack. The theoretical and experimental lift curves are in fairly good agreement. For both airfoils at a Rn of 400,000, a laminar separation bubble is predicted on the upper surface for angles of attack within the low-drag range of the drag polar. These Eppler airfoils are similar in that the velocity distribution is characterized at a particular angle of attack by a constant velocity rooftop (shown in Fig. 11), followed by a slightly concave velocity recovery.

While not compared in this paper, when tested by T. J. Mueller and L. J. Pohlen [7] at the University of Notre Dame, the Miley M06-13-128 airfoil [4], which has a very concave velocity distribution with no aft loading, demonstrated this type of hysteresis for Rn's less than 150,000.

3. Airfoils without hysteresis. Airfoils in this group are the NACA0009 and FX60-100, shown in Figs. 15-16 and 17-18. These airfoils have a critical Rn below 60,000. Agreement for the NACA0009 is inconsistent; but, as expected for thin airfoil with no camber, it does have low drag. The FX60-100 has aft loading which does not result in steep adverse pressure gradients at the trailing edge like that present in the case of the FX63-137. Agreement between the lift curves for both airfoils is good. Like the first group of airfoils with high-lift hysteresis, these airfoils have convex recovery regions.

Appendix III presents the theoretical section characteristics and a discussion of several popular R/C sailplane airfoils.

LOW REYNOLDS NUMBER AIRFOIL DESIGN CONSIDERATIONS

At low Rn's it is desirable to have the flow transition early allowing for quick reattachment and thereby avoiding a long laminar separation bubble. As discussed previously, a turbulator effectively achieves this but results in a drag greater than necessary at higher Rn's. In designing airfoils specifically for R/C sailplanes operating in the Rn regime from 100,000 (C_{ℓ}=1.2) to 600,000 (C_{ℓ}=0.1), it is desirable on the upper surface to have transition occur early at low Rn's (high C_{ℓ}'s) and later at high Rn's (low C_{ℓ}'s). The AQUILA airfoil, presented in Appendix III, illustrates this movement of the theoretical upper surface transition point. This movement can only be achieved by the proper design of the velocity distribution along the upper-forward surface of the airfoil so that a laminar separation bubble is not predicted. Also, this type of design shows a theoretical drag which slowly increases with increasing lift coefficients rather than a theoretical drag which quickly increases like the designs of Eppler.

Here the comment should be made that while the Eppler airfoils are excellent in that they have low drag and wide drag polars at Rn's above around 200 000, they suffer from large laminar separation bubbles at Rn's below this. Because of this, the Eppler airfoils perform well on F3B type models but not so well on soaring type models which typically operate at Reynolds number less than 200,000. Not surprisingly with the increasing popularity of the Eppler sections,

12

there has been a trend to increase the chord lengths and wing loadings both of which increase the Reynolds number. Also, there seems to be a consensus among modelers that the Eppler sections must be flown "on step," i.e. fast. This too increases the Reynolds number.

From the comparisons, it is concluded that the type of velocity recovery employed should be linear to convex in order to prevent moderate-lift hysteresis.

As demonstrated in the comparisons, the theoretical and experimental lift and drag coefficients are in poor agreement for airfoils with large amounts of aft loading, or thick trailing edges which result in steep adverse pressure gradients on the upper surface near the trailing edge. Such a gradient likely leads to turbulent separation on the upper surface that extends further upstream than can be predicted by conventional boundary-layer methods. Examples of airfoils with large amounts of aft loading are the FX63-137 and E214 shown in Appendix III.

SOME NEW AIRFOILS DESIGNED FOR R/C SAILPLANES

Based on the previously discussed low Rn airfoil design considerations, several airfoils were designed by the author using the Eppler computer program - the same program that Eppler used to design the E193, E201, E392, etc..

The author's airfoil nomenclature is as follows: the first four digits are unique to each individual airfoil, larger numbers being later designs; the next three digits indicate the section thickness ratio times 1000; and the last two digits designate the year of design.

S2046-090-83, Figs. 19-20 - This 9% thick airfoil is based on the HQ2.5/9 shown in Appendix III. The velocity distributions of the HQ2.5/9 show that it pulls a suction peak (shown in Fig. 62) on the leading edge of the lower surface for angles of attack less than four degrees. This suction peak increases the bias toward laminar separation on the lower surface at low angles of attack. In redesigning the HQ2.5/9, emphasis was placed on mantaining the same section thickness and drag polar structure while mitagating the lower surface suction peak. The resulting airfoil is slightly thicker than the HQ2.5/9 along the lower-forward surface. The new airfoil should out-perform the HQ2.5/9.

S2091-101-83, Figs. 21-22 - This airfoil is based on the AQUILA airfoil. Because of the flat-bottom contour of the AQUILA airfoil, it performs poorly at low angles of attack such that an R/C sailplane utilizing this airfoil suffers from poor wind penetration as a result of high drag at low angles of attack. The new airfoil has an extended low-lift, low-drag range, which allows for better penetration, without comprising the high-lift capability of the AQUILA airfoil. This airfoil is a good example of convex recovery with no steep pressure gradients on the upper surface near the trailing edge. As indicated in the Theoretical Boundary-Layer Summary Table, this airfoil is expected to perform as predicted. The author highly recommends it for use on a precision/duration type R/C sailplane.

S3002-099-83, Figs. 23-24-25 - This airfoil was designed for used with flaps. For zero flap deflection at a Rn of 100,000, its performance at high lift coefficients compares with that of the 2046 and

2091. Notice that the aft loading does not lead to steep adverse pressure gradients near the trailing edge. Figure 25 clearly illustrates the advantage of using flaps - that being a wider operating range. At the low lift coefficients (near C_l=0.1, δ_f =-5 deg), the lower surface shows some separation; however, here the Rn of an R/C sailplane is much higher than 200 000. Therefore, this separation is of little concern for this application. At the high lift coefficients (near C_l= 1.1, δ_f =+5 deg), little separation is predicted. For lift coefficients less than 1.1 at positive five degrees flap deflection, both the lower and upper surfaces show separation at the low Rn's, and for this reason, excessive positive flap deflection at low lift coefficients and low Rn's is not desirable. Large positive flap deflections are suggested only for towing purposes, while small positive flap deflections are suggested for soaring in light lift.

S2027-145-83, Figs. 26-27 - This airfoil likely has a very soft stall as indicated by the smooth progression of the separation point on the upper surface. Close inspection of the airfoil reveals that both the upper and lower aft surface contours are concave rather than convex like the MB253515 and the thick low Reynolds number Eppler airfoils. This convexity should not be neglected in constructing a wing using this airfoil. Also, no attempt should be made to sharpen the leading edge, as such modification would lead to permature separation at the leading edge and lower the maximum lift.

S3010-103-84, Figs. 28-29 - In viewing the Theoretical Boundary Layer Summary Table, the S3010 is expected to operate efficiently at very low Reynolds numbers. Because of this, it is well suited for R/C

hand launch gliders.

S3021-095-84, Figs. 30-31 - At a glance, the semi-flat-bottomed S3021 looks very much like the famed E205 airfoil. The major difference between the two is at the high lift coefficients. Unlike the E205, at high lift coefficients, the upper surface transition point of the S3021 progresses gradually towards the leading edge with increasing angle of attack. The result is improved performance at high lift (since the laminar separation bubble is shorter) while the integrity of the Eppler section at low lift is mantained.

S4022-113-84, Figs. 32-33 - Since this airfoil has large amounts of aft loading, its theoretical lift and drag coefficients probably would not agree with experimental data. The actual performance of the S4022 is most likely similar to the FX63-137 with the exception that its drag polar is narrower by virtue of the S4022 being thinner than the FX63-137.

S4053-089-84, Figs. 34-35 - The author was motivated to design this airfoil at the request of Stan Watson who wished to have a "thinned out E193." The S4053 designed like an Eppler section will perform like one; it must be flown at Rn's near 200,000.

S4061-096-84, Figs. 36-37 - This airfoil would be an excellent choice for a cross-country sailplane where high lift-to-drag ratios are of most importance.

S4110-084-84, Figs. 38-39 - By smoothing the upper surface velocity distributions of the S2046 and combining it with the lower surface of the S2091, the S4110 results. Since the low drag range is so narrow like the HQ2.5/9, it is suggested that flaps be used on this

airfoil.

S4158-109-84, Figs. 40-41 - The unique S4158 must be considered strictly experimental. At the low lift and high Rn's, the flow on the upper surface is predicted to transition around 68% of the chord where it then incounters a steep adverse pressure gradient similar the a low drag stratford recovery. To promote transition at this point a turbulator could be place slightly ahead at 60%. At intermediate lift coefficients, this airfoil probably has a high drag knee and, therefore, should be flown at high Rn's to avoid this added drag.

S4180-098-84, Figs. 42-43 - The S4180 was designed primarily for soaring. Its ability to penetrate equals that of the AQUILA airfoil. According to the Theoretical Boundary-Layer Summary Table, this airfoil should out-perform the AQUILA in distance and duration.

S4233-136-84, Figs. 44-45 - This airfoil is a thinner, lower drag version of the S2027.

S4310-109-84 and S4320-094-84, Figs. 46-47 and 48-49 - Like the S3021 these airfoils are expected to be improvements over the Eppler sections.

As discussed, the selection of an airfoil should not be based solely on comparisons of the theoretical section characteristics predicted by the Eppler computer program. In addition, the velocity distributions, Theoretical Boundary-Layer Summary Table, and movement of the theoretical transition point should all be carefully examined before final selection.

CONCLUDING REMARKS

In designing airfoils for low Rn's, a convex recovery is favored over a concave recovery, thus preventing moderate-lift hysteresis and its associated lift and drag penalties. Large amounts of aft loading which result in steep adverse pressure gradients should be avoided, and the transition point should be designed to progress forward toward the leading edge with increasing angles of attack in order to minimize the areas of laminar and turbulent separation that are detrimental to airfoil performance. Some new airfoils have been designed with these considerations and should prove to be successful specifically in application to R/C sailplanes. To use the Eppler computer program for the design and analysis of low Rn airfoils, the limitations of the boundary-layer analysis, as discussed, must be considered when designing and choosing an airfoil for use in the R/C sailplane Rn regime.

ACKNOWLEDGEMENTS

The author expresses special thanks to Dr. Mark D. Maughmer, Professor of Aerospace Engineering at Pennsylvania State University (formerly of the University of Illinois), for making available the Eppler computer program. In addition, the author especially thanks him for their many discussions throughout the course of this work.

APPENDIX I

The Reynolds number is defined as

$$R_n = \frac{Vc}{\nu} \qquad (I-1)$$

where

c = wing chord
V = velocity
ν = kinematic viscosity

At standard sea level conditions

$$\nu = 1.5723 \times 10^{-4} \ ft^2/sec \qquad (I-2)$$

Thus

$$R_n = 6360 \ V c \ , \ sec/ft^2 \qquad (I-3)$$

The lift produced by the sailplane is given as

$$L = \tfrac{1}{2} \rho V^2 S C_L \qquad (I-4)$$

where ρ = air density
S = wing area
C_L = total aircraft lift coefficient

For steady, level flight the lift is equal to the weight.

$$W = L \qquad (I-5)$$

Substituting equation (I-5) into (I-4) gives

$$W = \tfrac{1}{2} \rho V^2 S C_L \qquad (I-6)$$

Solving for the velocity yields

$$V = \sqrt{\frac{2 \ W/S}{\rho \ C_L}} \qquad (I-7)$$

where W/S is termed the wing loading.

Using equation (I-7), (I-3) may be expressed as

$$R_n = 6360\sqrt{\frac{2W/S}{\rho C_L}}\, C \qquad (I\text{-}8)$$

From equation (I-8) it is seen that increasing the wing loading and the chord length increase the Reynolds number and increasing the aircraft lift coefficient decreases the Reynolds number. It should be pointed out the the aircraft lift coefficient is commonly less than the wing lift coefficient. And the wing lift coefficient is typically less than the airfoil lift coefficient.

APPENDIX II

Symbols

c	airfoil chord, ft
C_l	airfoil lift coefficient
C_d	airfoil drag coefficient
$C_{m\ c/4}$	airfoil pitching-moment coefficient at quarter-chord point
Rn	Reynolds number based on free-stream conditions and airfoil chord, for airfoil at standard sea level conditions, 6380VC where [VC]=[ft /sec]
t	airfoil thickness ratio
V	local velocity, ft/sec
V_∞	free-stream velocity, ft/sec
V/V_∞	nondimensional velocity
x	airfoil abscissa, ft
x/c	percent chord
α	angle of attack, degrees
α_o	zero-lift angle of attack relative to chord line - zero-lift line, degrees

Abbreviations

T.	boundary-layer transition point
S.	boundary-layer separation point
U.	upper surface of airfoil
L.	lower surface of airfoil

APPENDIX III

The following airfoils have been used on R/C sailplanes with much success. Of course, this success depends not only on the airfoil, but also, on the sailplane and ,most importantly, the skills of the pilot.

ANTARES, Figs. 50-51 - This airfoil, used on the Antares sailplane designed by Scott Christensen of Top Flite, is a "composite" airfoil. The upper surface is from the E193 and the lower surface from the E205. The resulting hybrid appears no different than the designs of Eppler.

AQUILA, Figs. 52-53 - This flat-bottom airfoil is used on the Airtronics Aquila R/C sailplane (now out-of-production) designed by Lee Renaud. Close inspection of the airfoil reveals that the upper-surface contour was borrowed from the E205. It is interesting to note that the upper-surface contour does not yield the same velocity distributions as the E205. The Theoretical Boundary-Layer Summary Table shows that at several angles of attack within the drag bucket, a laminar separation bubble is not predicted.

E205, E211, E214 and E374, Figs. 54-55, 56-57, 58-59, and 60-61 - These airfoils are designs of Eppler.

HQ2.5/9, Figs. 62-63 - Designed by Dr. Helmut Quabeck this airfoil was used by Ralf Decker of West Germany to win the 1983 R/C Soaring Championships held in York, England. By design, this airfoil is flown with flaps.

MB253515, Figs. 64-65 - This 15% thick ai foil, designed by Michael Bame, is thick enough to allow for use with powerful winches. Despite its thickness it has proven to be formidable airfoil in F3B

competition. The waviness of the velocity distribution is characteristic of airfoils drawn with french curves as this one was. Note the convex recovery region.

REFERENCES

1. Eppler, Richard and Somers, Dan M., "A Computer Program for the Design and Analysis of Low-Speed Airfoils," NASA TM-80210, August, 1980.

2. Eppler, Richard and Somers, Dan M., "Low Speed Airfoil Design and Analysis " Proceedings of the NASA Advanced Technology Airfoil Research Conference, NASA CP-2045, Part 1, March 1978.

3. Althaus, Dieter, Profilpolaren Fur Den Modellflug, Villingen-Schwennigen: Necker-Verlag, 1980.

4. Miley, S. J., "On the Design of Airfoils for Low Reynolds Numbers," Proceedings of the Second International Symposium on the Technology and Science of Low-Speed Motorless Flight, The Soaring Society of America, Inc. September 1974.

5. Schlichting, Herman, Boundary-Layer Theory, 7th ed. Trans. by J. Kestin, New York: McGraw-Hill, 1979.

6. Horstmann, K. H., Quast, A., "Reduction of Section Drag by Blowing Through Rows of Holes in Areas of Laminar Separation Bubbles," Technical Soaring, Vol. VII, No. 1, September 1981.

7. Mueller, T. J. and Pohlen, L. J., "Boundary Layer Characteristics of the Miley Airfoil at Low Reynolds Numbers," AIAA-83-1795, July 1983.

8. Selig, Michael S., "The Design of Airfoils at Low Reynolds Numbers," Paper presented at the AIAA 1984 Student Paper Conference held at Purdue University on March 23-24, 1984.

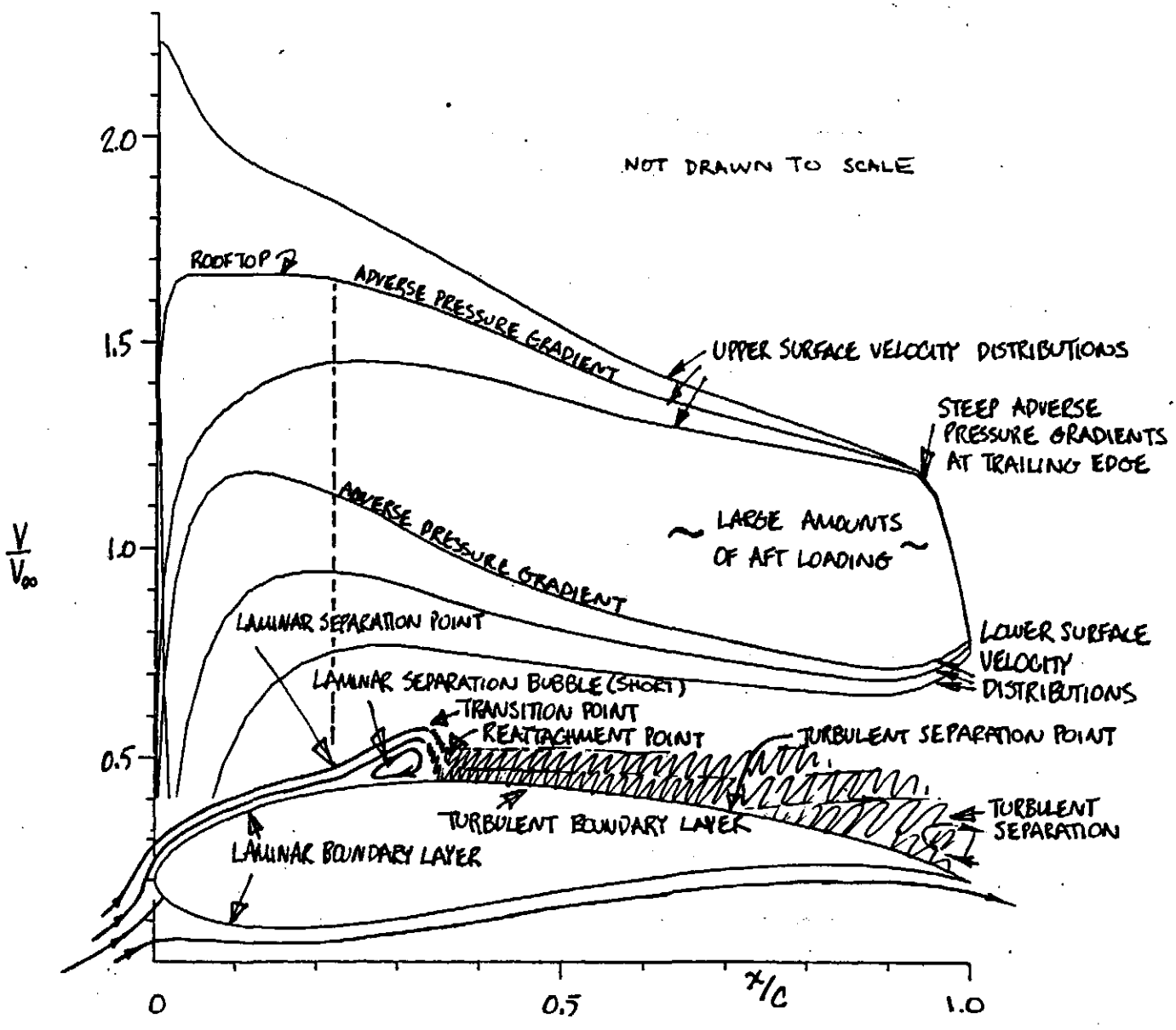

FIGURE 1.- ILLUSTRATION OF ATTACHED FLOW, FOLLOWED BY TURBULENT SEPARATION ON UPPER SURFACE WITH LAMINAR FLOW ON LOWER SURFACE.

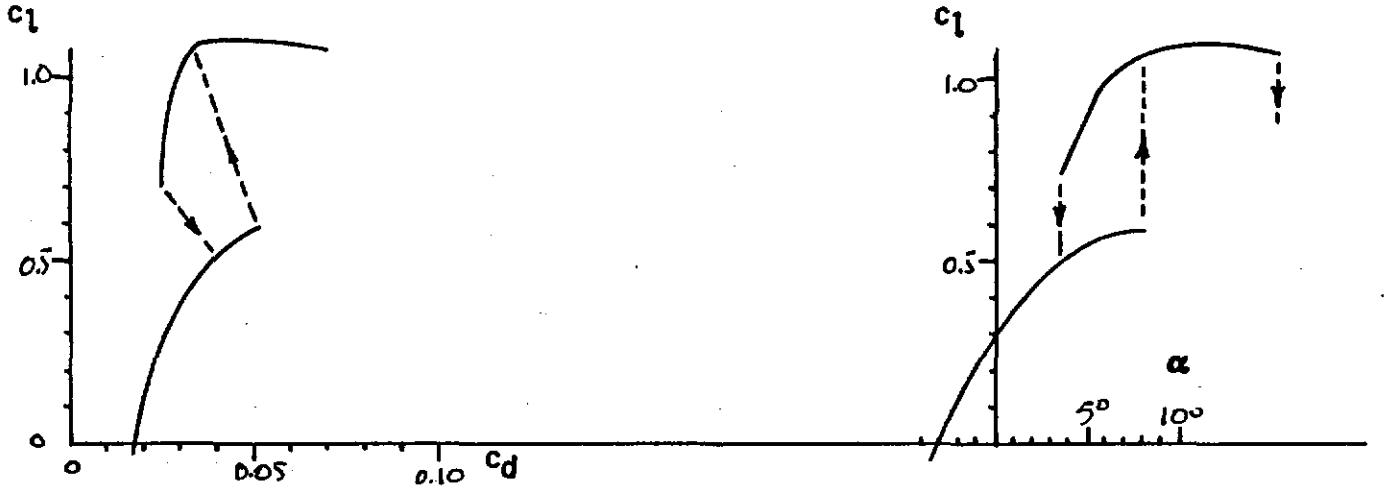

FIGURE 3.- TYPICAL SECTION CHARACTERISTICS OF AN AIRFOIL THAT EXHIBITS MODERATE-LIFT HYSTERSIS.

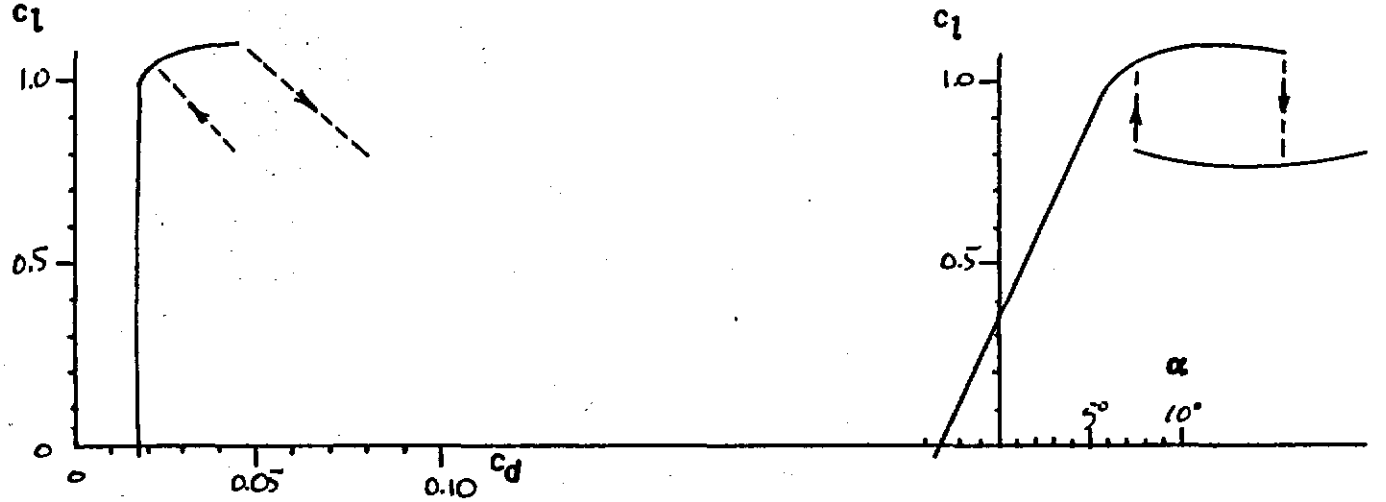

FIGURE 2.- TYPICAL SECTION CHARACTERISTICS OF AN AIRFOIL THAT EXHIBITS HIGH-LIFT HYSTERSIS.

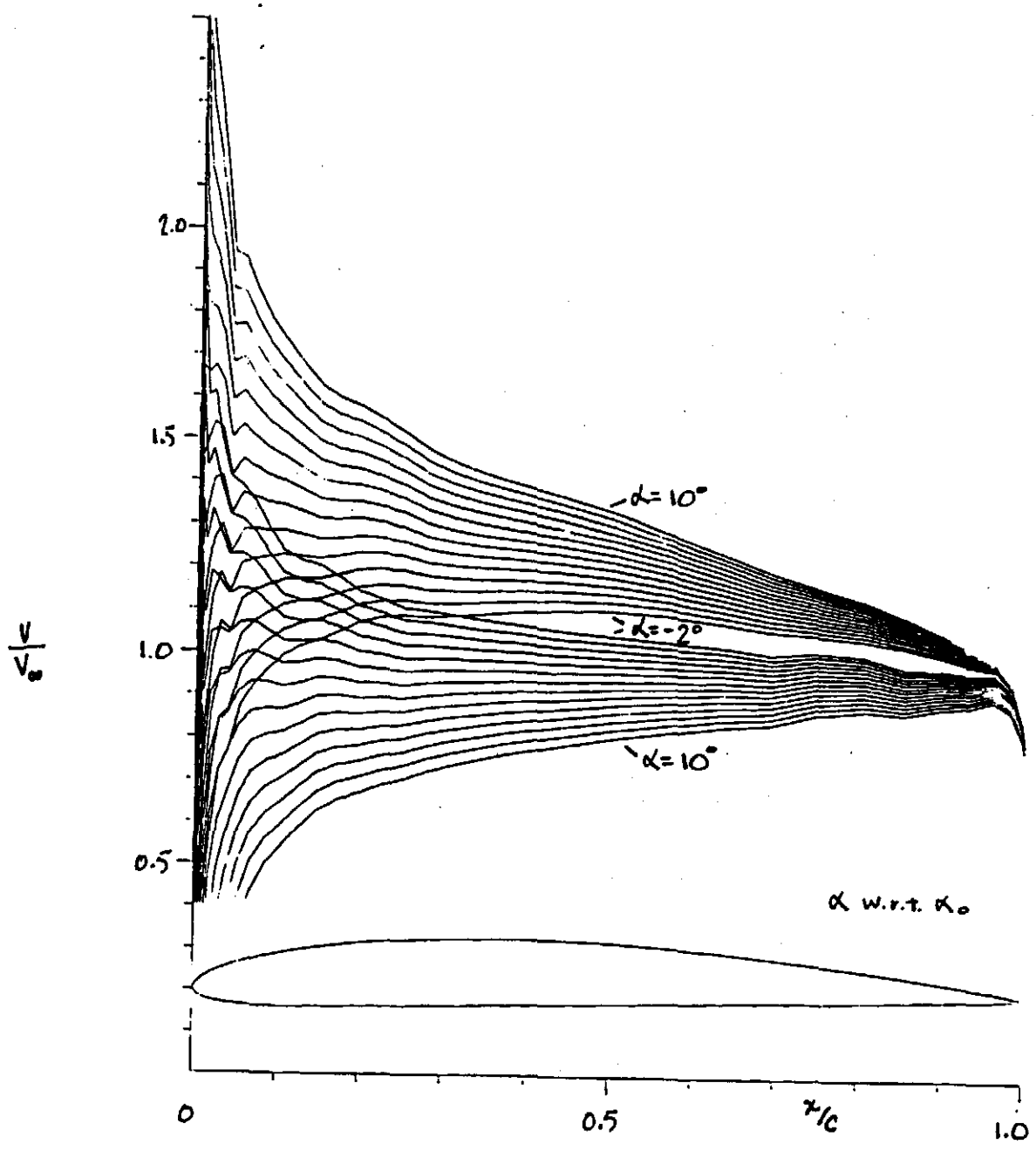

FIGURE 4.- VELOCITY DISTRIBUTIONS FOR THE ORIGINAL GOE 795 COORDINATES.

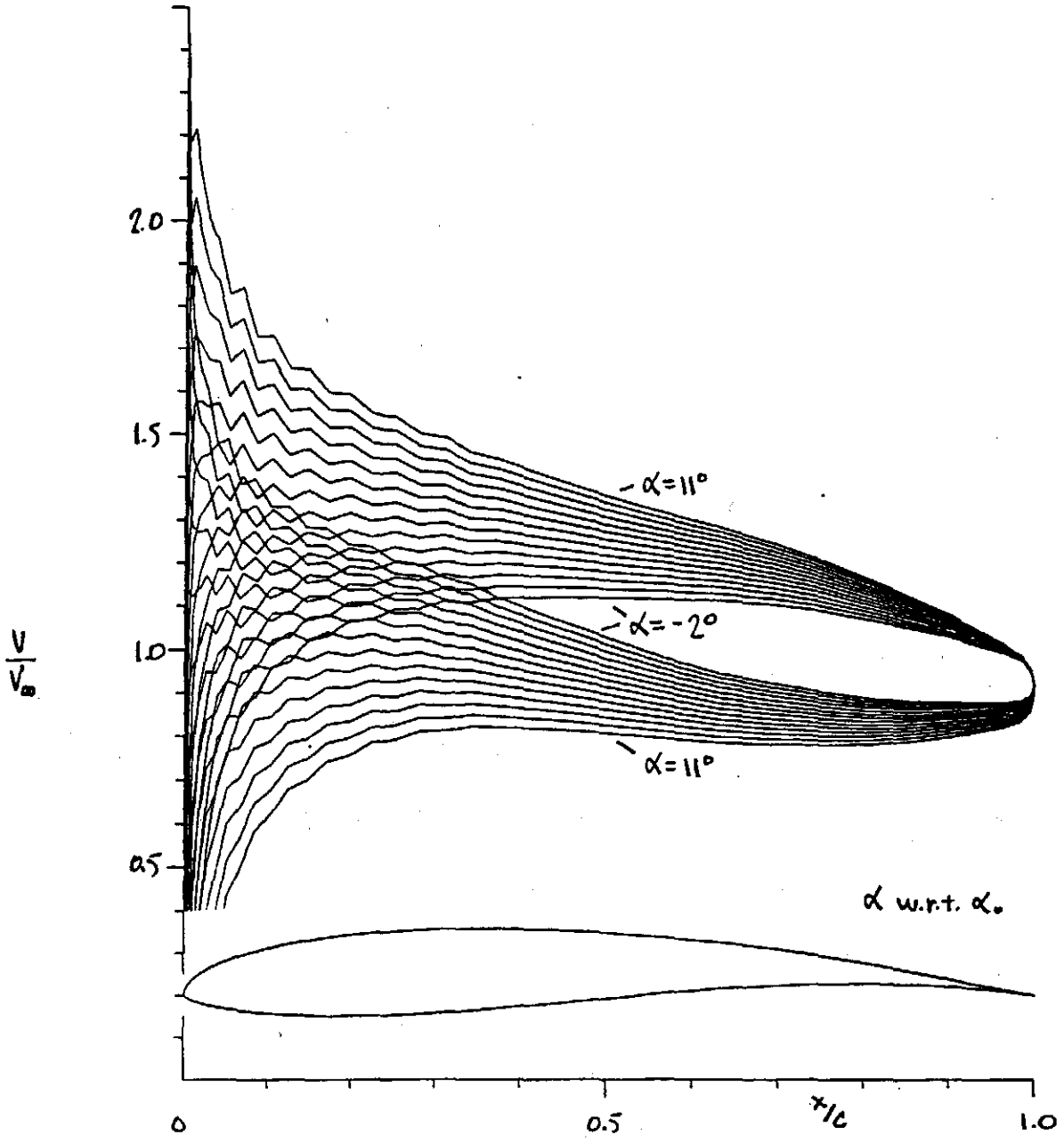

FIGURE 5.- VELOCITY DISTRIBUTIONS FOR THE ORIGINAL FX 60-100 COORDINATES.

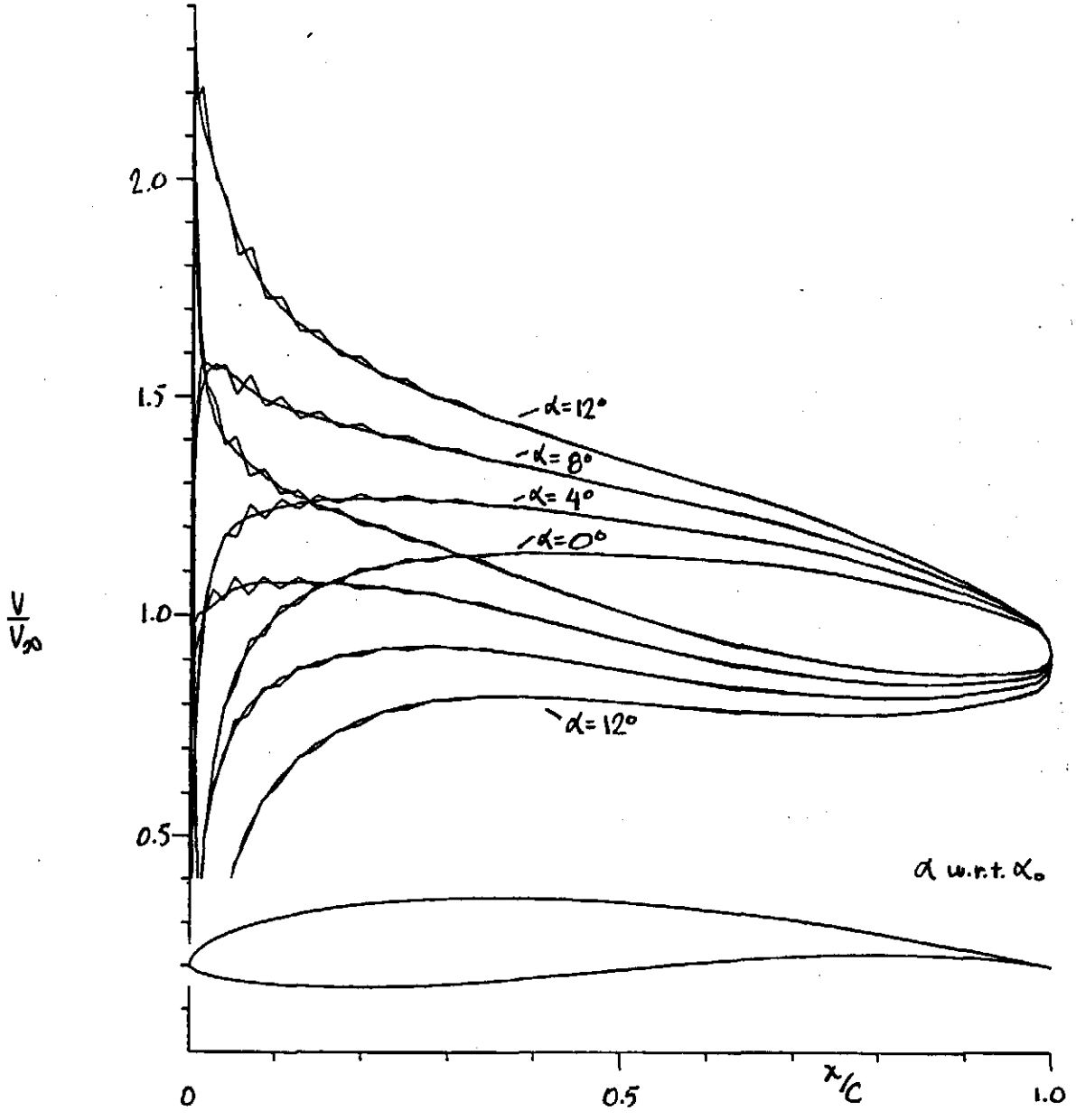

FIGURE 6.- VELOCITY DISTRIBUTIONS FOR THE ORIGINAL AND SMOOTHED FX 60-100 COORDINATES.

THEORETICAL BOUNDARY-LAYER SUMMARY TABLE										
AIRFOIL	*-LAMINAR SEPARATION BUBBLE WARNING O-NO SEPARATION BUBBLE WARNING ●-NO BUBBLE, TRANSITION BEFORE 0.05C --SEPARATION AT LEADING EDGE (STALL)									
CLARK-Y	+-ANGLE OF ATTACK WITHIN DRAG BUCKET									
ALPHA (deg)	REYNOLDS NUMBER									
	60000		100000		200000		400000			
	us	ls	us	ls	us	ls	us	ls	us	ls
-1	-	-	-	-	●	●	●	●		
0	-	-	●	●	●	●	●	●		
1	●	●	●	●	●	●	●	●		
+ 2	●	●	●	●	●	●	●	●		
+ 3	●	●	●	●	●	●	●	●		
+ 4	●	●	●	●	●	●	●	●		
+ 5	●	●	●	●	●	●	●	●		
+ 6	●	●	●	●	●	●	●	●		
+ 7	●	●	●	●	●	●	●	●		
+ 8	●	●	●	●	●	●	O	●		
+ 9	●	●	●	●	●	●	O	●		
+10	●	●	●	●	●	●	O	●		
11	●	●	●	●	●	●	●	●		
12	●	●	●	●	●	●	●	●		

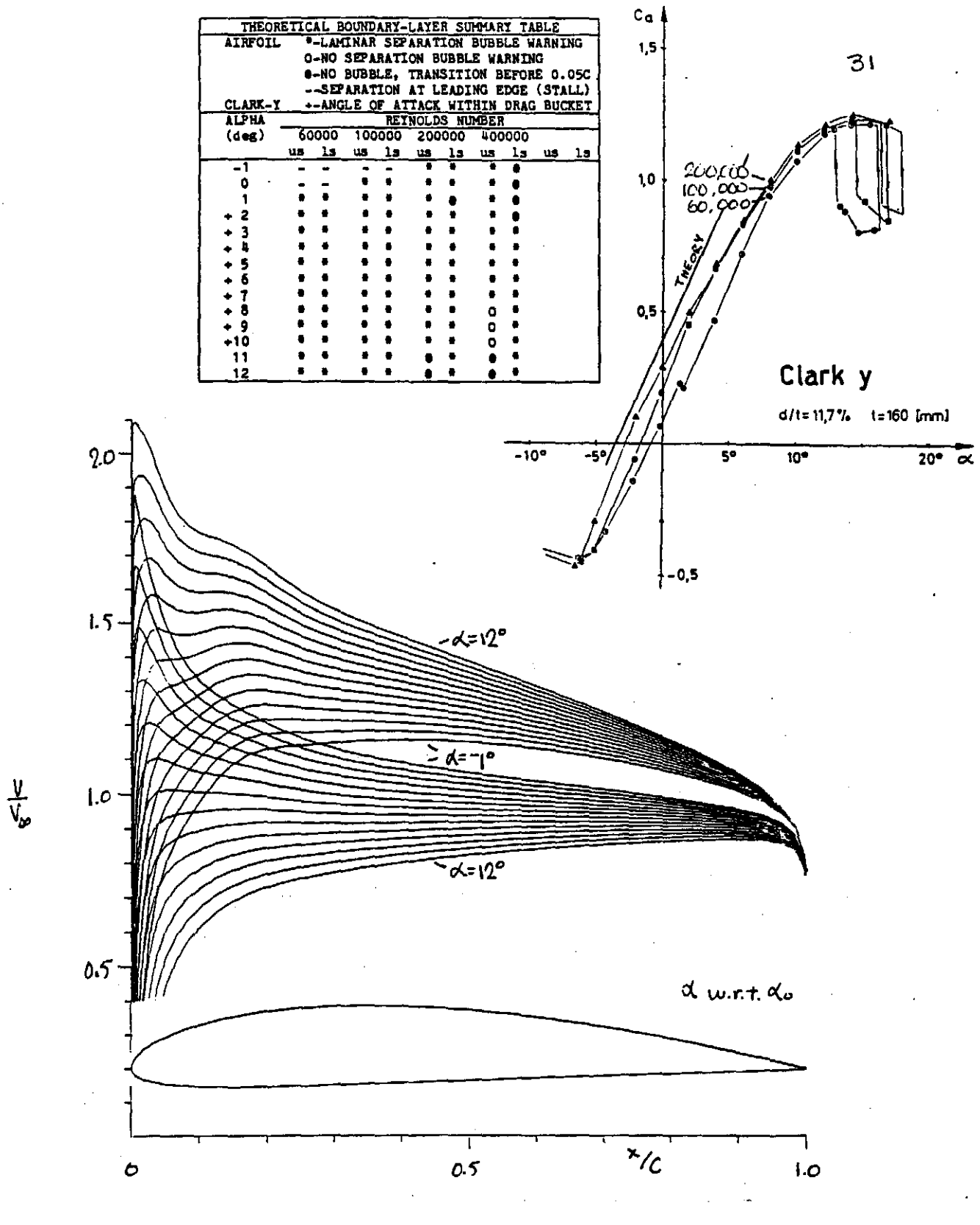

FIGURE 7. - VELOCITY DISTRIBUTIONS FOR THE CLARK-Y AIRFOIL.

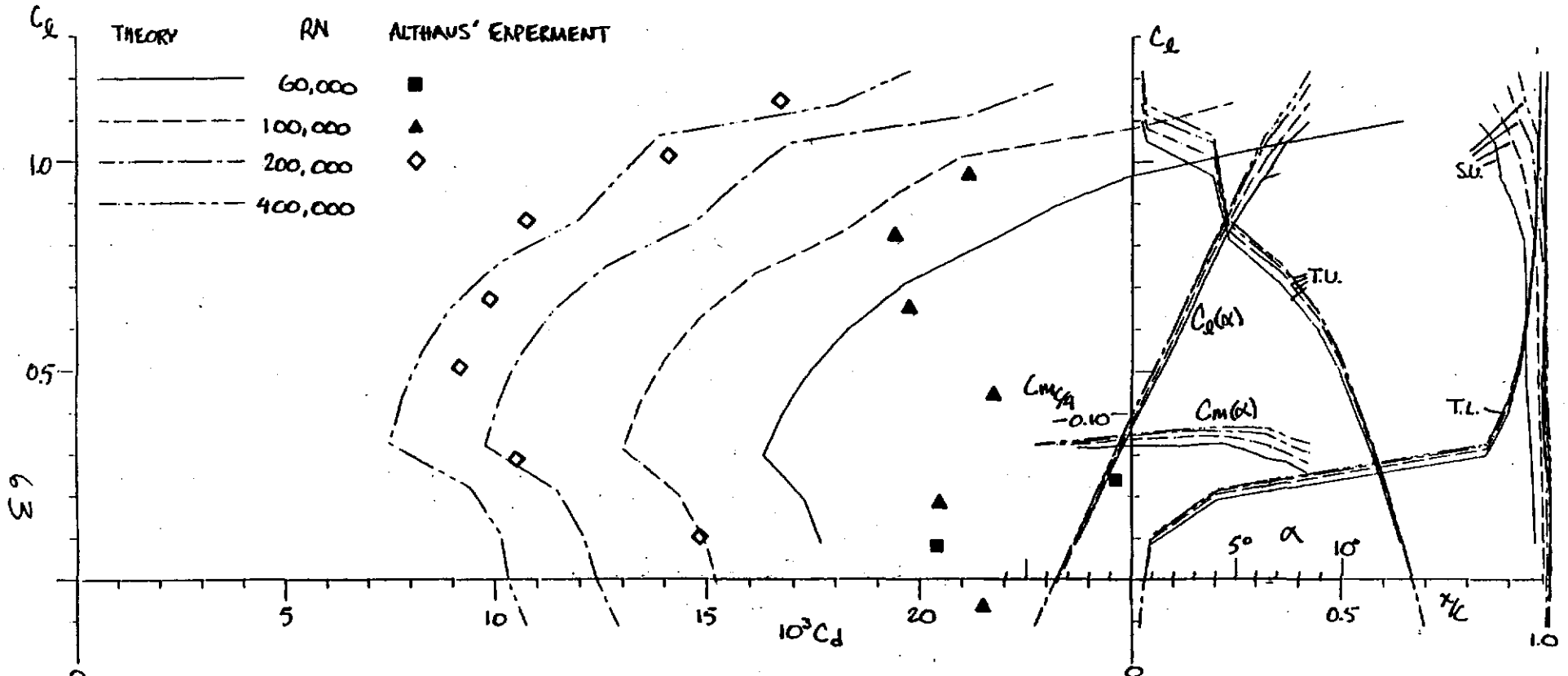

FIGURE 8.- COMPARISON OF THE THEORETICAL AND EXPERIMENTAL SECTION CHARACTERISTICS FOR THE CLARK-Y AIRFOIL.

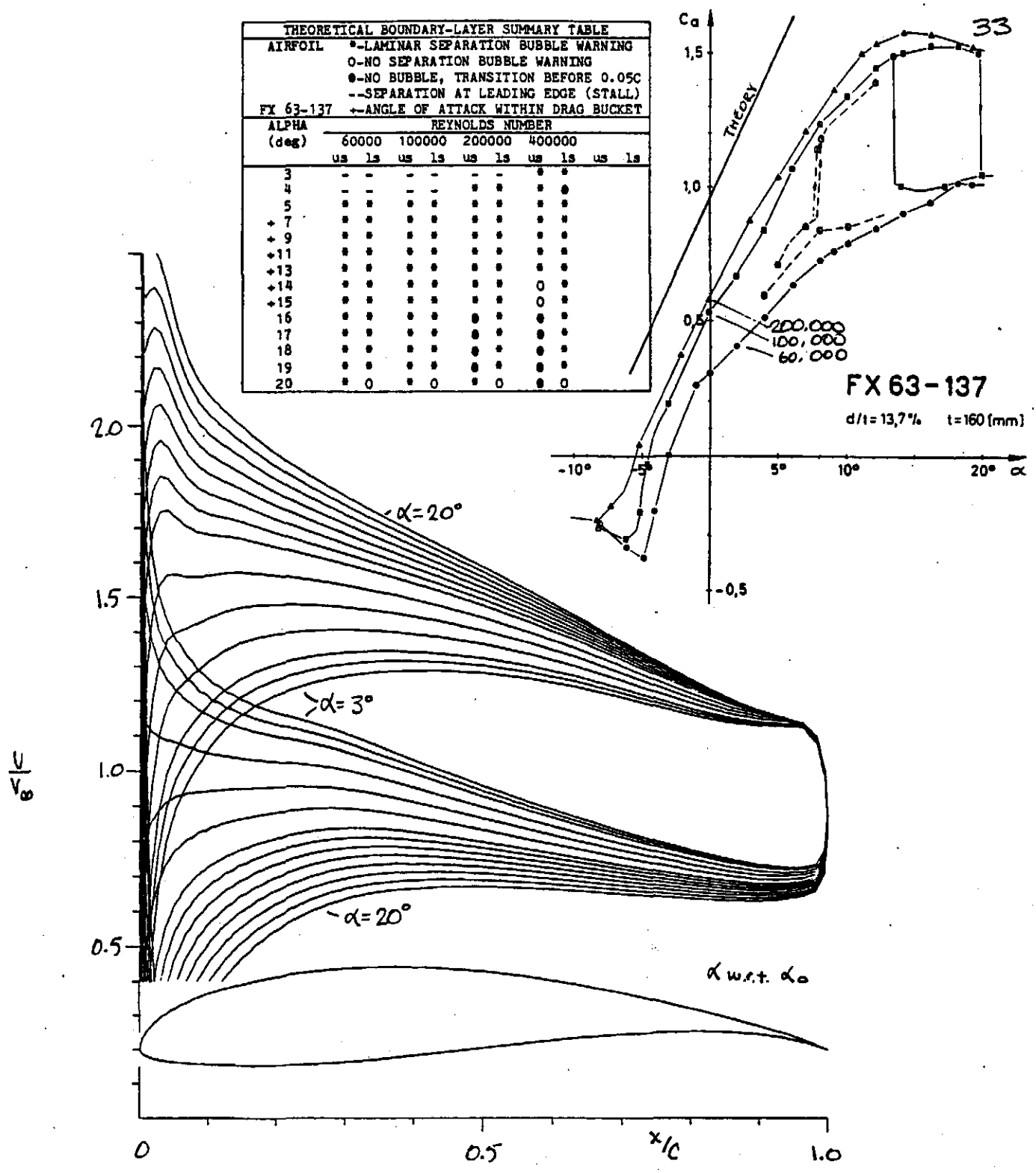

FIGURE 9.- VELOCITY DISTRIBUTIONS FOR THE FX 63-137 AIRFOIL.

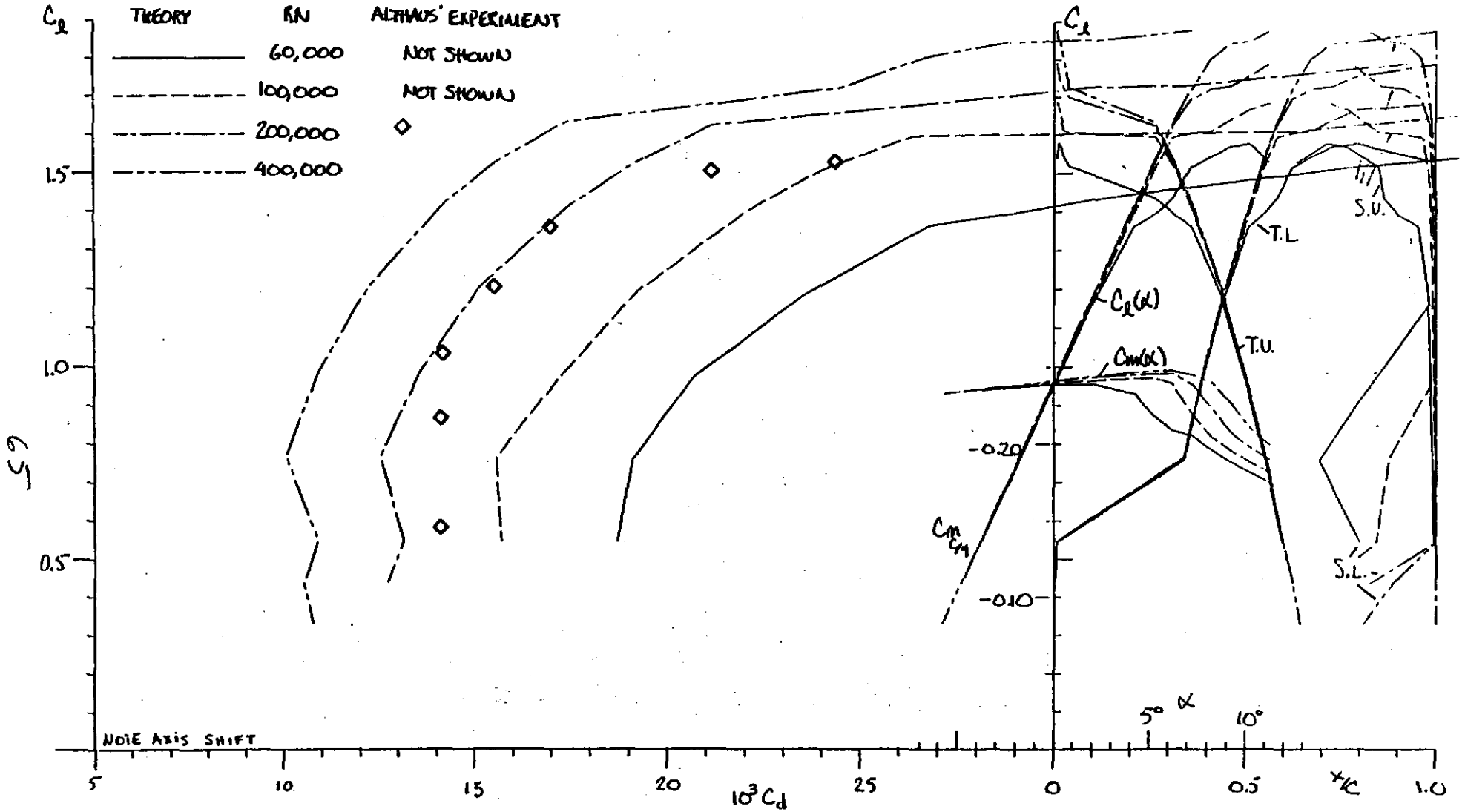

FIGURE 10. - COMPARISON OF THE THEORETICAL AND EXPERIMENTAL SECTION CHARACTERISTICS FOR THE FX 63-137 AIRFOIL.

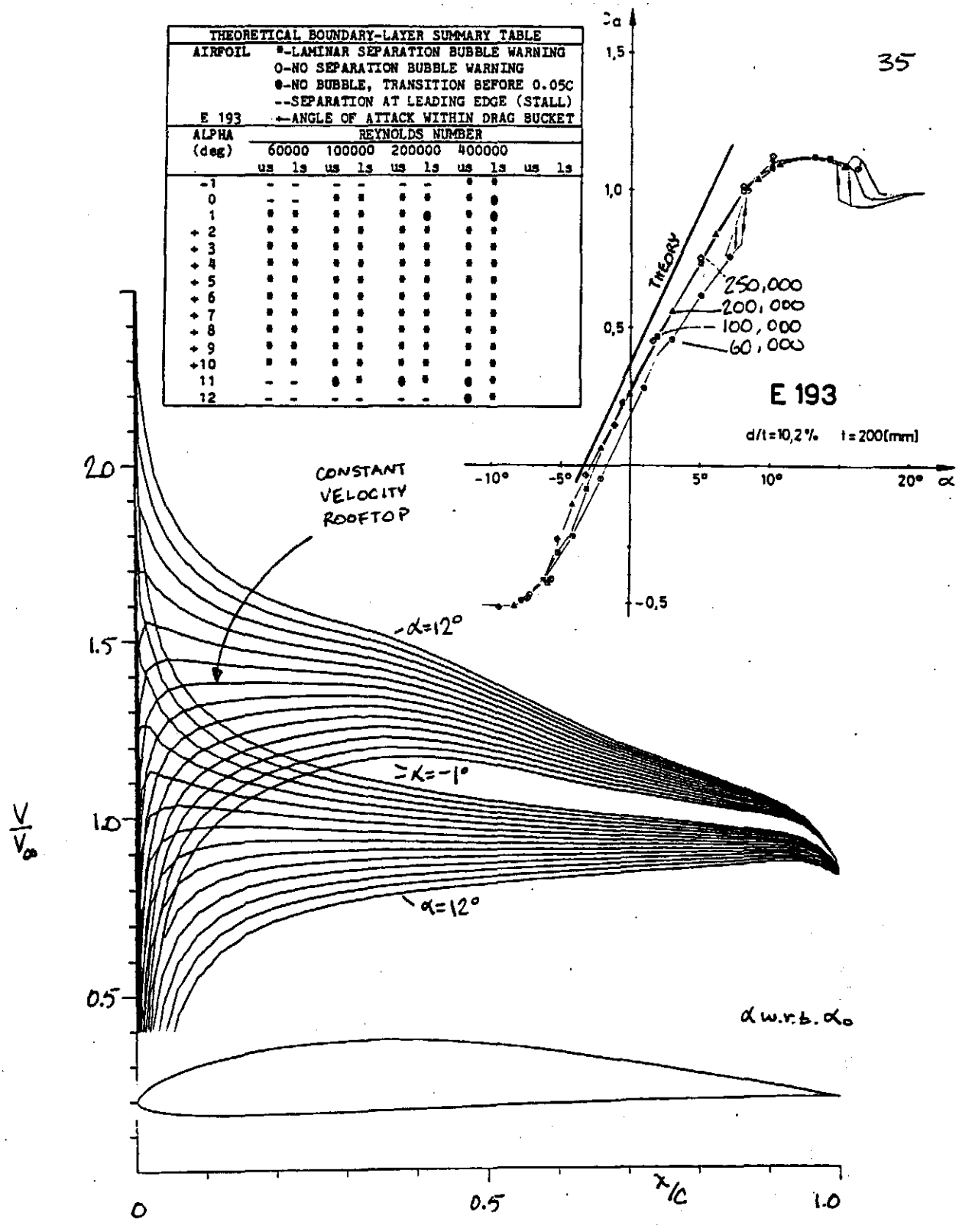

FIGURE 11.- VELOCITY DISTRIBUTIONS FOR THE E193 AIRFOIL.

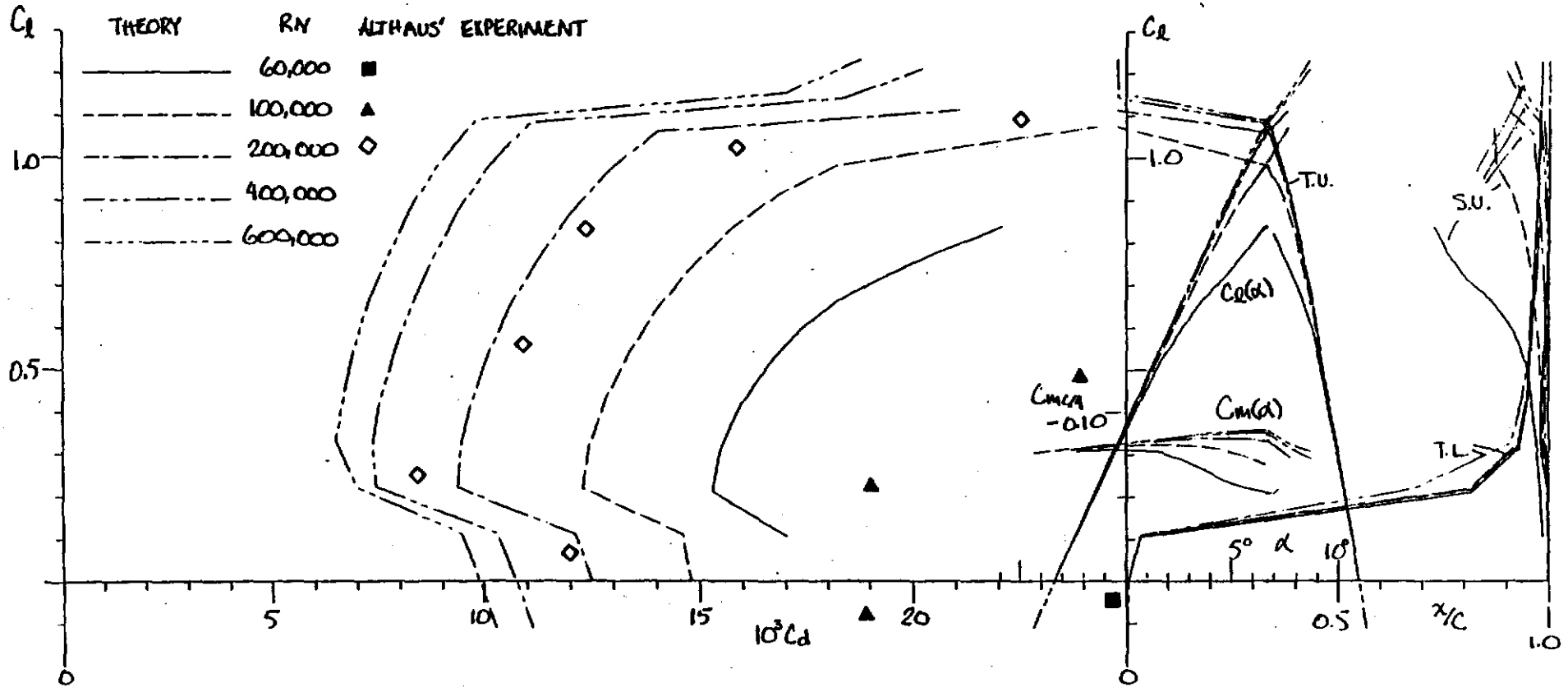

FIGURE 12.- COMPARISON OF THE THEORETICAL AND EXPERIMENTAL SECTION CHARACTERISTICS FOR THE E193 AIRFOIL.

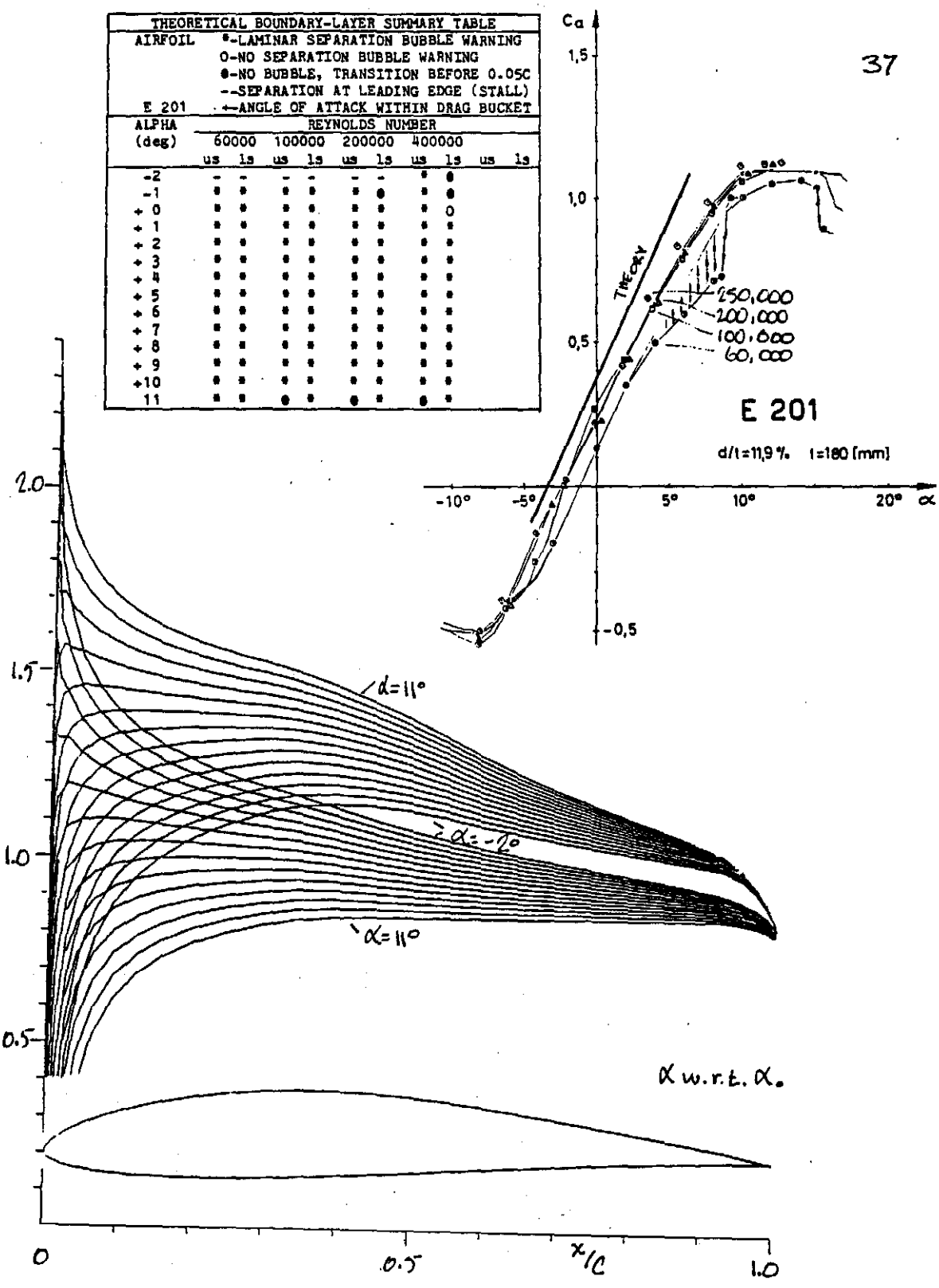

FIGURE 13.- VELOCITY DISTRIBUTIONS FOR THE E201 AIRFOIL.

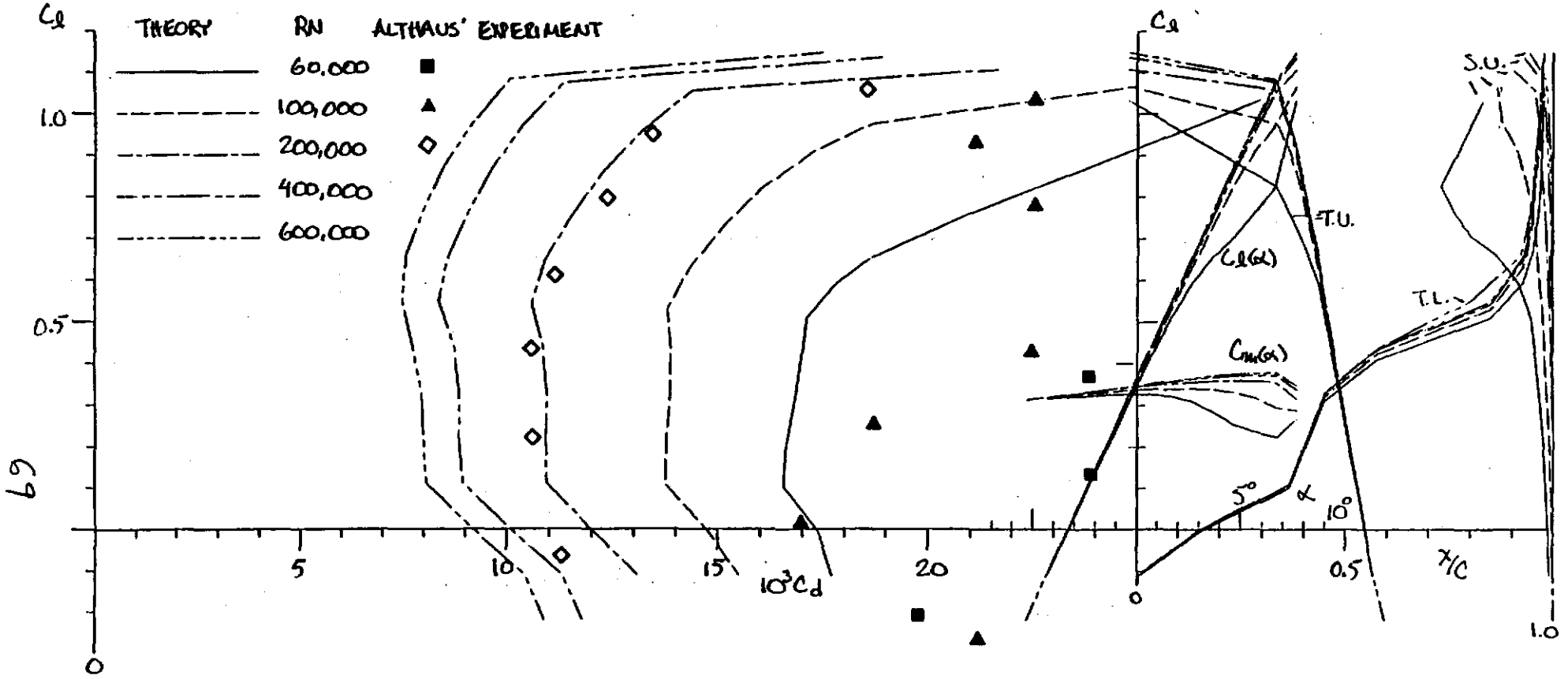

FIGURE 19.- COMPARISON OF THE THEORETICAL AND EXPERIMENTAL SECTION CHARACTERISTICS FOR THE E201 AIRFOIL.

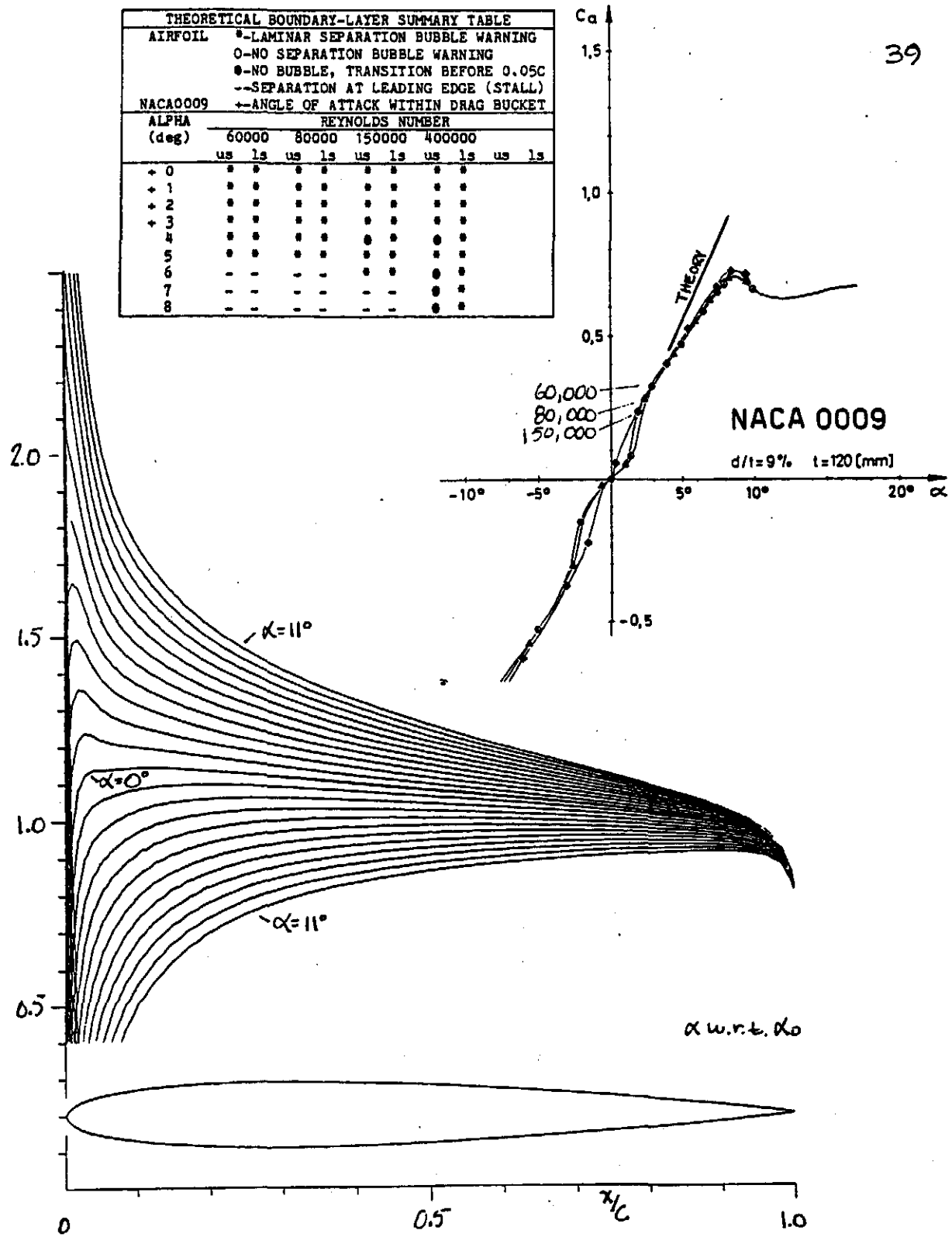

FIGURE 15 .- VELOCITY DISTRIBUTIONS FOR THE NACA 0009 AIRFOIL.

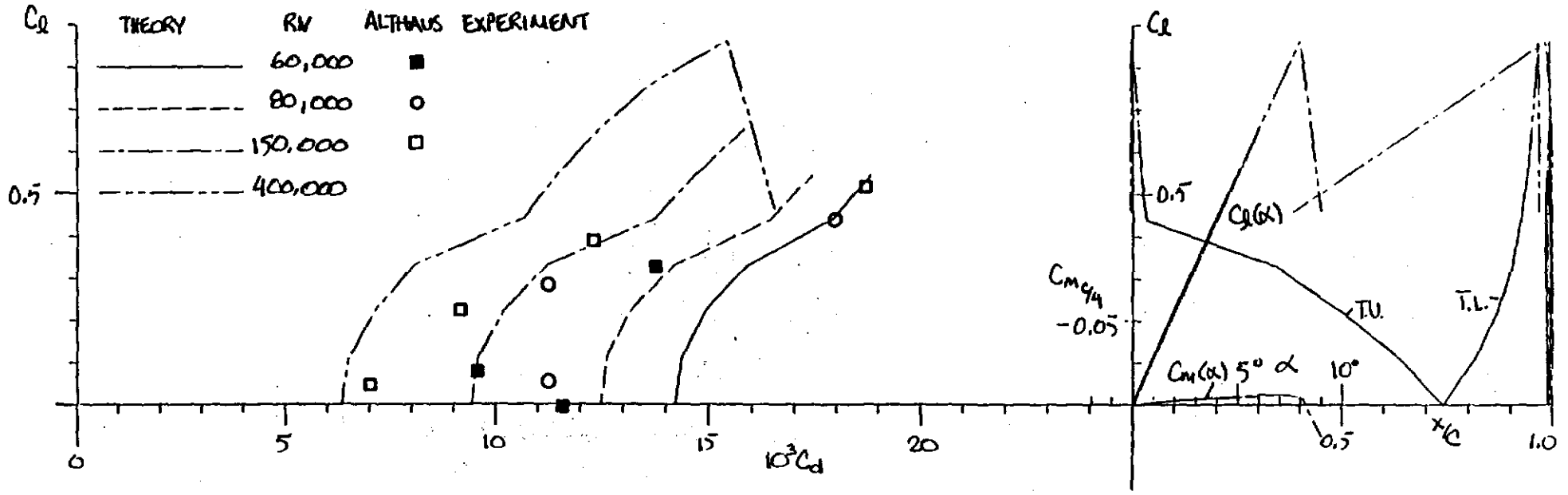

FIGURE 16.- COMPARISON OF THE THEORETICAL AND EXPERIMENTAL SECTION CHARACTERISTICS FOR THE NACA 0009 AIRFOIL.

THEORETICAL BOUNDARY-LAYER SUMMARY TABLE										
AIRFOIL	*-LAMINAR SEPARATION BUBBLE WARNING O-NO SEPARATION BUBBLE WARNING ●-NO BUBBLE, TRANSITION BEFORE 0.05C --SEPARATION AT LEADING EDGE (STALL)									
FX 60-100	+-ANGLE OF ATTACK WITHIN DRAG BUCKET									
ALPHA (deg)	REYNOLDS NUMBER									
	60000		100000		200000		400000			
	us	ls	us	ls	us	ls	us	ls	us	ls
1	-	-	-	-	-	-	●	●		
2	●	●	●	●	●	●	●	●		
+ 3	●	●	●	●	●	●	●	●		
+ 4	●	●	●	●	●	●	●	●		
+ 5	●	●	●	●	●	●	●	●		
+ 6	●	●	●	●	●	●	●	●		
+ 7	●	●	●	●	●	●	●	●		
+ 8	●	●	●	●	●	●	●	●		
+ 9	●	●	●	●	●	●	●	●		
+10	●	O	●	O	O	O	O	O		
11	●	O	●	O	●	O	●	O		
12	●	O	●	O	●	O	●	O		

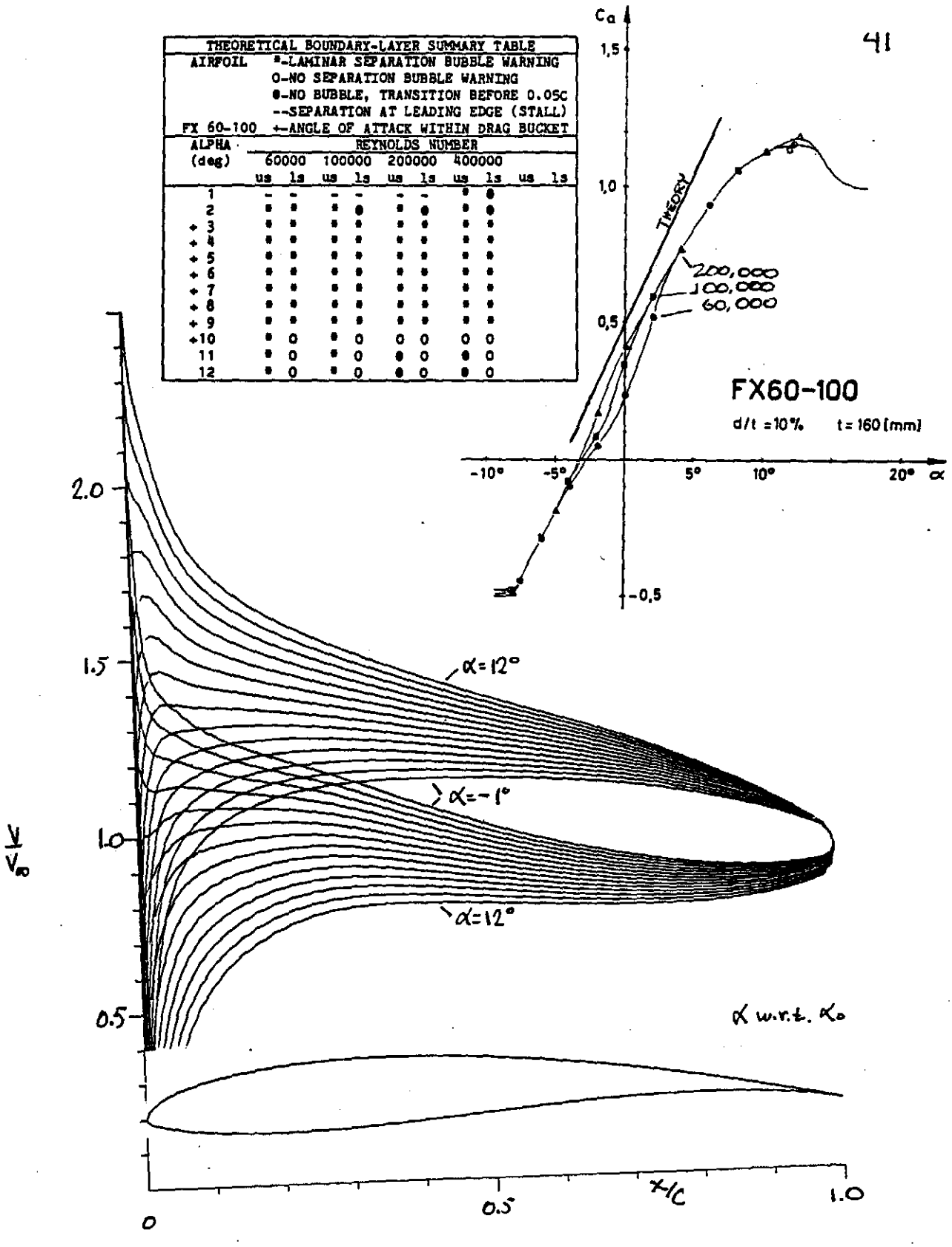

FIGURE 17.- VELOCITY DISTRIBUTIONS FOR THE FX 60-100 AIRFOIL.

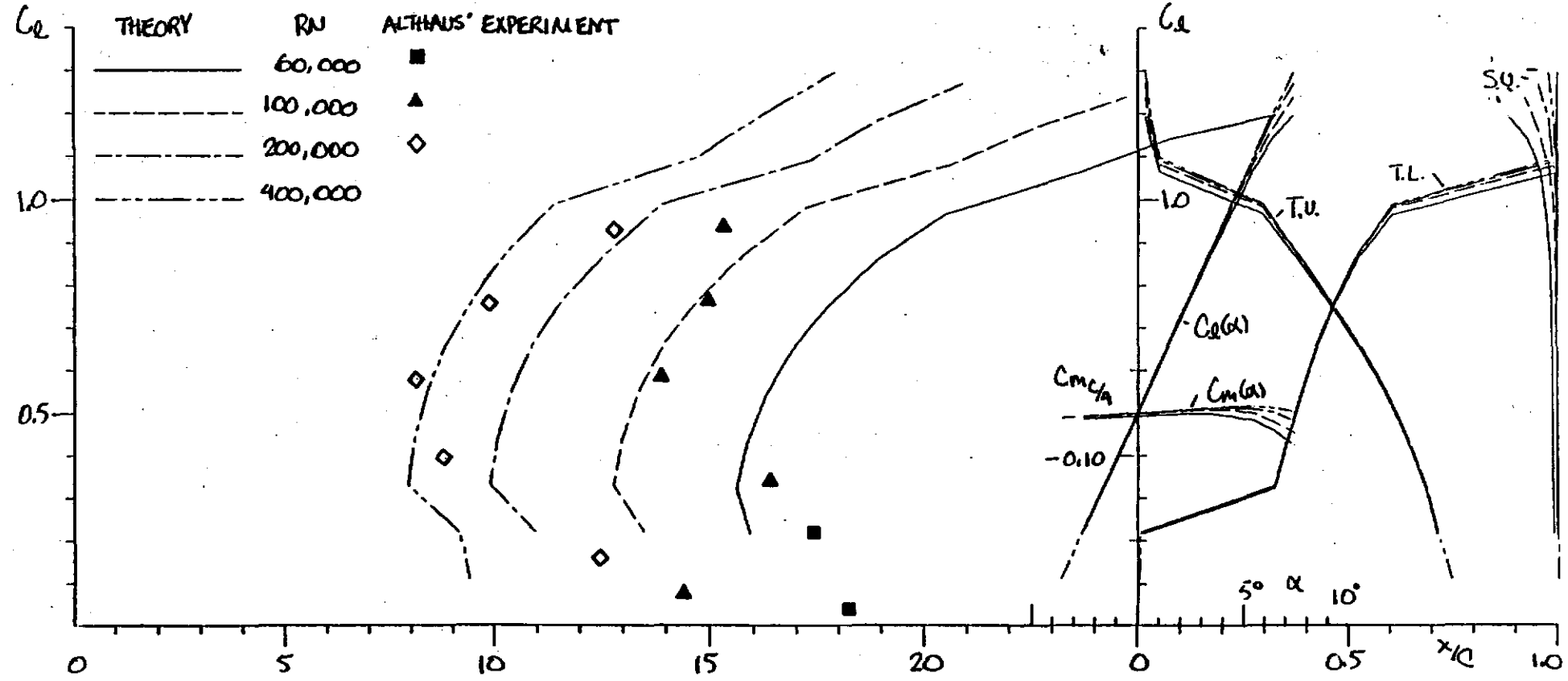

FIGURE 18. - COMPARISON OF THE THEORETICAL AND EXPERIMENTAL SECTION CHARACTERISTICS FOR THE FX 60-100 AIRFOIL.

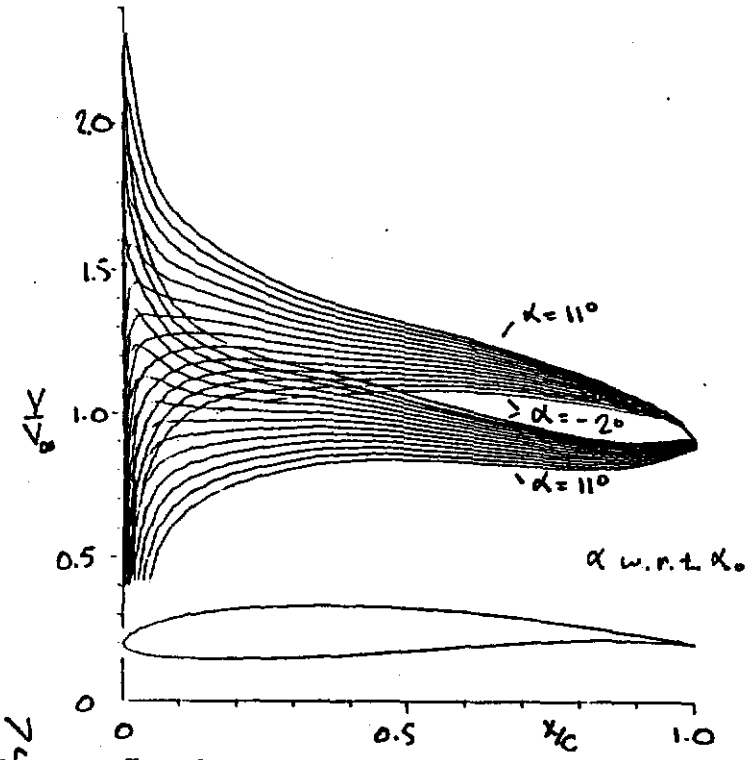

FIG. 19 - VELOCITY DISTRIBUTIONS FOR THE S2046-090-83.

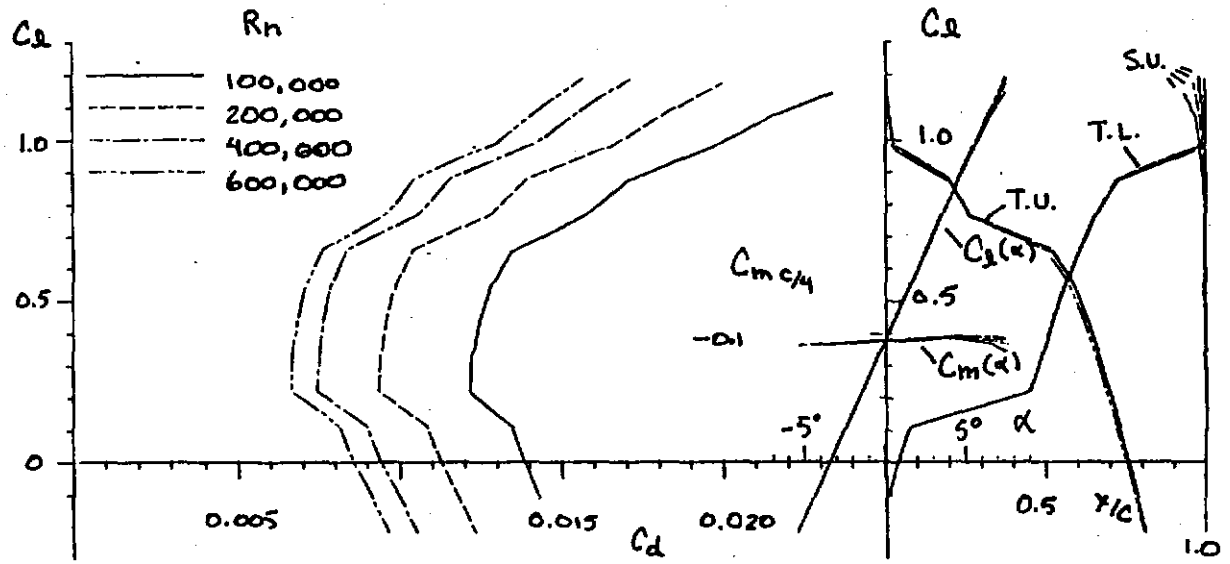

FIG. 20 - THEORETICAL SECTION CHARACTERISTICS FOR THE S2046-090-83.

THEORETICAL BOUNDARY-LAYER SUMMARY TABLE									
AIRFOIL	*-LAMINAR SEPARATION BUBBLE WARNING O-NO SEPARATION BUBBLE WARNING ●-NO BUBBLE, TRANSITION BEFORE 0.05C --SEPARATION AT LEADING EDGE (STALL)								
2046-090-83	+-ANGLE OF ATTACK WITHIN DRAG BUCKET								
ALPHA (deg)	REYNOLDS NUMBER								
			100000		200000		400000		600000	
	us	ls	us	ls	us	ls	us	ls	us	ls
-2			-	-	*	*	*	●	*	●
-1			*	*	*	●	*	●	*	●
0			*	*	*	●	*	●	*	●
+ 1			*	*	*	*	*	O	*	O
+ 2			*	*	*	*	*	*	*	*
+ 3			*	*	*	*	*	*	*	*
+ 4			*	*	*	*	*	*	*	*
+ 5			*	*	*	*	*	*	*	*
+ 6			*	*	*	*	*	*	*	*
+ 7			*	*	*	*	O	*	O	*
+ 8			*	*	*	*	O	*	O	*
9			*	O	●	O	●	O	●	O
10			*	O	●	O	●	O	●	O
11			*	O	*	O	●	O	●	O

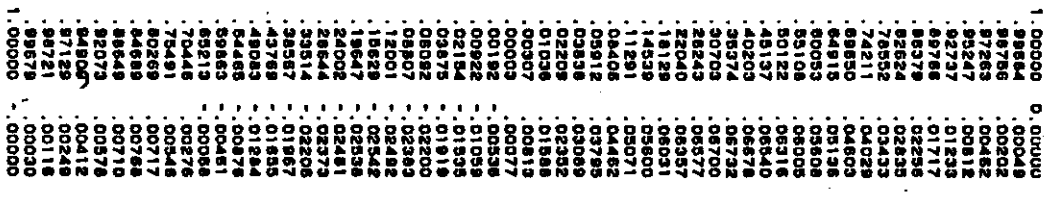

S2046-090-83 COORDINATES

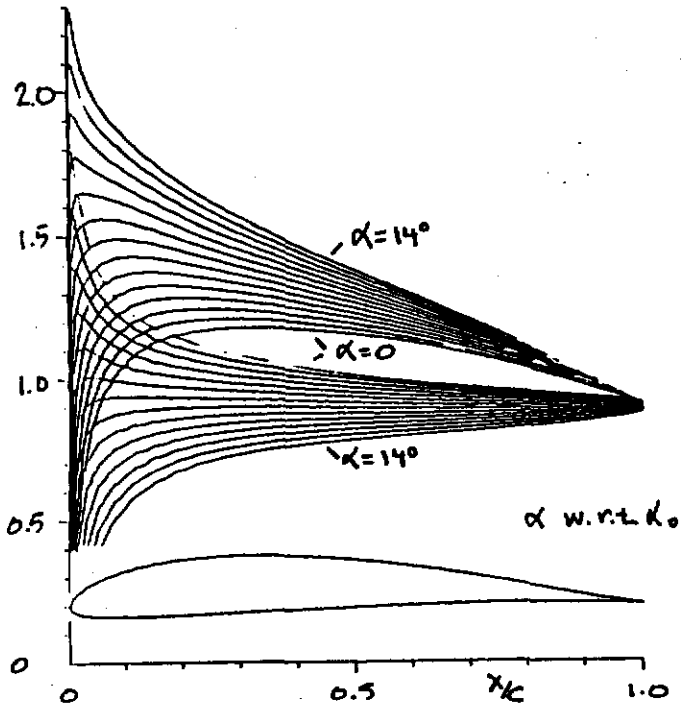

FIG. 21- VELOCITY DISTRIBUTIONS FOR THE S2091-101-83.

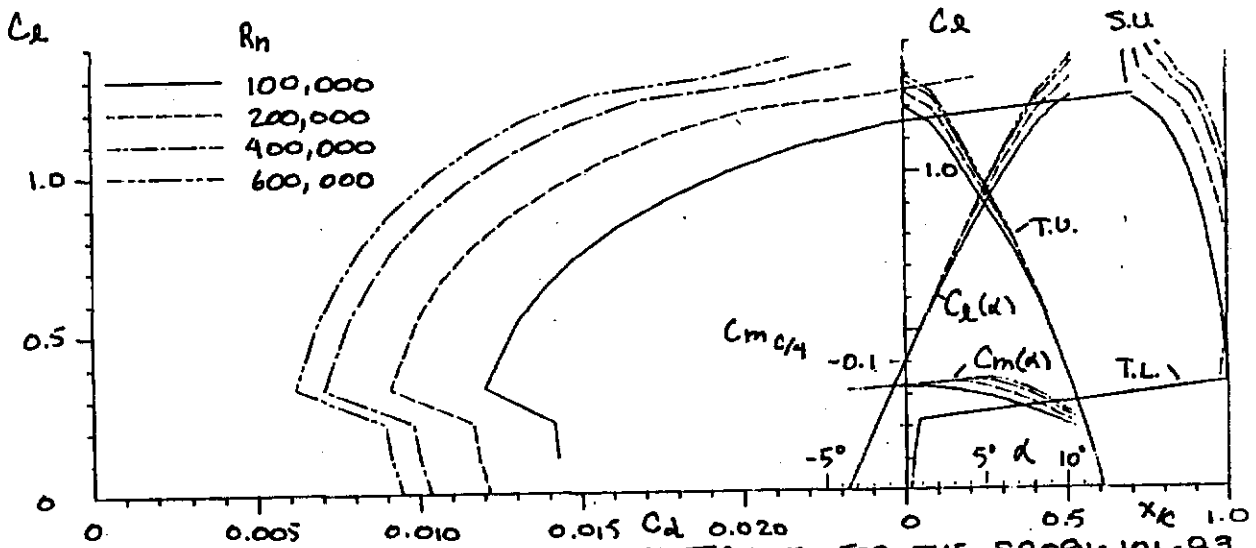

FIG. 22 - THEORETICAL SECTION CHARACTERISTICS FOR THE S2091-101-83.

THEORETICAL BOUNDARY-LAYER SUMMARY TABLE										
AIRFOIL	*-LAMINAR SEPARATION BUBBLE WARNING O-NO SEPARATION BUBBLE WARNING ●-NO BUBBLE, TRANSITION BEFORE 0.05C --SEPARATION AT LEADING EDGE (STALL)									
2091-101-83	+-ANGLE OF ATTACK WITHIN DRAG BUCKET									
ALPHA (deg)	REYNOLDS NUMBER									
			100000		200000		400000		600000	
	us	ls	us	ls	us	ls	us	ls	us	ls
0			*	*	*	*	*	●	*	●
1			*	*	*	*	*	●	*	●
+ 2			*	*	*	●	*	●	*	●
+ 3			*	*	*	*	*	*	*	*
+ 5			*	O	*	O	*	O	*	O
+ 6			*	O	*	O	*	O	O	O
+ 7			*	O	*	O	*	O	O	O
+ 8			*	O	*	O	*	O	O	O
+ 9			*	O	*	O	O	O	O	O
+10			*	O	*	O	O	O	O	O
+11			*	O	*	O	O	O	O	O
+12			*	O	O	O	O	O	O	O
13			●	O	●	O	●	O	●	O
14			*	O	●	O	●	O	●	O

x/c	y/c
1.00000	.00000
.99674	.00035
.98707	.00150
.97128	.00367
.94970	.00698
.92282	.01150
.89147	.01713
.85594	.02373
.81693	.03107
.77501	.03888
.73070	.04688
.68454	.05479
.63700	.06231
.58856	.06920
.53965	.07526
.49073	.08029
.44220	.08416
.39450	.08677
.34805	.08805
.30323	.08794
.26043	.08644
.22002	.08356
.18232	.07934
.14785	.07382
.11922	.06708
.08823	.05927
.06384	.05060
.04320	.04130
.02645	.03168
.01374	.02205
.00517	.01289
.00077	.00401
.00058	-.00312
.00575	-.00884
.01582	-.01315
.03263	-.01645
.05387	-.01844
.08063	-.01938
.11236	-.01939
.14883	-.01873
.19060	-.01750
.23417	-.01581
.28205	-.01374
.33271	-.01142
.38558	-.00894
.43995	-.00643
.49528	-.00398
.55088	-.00171
.60605	.00025
.66005	.00182
.71218	.00296
.76168	.00367
.80798	.00397
.85036	.00391
.88834	.00354
.92140	.00295
.94911	.00222
.97108	.00144
.98708	.00073
.99674	.00020
1.00000	.00000

S2091-101-83 COORDINATES

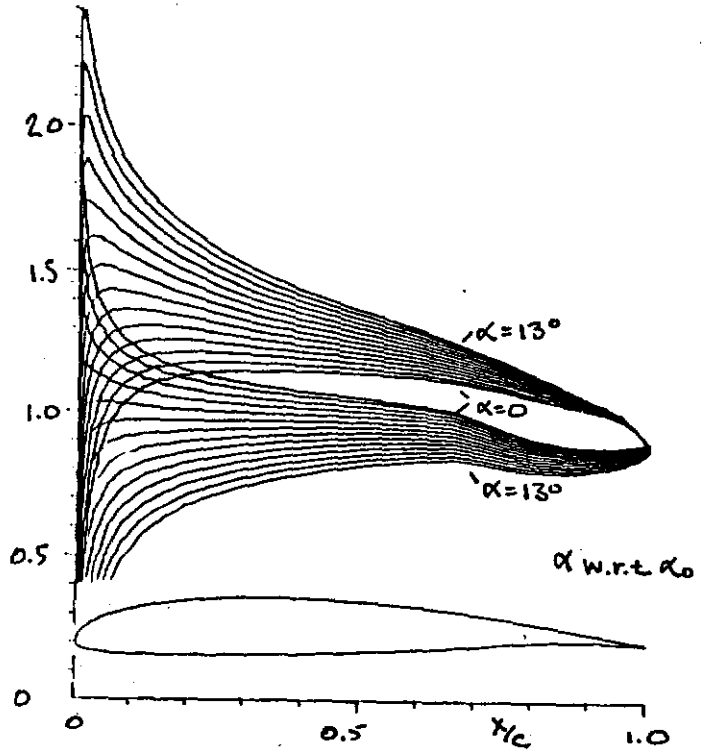

FIG. 23- VELOCITY DISTRIBUTIONS FOR THE S3002-099-83.

THEORETICAL BOUNDARY-LAYER SUMMARY TABLE AIRFOIL *-LAMINAR SEPARATION BUBBLE WARNING O-NO SEPARATION BUBBLE WARNING ●-NO BUBBLE, TRANSITION BEFORE 0.05C --SEPARATION AT LEADING EDGE (STALL) 3002-099-83 +-ANGLE OF ATTACK WITHIN DRAG BUCKET											
ALPHA (deg)	REYNOLDS NUMBER										
			100000		200000		400000		600000		
	us	ls	us	ls	us	ls	us	ls	us	ls	
0			*	●	*	●	*	●	*	●	
1			*	*	*	*	*	●	*	●	
+ 2			*	*	*	*	*	*	*	*	
+ 3			*	*	*	*	*	*	*	*	
+ 4			*	*	*	*	*	*	*	*	
+ 5			*	*	*	*	*	*	*	*	
+ 6			*	*	*	*	*	*	*	*	
+ 7			*	*	*	*	*	*	O	O	
+ 8			*	*	*	*	O	O	O	O	
+ 9			*	*	*	*	O	O	O	O	
+10			*	*	O	*	O	O	O	O	
+11			*	*	●	*	●	●	●	●	
12			*	*	●	*	●	*	●	●	
13			*	*	●	*	●	*	●	●	

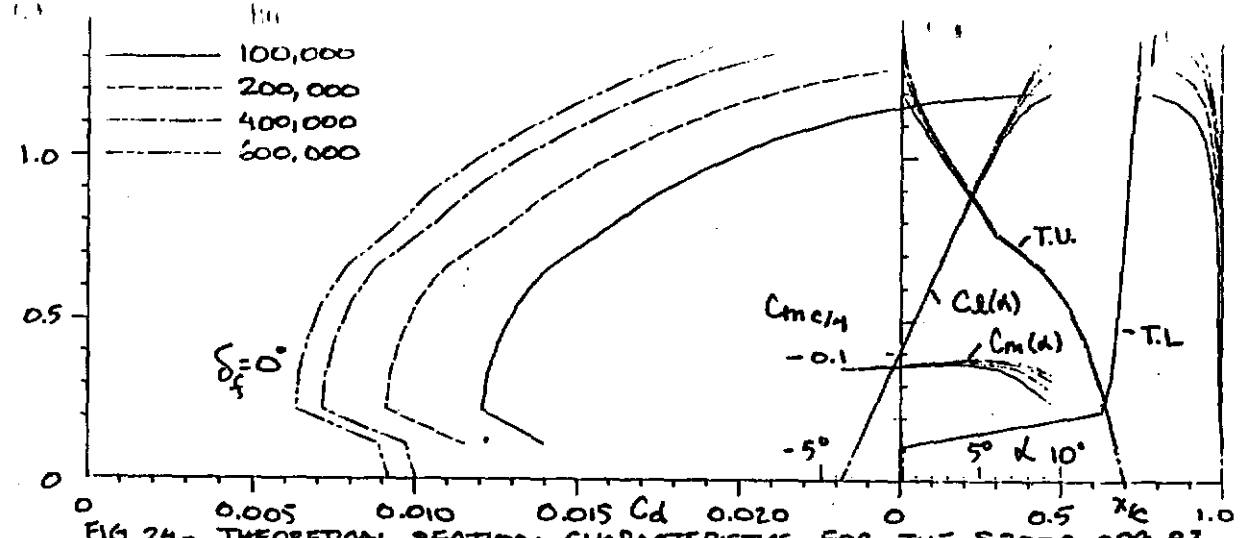

FIG. 24- THEORETICAL SECTION CHARACTERISTICS FOR THE S3002-099-83.

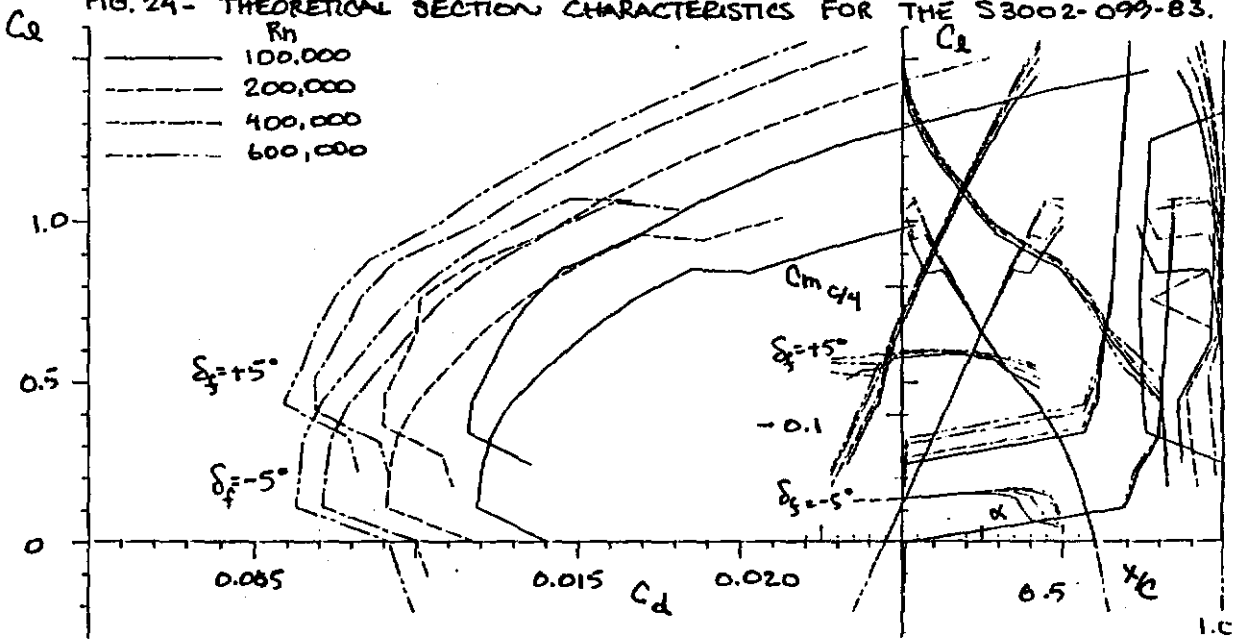

FIG. 25- THEORETICAL SECTION CHARACTERISTICS FOR THE S3002-099-83 AT A FLAP DEFLECTION OF $\delta_f = +5°$ AND $\delta_f = -5°$.

x	y
1.00000	0.00000
.99672	.00033
.98688	.00125
.97052	.00257
.94770	.00402
.91863	.00527
.88373	.00590
.84358	.00550
.79932	.00382
.75185	.00081
.70250	-.00311
.65189	-.00697
.60027	-.01020
.54750	-.01294
.49424	-.01527
.44102	-.01717
.38835	-.01869
.33684	-.01988
.28711	-.02078
.23978	-.02136
.19537	-.02159
.15449	-.02145
.11781	-.02097
.08582	-.01976
.05763	-.01796
.03507	-.01576
.01778	-.01223
.00602	-.00831
.00051	-.00333
.00048	.00360
.00440	.01211
.01234	.02105
.02450	.03000
.04087	.03873
.06135	.04701
.08583	.05460
.11417	.06135
.14619	.06711
.18165	.07181
.22028	.07537
.26175	.07778
.30572	.07900
.35178	.07915
.39944	.07823
.44820	.07627
.49758	.07328
.54711	.06930
.59634	.06441
.64481	.05868
.69214	.05226
.73787	.04536
.78161	.03825
.82286	.03124
.86104	.02463
.89553	.01862
.92578	.01330
.95131	.00867
.97191	.00483
.98723	.00205
.99678	.00048
1.00000	0.00000

S3002-099-83 COORDINATES

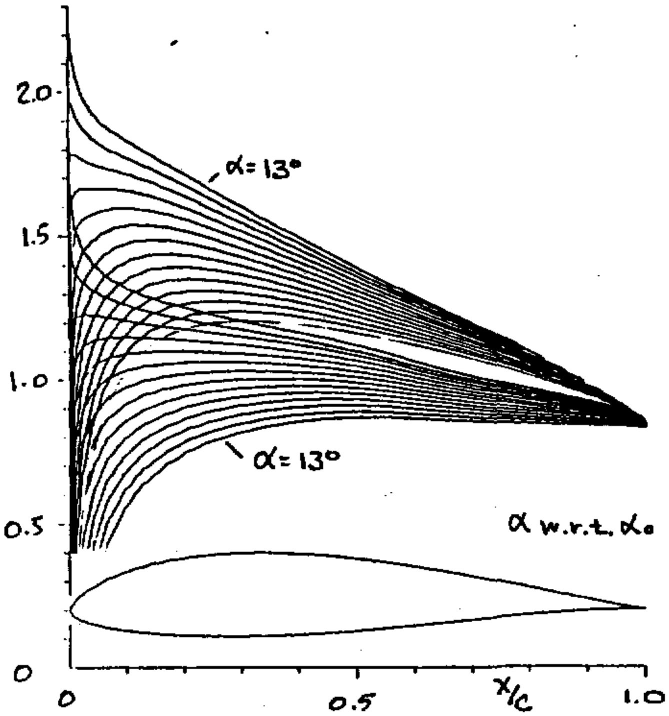

FIG. 26 - VELOCITY DISTRIBUTIONS FOR THE S2027-145-83.

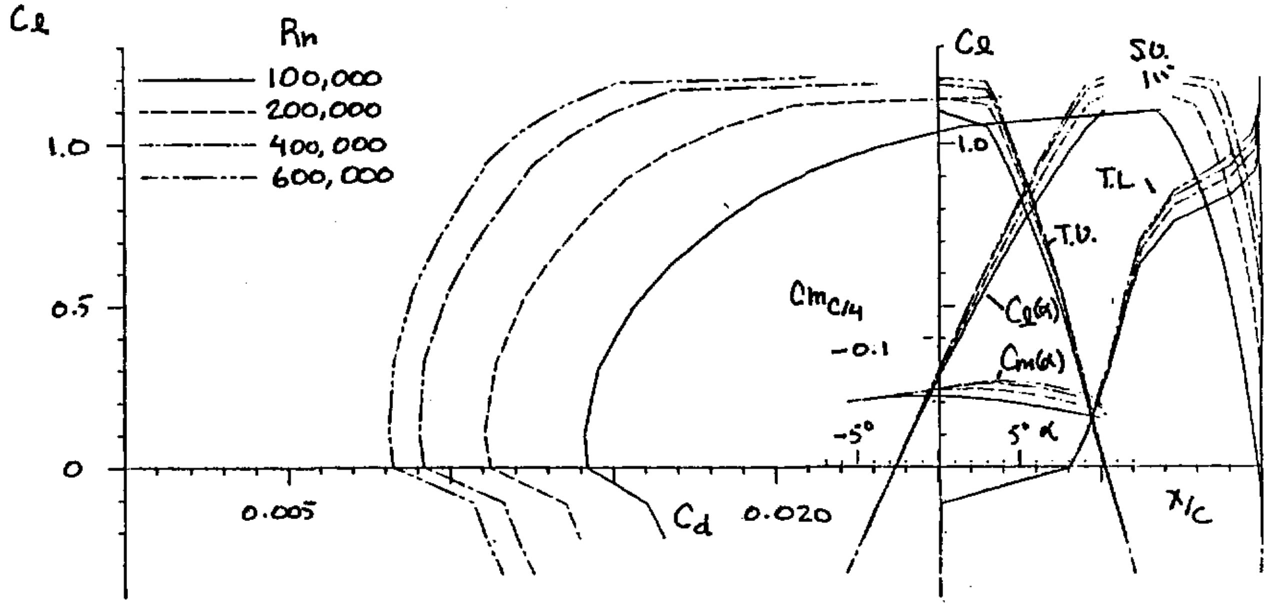

FIG. 27- THEORETICAL SECTION CHARACTERISTICS FOR THE S2027-145-83.

THEORETICAL BOUNDARY-LAYER SUMMARY TABLE										
AIRFOIL	*-LAMINAR SEPARATION BUBBLE WARNING O-NO SEPARATION BUBBLE WARNING ●-NO BUBBLE, TRANSITION BEFORE 0.05C --SEPARATION AT LEADING EDGE (STALL) +-ANGLE OF ATTACK WITHIN DRAG BUCKET									
2027-145-83										
ALPHA (deg)	REYNOLDS NUMBER									
			100000		200000		400000		600000	
	us	ls	us	ls	us	ls	us	ls	us	ls
-3			*	*	*	*	*	*	*	●
-2			*	*	*	●	*	●	*	●
-1			*	●	*	●	*	●	*	●
+ 0			*	*	*	*	*	*	*	*
+ 1			*	*	*	*	*	*	O	*
+ 3			*	*	*	*	*	*	O	*
+ 5			*	*	*	*	*	*	O	*
+ 7			*	*	*	*	*	*	O	*
+ 8			*	*	*	*	*	*	O	*
+ 9			*	*	*	*	O	*	O	*
+10			*	*	*	*	O	*	O	*
+11			*	O	*	O	O	O	O	*
+12			*	O	*	O	O	O	O	O
13			●	O	●	O	●	O	●	O

x	y
1.00000	0.00000
.99647	.00037
.98604	.00164
.96916	.00413
.94635	.00798
.91825	.01321
.88546	.01970
.84870	.02725
.80852	.03560
.76553	.04444
.72028	.05346
.67332	.06236
.62516	.07084
.57628	.07865
.52717	.08554
.47831	.09130
.43016	.09571
.38310	.09867
.33747	.09976
.29351	.09929
.25186	.09709
.21254	.09321
.17589	.08769
.14216	.08064
.11153	.07224
.08419	.06274
.06033	.05240
.04012	.04159
.02380	.03064
.01156	.01992
.00357	.00980
.00004	.00090
.00226	-.00627
.01078	-.01262
.02476	-.01894
.04376	-.02488
.06752	-.03027
.09581	-.03497
.12833	-.03890
.16474	-.04200
.20467	-.04420
.24773	-.04548
.29350	-.04574
.34154	-.04504
.39139	-.04336
.44256	-.04076
.49465	-.03721
.54723	-.03285
.59994	-.02792
.65225	-.02282
.70342	-.01790
.75270	-.01340
.79932	-.00946
.84257	-.00617
.88176	-.00360
.91625	-.00174
.94545	-.00055
.96884	.00005
.98597	.00020
.99646	.00009
1.00000	-.00000

S2027-145-83 COORDINATES

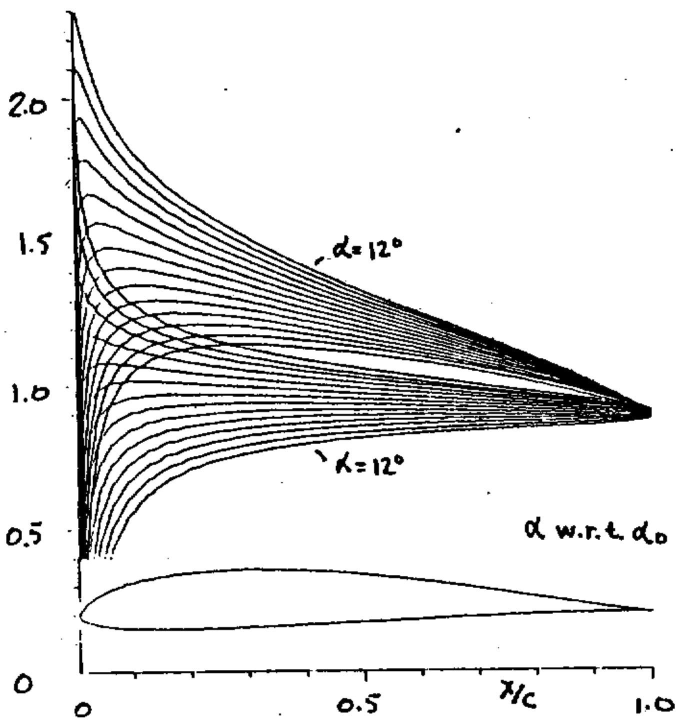

FIG. 28 - VELOCITY DISTRIBUTIONS FOR THE S3010-103-84.

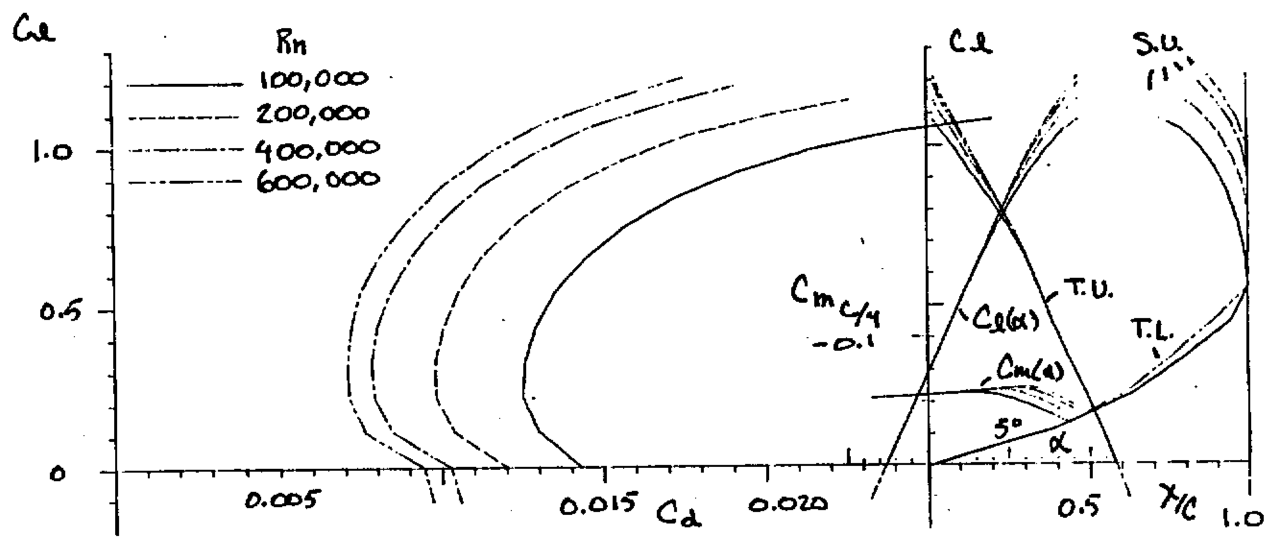

FIG. 29 - THEORETICAL SECTION CHARACTERISTICS FOR THE S3010-103-84.

THEORETICAL BOUNDARY-LAYER SUMMARY TABLE

AIRFOIL 3010-103-84

*-LAMINAR SEPARATION BUBBLE WARNING
O-NO SEPARATION BUBBLE WARNING
●-NO BUBBLE, TRANSITION BEFORE 0.05C
--SEPARATION AT LEADING EDGE (STALL)
+-ANGLE OF ATTACK WITHIN DRAG BUCKET

ALPHA (deg)			REYNOLDS NUMBER 100000		200000		400000		600000	
	us	ls	us	ls	us	ls	us	ls	us	ls
-1			*	-	*	-	*	●	*	●
0			*	●	*	●	*	●	*	●
+ 1			*	*	*	*	*	*	*	*
+ 2			*	*	*	*	*	*	*	*
+ 3			*	*	*	*	*	*	*	*
+ 4			*	*	*	*	*	*	O	*
+ 5			*	O	*	O	*	O	O	O
+ 6			*	O	*	O	O	O	O	O
+ 7			*	O	*	O	O	O	O	O
+ 8			*	O	*	O	O	O	O	O
+ 9			*	O	O	O	O	O	O	O
+10			*	O	O	O	O	O	O	O
11			*	O	●	O	●	O	●	O
12			*	O	●	O	●	O	●	O

x	y
1.00000	0.00000
.99674	.00027
.98706	.00118
.97122	.00293
.94959	.00564
.92264	.00936
.89090	.01405
.85493	.01960
.81531	.02565
.77261	.03259
.72739	.03958
.68021	.04656
.63158	.05337
.58203	.05971
.53204	.06541
.48213	.07029
.43275	.07422
.38436	.07706
.33750	.07870
.29250	.07902
.24970	.07798
.20944	.07558
.17206	.07184
.13785	.06689
.10706	.06076
.07990	.05360
.05655	.04556
.03713	.03683
.02173	.02766
.01042	.01835
.00319	.00927
.00005	.00100
.00181	-.00543
.00932	-.01048
.02239	-.01506
.04061	-.01894
.06381	-.02203
.09180	-.02427
.12435	-.02567
.16119	-.02625
.20200	-.02610
.24635	-.02531
.29376	-.02399
.34371	-.02221
.39565	-.02009
.44899	-.01769
.50312	-.01514
.55743	-.01252
.61127	-.00994
.66399	-.00749
.71495	-.00526
.76350	-.00332
.80901	-.00172
.85087	-.00051
.88851	.00031
.92140	.00075
.94906	.00086
.97104	.00072
.98703	.00042
.99674	.00013
1.00000	-.00000

S3010-103-84 COORDINATES

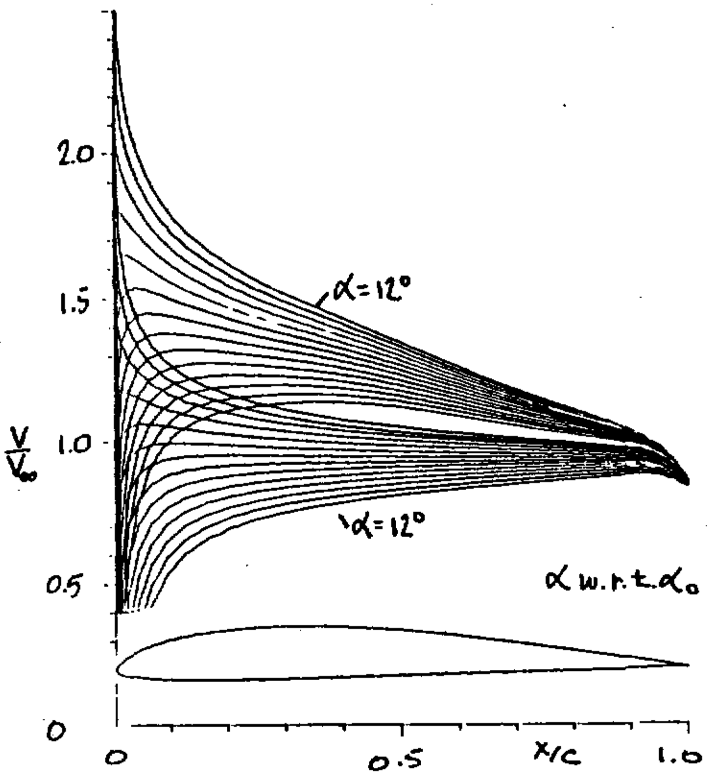

FIG. 30- VELOCITY DISTRIBUTIONS FOR THE S3021-095-84.

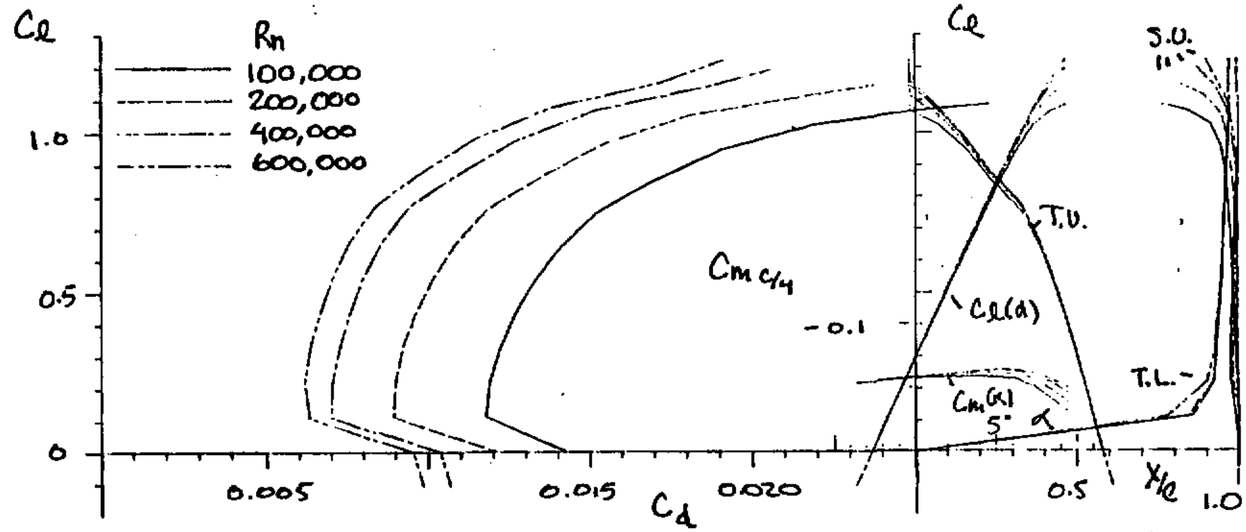

FIG. 31 - THEORETICAL SECTION CHARACTERISTICS FOR THE S3021-095-84.

THEORETICAL BOUNDARY-LAYER SUMMARY TABLE										
AIRFOIL	*-LAMINAR SEPARATION BUBBLE WARNING O-NO SEPARATION BUBBLE WARNING ●-NO BUBBLE, TRANSITION BEFORE 0.05C --SEPARATION AT LEADING EDGE (STALL) +-ANGLE OF ATTACK WITHIN DRAG BUCKET									
3021-095-84										
ALPHA (deg)	REYNOLDS NUMBER									
			100000		200000		400000		600000	
	us	ls	us	ls	us	ls	us	ls	us	ls
-1			*	-	*	-	*	●	*	●
0			*	*	*	●	*	●	*	●
+ 1			*	*	*	*	*	*	*	*
+ 2			*	*	*	*	*	*	*	*
+ 3			*	*	*	*	*	*	*	*
+ 4			*	*	*	*	*	*	*	*
+ 5			*	*	*	*	*	*	*	*
+ 6			*	*	*	*	*	*	*	*
+ 7			*	*	*	*	*	*	O	*
+ 8			*	*	*	*	O	*	O	*
+ 9			*	*	*	*	O	*	O	*
+10			*	*	O	*	O	*	O	*
11			●	*	●	*	●	*	●	*
12			*	*	●	*	●	*	●	*

x	y
1.00000	0.00000
.99663	.00039
.98679	.00172
.97104	.00419
.94996	.00769
.92398	.01193
.89336	.01670
.85840	.02199
.81959	.02778
.77748	.03394
.73266	.04039
.68572	.04695
.63730	.05342
.58801	.05955
.53839	.06505
.48891	.06964
.43996	.07312
.39191	.07537
.34513	.07632
.29999	.07596
.25685	.07433
.21611	.07151
.17816	.06763
.14331	.06243
.11182	.05631
.08393	.04930
.05983	.04157
.03968	.03329
.02358	.02472
.01160	.01615
.00374	.00799
.00008	.00099
.00191	-.00427
.00984	-.00852
.02320	-.01232
.04178	-.01547
.06542	-.01789
.09394	-.01957
.12712	-.02053
.16464	-.02085
.20613	-.02059
.25118	-.01986
.29928	-.01878
.34988	-.01742
.40237	-.01592
.45611	-.01433
.51046	-.01273
.56475	-.01118
.61833	-.00963
.67055	-.00821
.72078	-.00690
.76839	-.00571
.81282	-.00462
.85354	-.00365
.89004	-.00278
.92186	-.00193
.94875	-.00107
.97046	-.00038
.98659	.00003
.99660	.00008
1.00000	-.00000

S3021-095-84 COORDINATES

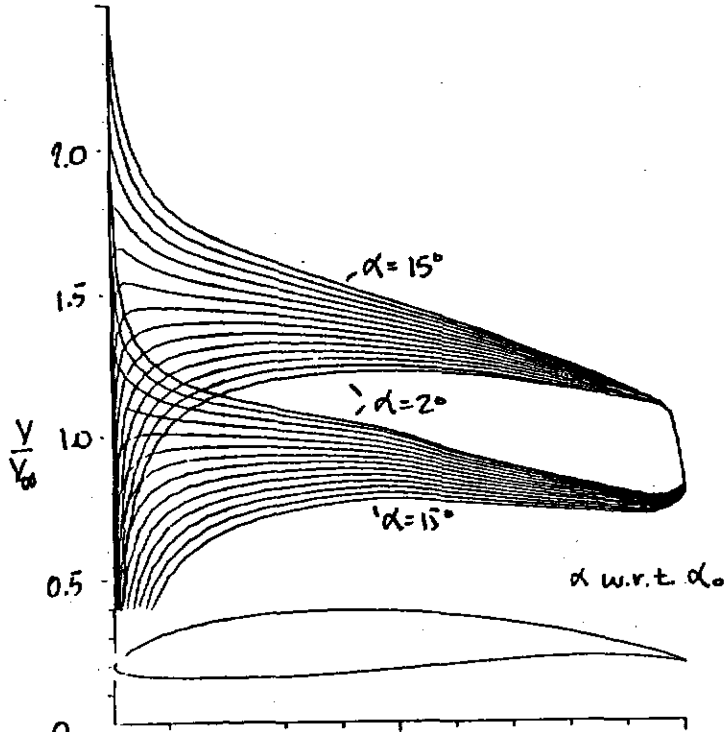

FIG. 32 - VELOCITY DISTRIBUTIONS FOR THE S4022-113-84.

THEORETICAL BOUNDARY-LAYER SUMMARY TABLE										
AIRFOIL 4022-113-84	*-LAMINAR SEPARATION BUBBLE WARNING O-NO SEPARATION BUBBLE WARNING ●-NO BUBBLE, TRANSITION BEFORE 0.05C --SEPARATION AT LEADING EDGE (STALL) +-ANGLE OF ATTACK WITHIN DRAG BUCKET									
ALPHA (deg)	REYNOLDS NUMBER									
			100000		200000		400000		600000	
	us	ls	us	ls	us	ls	us	ls	us	ls
2			*	-	*	-	*	*	*	*
3			*	*	*	*	*	-	*	-
+ 4			*	*	*	*	*	*	*	*
+ 5			*	*	*	*	*	*	*	*
+ 6			*	*	*	*	*	*	*	*
+ 7			*	*	*	*	*	*	*	*
+ 8			*	*	*	*	*	*	*	*
+ 9			*	*	*	*	*	*	*	*
+10			*	*	*	*	*	*	*	*
+11			*	*	*	*	*	*	O	*
+12			*	*	*	*	*	*	O	*
+13			*	*	*	*	O	*	O	*
14			*	*	●	*	●	*	●	*
15			●	O	●	O	●	O	●	O

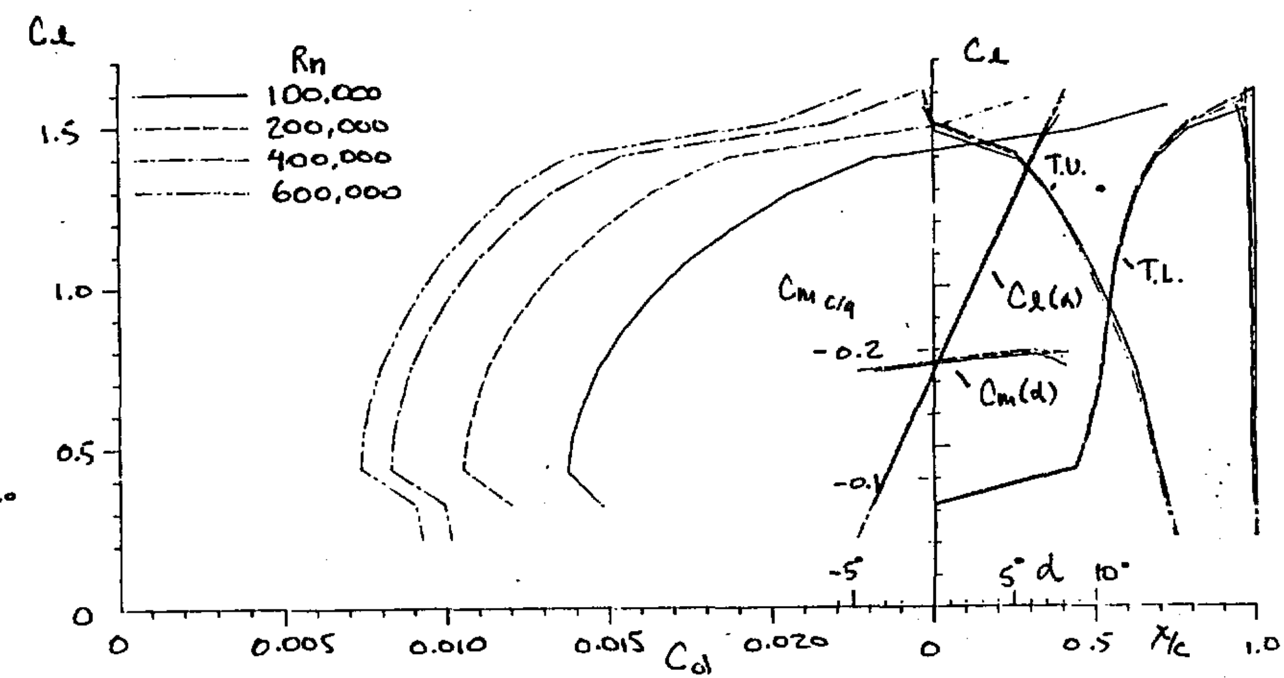

FIG. 33 - THEORETICAL SECTION CHARACTERISTICS FOR THE S4022-113-84.

1.00000	0.00000
.99679	.00128
.98795	.00501
.97456	.01036
.95656	.01638
.93361	.02295
.90652	.03009
.87510	.03768
.83996	.04557
.80156	.05358
.76043	.06152
.71703	.06914
.67185	.07619
.62532	.08241
.57782	.08760
.52975	.09167
.48158	.09453
.43371	.09608
.38660	.09628
.34064	.09512
.29623	.09256
.25373	.08871
.21350	.08361
.17587	.07741
.14120	.07023
.10980	.06225
.08196	.05361
.05792	.04451
.03789	.03515
.02206	.02575
.01050	.01649
.00313	.00776
.00001	.00038
.00246	-.00502
.01117	-.00919
.02553	-.01287
.04522	-.01594
.07000	-.01834
.09959	-.02006
.13368	-.02111
.17189	-.02152
.21378	-.02129
.25888	-.02044
.30669	-.01897
.35670	-.01685
.40836	-.01409
.46124	-.01081
.51493	-.00635
.56931	-.00152
.62394	.00324
.67803	.00747
.73071	.01084
.78110	.01311
.82829	.01415
.87139	.01390
.90955	.01242
.94190	.00982
.96749	.00648
.98569	.00321
.99645	.00085
1.00000	.00000

S4022-113-84 COORDINATES

80

16

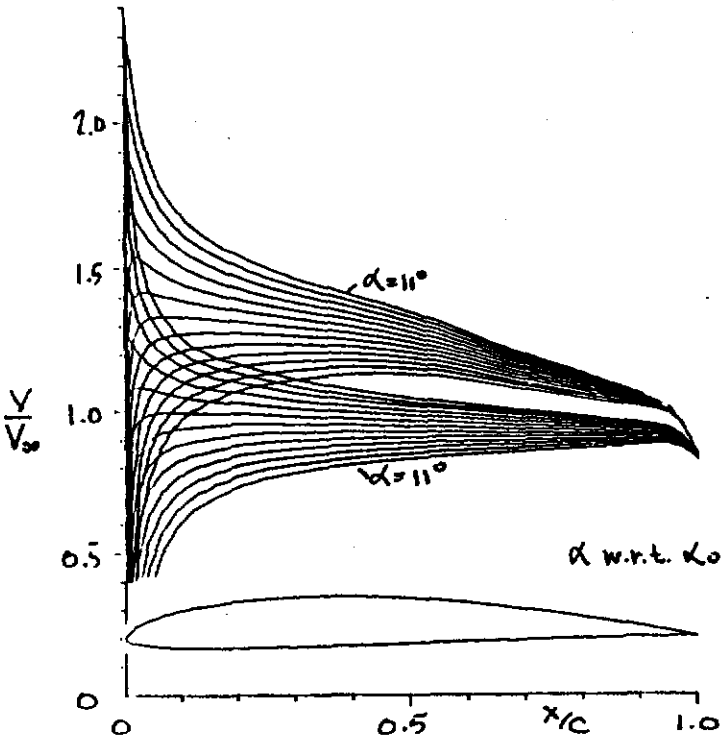

FIG. 34 - VELOCITY DISTRIBUTIONS FOR THE S4053-089-84.

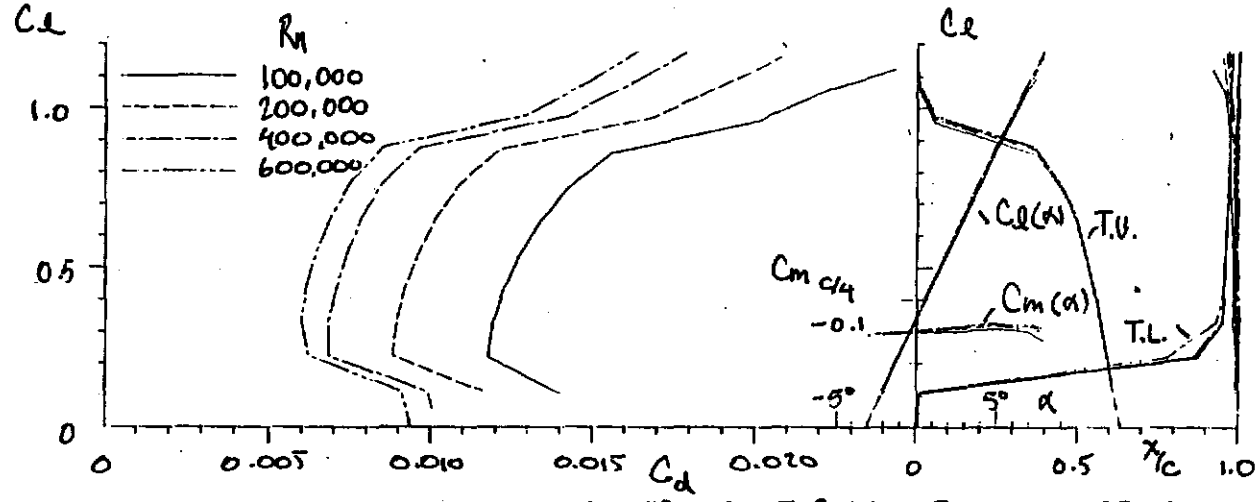

FIG. 35 - THEORETICAL SECTION CHARACTERISTICS FOR THE S4053-089-84.

18

THEORETICAL BOUNDARY-LAYER SUMMARY TABLE										
AIRFOIL	*-LAMINAR SEPARATION BUBBLE WARNING O-NO SEPARATION BUBBLE WARNING ●-NO BUBBLE, TRANSITION BEFORE 0.05C --SEPARATION AT LEADING EDGE (STALL)									
4053-089-84	+-ANGLE OF ATTACK WITHIN DRAG BUCKET									
ALPHA (deg)	REYNOLDS NUMBER									
			100000		200000		400000		600000	
	us	ls	us	ls	us	ls	us	ls	us	ls
-1			*	-	*	-	*	-	*	●
0			*	*	*	●	*	●	*	●
1			*	*	*	*	*	*	*	*
+ 2			*	*	*	*	*	*	*	*
+ 3			*	*	*	*	*	*	*	*
+ 4			*	*	*	*	*	*	*	*
+ 5			*	*	*	*	*	*	*	*
+ 6			*	*	*	*	*	*	*	*
+ 7			*	*	*	*	*	*	*	*
+ 8			*	*	*	*	*	*	O	*
+ 9			*	*	O	*	O	*	O	*
10			*	*	●	*	●	*	●	*
11			*	*	●	*	●	*	●	*

x	y
1.00000	0.00000
.99662	.00053
.98668	.00231
.97153	.00536
.95119	.00935
.92601	.01381
.89611	.01877
.86192	.02422
.82383	.03011
.78228	.03632
.73769	.04271
.69050	.04911
.64100	.05531
.59047	.06102
.54753	.06582
.49853	.06973
.44977	.07232
.40180	.07366
.35444	.07385
.30869	.07280
.26478	.07056
.22310	.06749
.18409	.06333
.14813	.05828
.11551	.05243
.08655	.04588
.06147	.03879
.04053	.03131
.02388	.02360
.01183	.01584
.00377	.00823
.00013	.00131
.00152	-.00382
.00678	-.00781
.02183	-.01118
.03960	-.01388
.06334	-.01592
.09177	-.01729
.12484	-.01808
.16249	-.01840
.20391	-.01829
.24875	-.01771
.29681	-.01671
.34698	-.01541
.39927	-.01392
.45286	-.01231
.50711	-.01064
.56138	-.00896
.61507	-.00731
.66752	-.00579
.71809	-.00443
.76614	-.00328
.81105	-.00238
.85226	-.00165
.88923	-.00113
.92145	-.00075
.94854	-.00047
.97028	-.00027
.98648	-.00018
.99655	-.00010
1.00000	.00000

COORDINATES FOR THE S4053-089-84

50

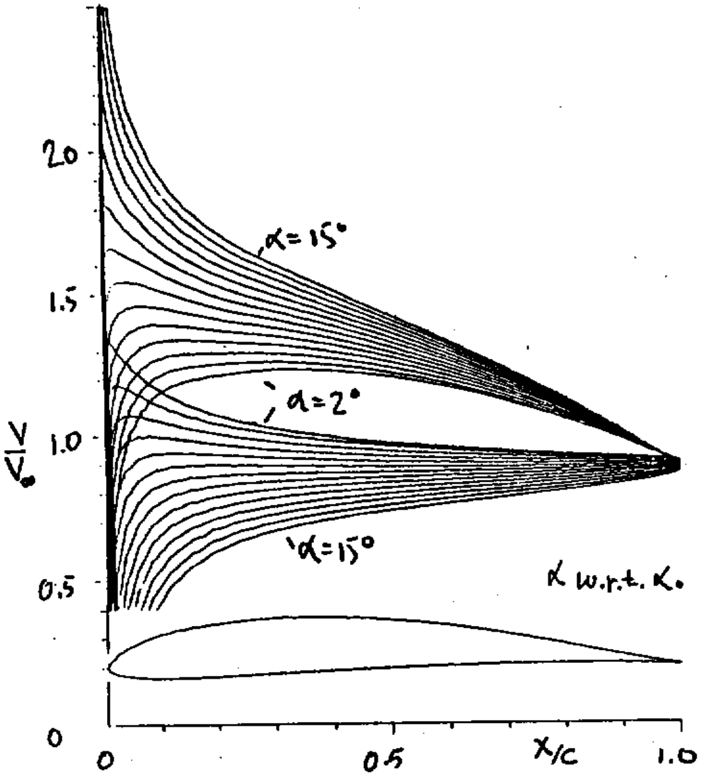

FIG. 36- VELOCITY DISTRIBUTIONS FOR THE S4061-096-84.

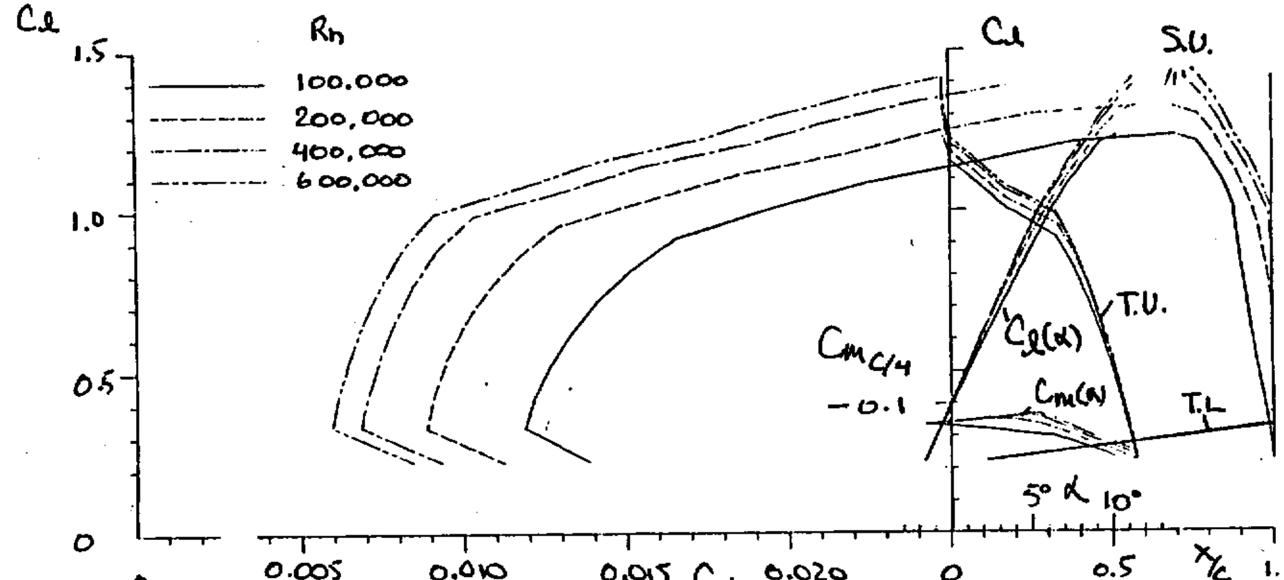

FIG. 37- THEORETICAL SECTION CHARACTERISTICS FOR THE S4061-096-84.

THEORETICAL BOUNDARY-LAYER SUMMARY TABLE										
AIRFOIL 4061-096-84	*-LAMINAR SEPARATION BUBBLE WARNING O-NO SEPARATION BUBBLE WARNING ●-NO BUBBLE, TRANSITION BEFORE 0.05C --SEPARATION AT LEADING EDGE (STALL) +-ANGLE OF ATTACK WITHIN DRAG BUCKET									
ALPHA (deg)	REYNOLDS NUMBER									
			100000		200000		400000		600000	
	us	ls	us	ls	us	ls	us	ls	us	ls
2			*	*	*	*	*	O	*	O
+ 3			*	*	*	*	*	*	*	*
+ 4			*	O	*	O	*	O	*	O
+ 5			*	O	*	O	*	O	*	O
+ 6			*	O	*	O	*	O	O	O
+ 7			*	O	*	O	*	O	*	O
+ 8			*	O	*	O	*	O	*	O
+ 9			*	O	*	O	*	O	O	O
+10			*	O	*	O	O	O	O	O
+11			*	O	O	O	O	O	O	O
12			*	O	●	O	●	O	●	O
12			*	O	●	O	●	O	●	O
13			*	O	●	O	●	O	●	O

X	Y
1.00000	0.00000
.99675	.00034
.98709	.00147
.97129	.00363
.94976	.00698
.92304	.01155
.89170	.01729
.85637	.02403
.81764	.03151
.77610	.03945
.73227	.04752
.68665	.05541
.63971	.06283
.59189	.06950
.54359	.07520
.49522	.07974
.44716	.08302
.39979	.08492
.35348	.08543
.30862	.08454
.26555	.08228
.22460	.07876
.18620	.07414
.15074	.06849
.11855	.06186
.08988	.05438
.06493	.04617
.04388	.03741
.02677	.02839
.01380	.01938
.00503	.01069
.00046	.00283
.00079	-.00320
.00681	-.00787
.01835	-.01209
.03499	-.01546
.05666	-.01780
.08328	-.01908
.11474	-.01932
.15085	-.01885
.19129	-.01724
.23565	-.01528
.28345	-.01292
.33413	-.01034
.38706	-.00772
.44159	-.00516
.49702	-.00279
.55265	-.00069
.60776	.00107
.66153	.00245
.71356	.00342
.76287	.00400
.80893	.00420
.85114	.00406
.88893	.00364
.92183	.00301
.94939	.00225
.97126	.00146
.98713	.00074
.99677	.00020
1.00000	.00000

S4061-096-84 COORDINATES

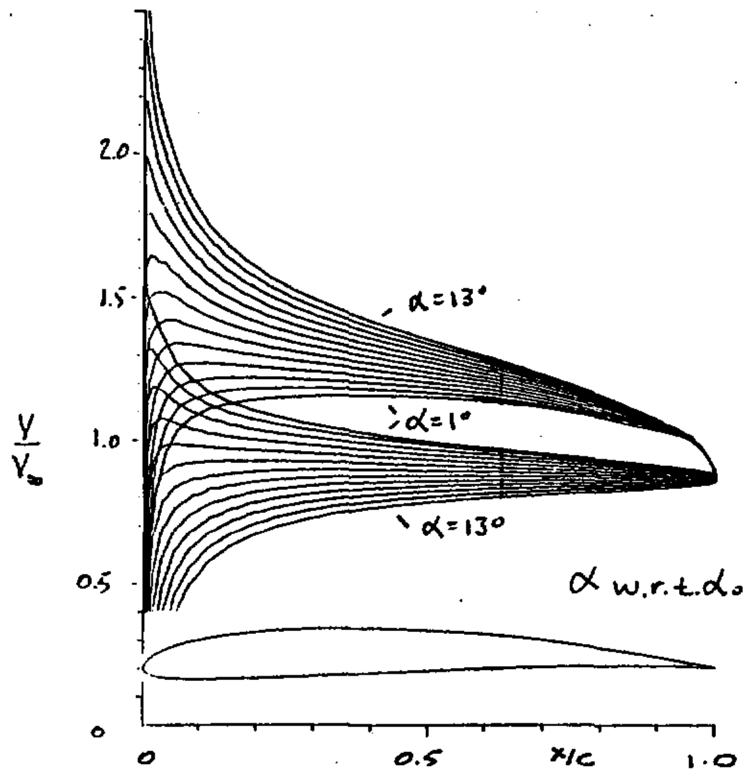

FIG. 38 - VELOCITY DISTRIBUTIONS FOR THE S4110-084-84.

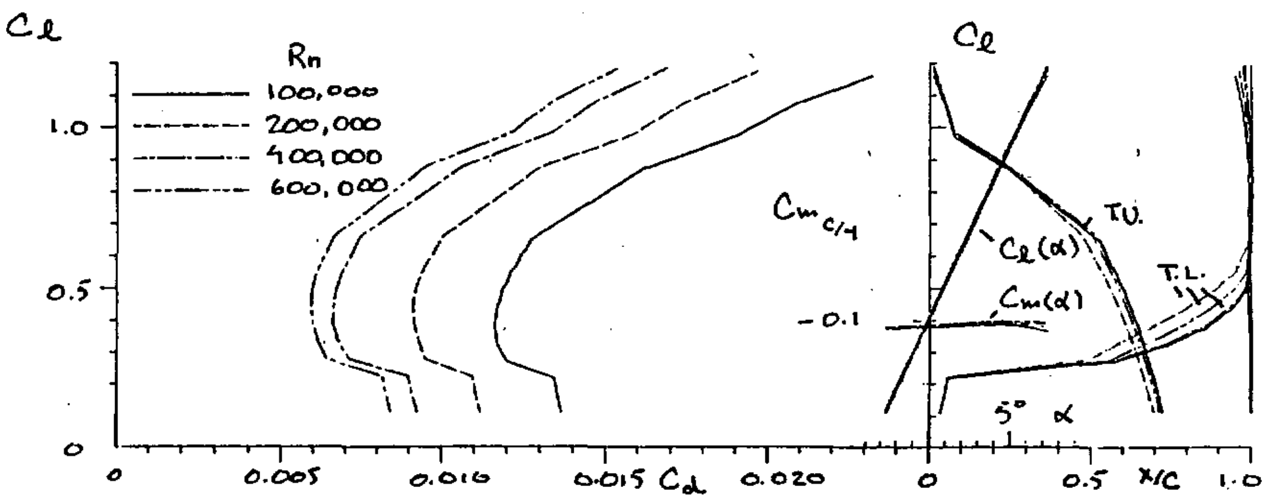

FIG. 39 - THEORETICAL SECTION CHARACTERISTICS FOR THE S4110-084-84.

THEORETICAL BOUNDARY-LAYER SUMMARY TABLE										
AIRFOIL	*-LAMINAR SEPARATION BUBBLE WARNING O-NO SEPARATION BUBBLE WARNING ●-NO BUBBLE, TRANSITION BEFORE 0.05C --SEPARATION AT LEADING EDGE (STALL)									
4110-084-84	+-ANGLE OF ATTACK WITHIN DRAG BUCKET									
ALPHA (deg)	REYNOLDS NUMBER									
			100000		200000		400000		600000	
	us	ls	us	ls	us	ls	us	ls	us	ls
1			*	*	*	*	*	●	*	●
2			*	*	*	O	*	O	*	O
+ 3			*	*	*	*	*	*	*	*
+ 4			*	*	*	*	*	*	*	*
+ 5			*	*	*	*	*	*	*	*
+ 6			*	O	*	O	*	O	*	O
+ 7			*	O	*	O	*	O	*	O
+ 8			*	O	*	O	O	O	O	O
+ 9			*	O	O	O	O	O	O	O
+10			*	O	O	O	O	O	O	O
11			*	O	●	O	●	O	●	O
12			*	O	●	O	●	O	●	O
13			*	O	●	O	●	O	●	O

X	Y
1.00000	0.00000
.99677	.00055
.98738	.00228
.97242	.00521
.95237	.00908
.92746	.01359
.89794	.01868
.86424	.02430
.82685	.03033
.78630	.03657
.74310	.04282
.69771	.04883
.65062	.05439
.60225	.05934
.55306	.06352
.50349	.06683
.45401	.06922
.40507	.07062
.35714	.07102
.31066	.07042
.26612	.06885
.22394	.06631
.18453	.06285
.14830	.05849
.11555	.05328
.08659	.04729
.06167	.04060
.04093	.03323
.02437	.02536
.01204	.01730
.00400	.00935
.00021	.00191
.00119	-.00408
.00755	-.00892
.01905	-.01317
.03554	-.01630
.05723	-.01820
.08413	-.01911
.11599	-.01920
.15247	-.01865
.19313	-.01757
.23751	-.01605
.28509	-.01417
.33537	-.01202
.38774	-.00970
.44162	-.00728
.49640	-.00487
.55146	-.00258
.60606	-.00053
.65957	.00121
.71127	.00260
.76051	.00360
.80665	.00418
.84906	.00436
.88717	.00416
.92046	.00363
.94843	.00285
.97068	.00193
.98686	.00102
.99670	.00029
1.00000	.00000

S4110-084-84 COORDINATES

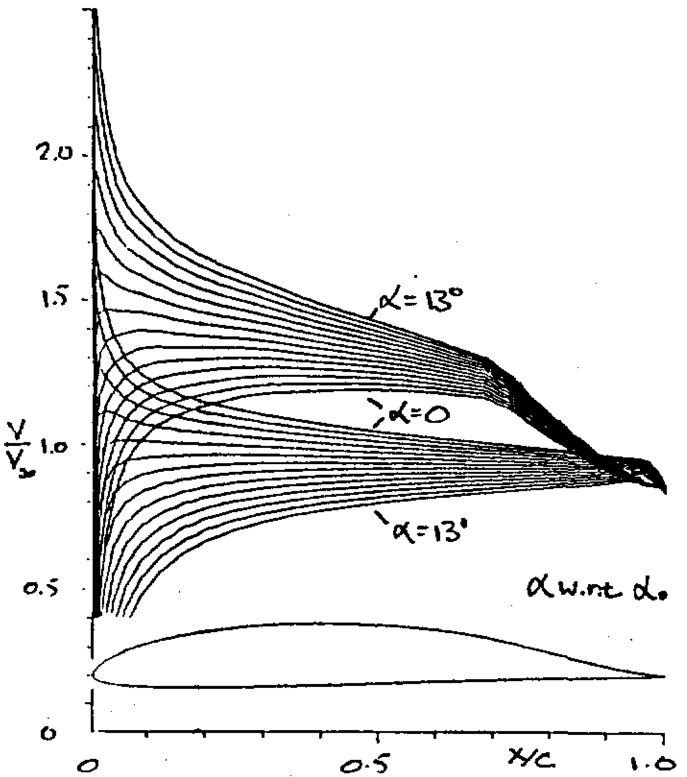

FIG. 40 - VELOCITY DISTRIBUTIONS FOR THE S4158-109-84.

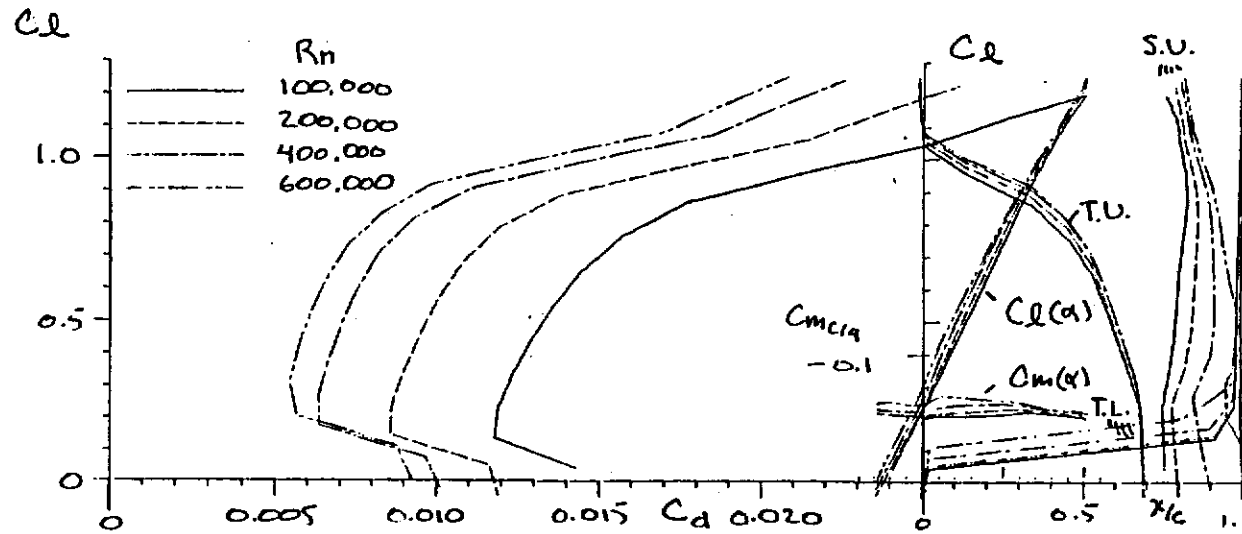

FIG. 41 - THEORETICAL SECTION CHARACTERISTICS FOR THE S4158-109-84.

THEORETICAL BOUNDARY-LAYER SUMMARY TABLE										
AIRFOIL	*-LAMINAR SEPARATION BUBBLE WARNING									
	O-NO SEPARATION BUBBLE WARNING									
	●-NO BUBBLE, TRANSITION BEFORE 0.05C									
	--SEPARATION AT LEADING EDGE (STALL)									
4158-109-84	+-ANGLE OF ATTACK WITHIN DRAG BUCKET									
ALPHA	REYNOLDS NUMBER									
(deg)			100000		200000		400000		600000	
	us	ls	us	ls	us	ls	us	ls	us	ls
0			*	-	*	*	*	●	*	●
1			*	*	*	●	*	●	*	●
+ 2			*	*	*	*	*	*	*	*
+ 3			*	*	*	*	*	*	*	*
+ 4			*	*	*	*	*	*	*	*
+ 5			*	*	*	*	*	*	*	*
+ 6			*	*	*	*	*	*	O	*
+ 7			*	*	*	*	*	*	O	*
+ 8			*	*	*	*	*	*	*	*
+ 9			*	*	*	*	*	*	O	*
+10			*	*	*	*	O	*	O	*
11			*	*	●	*	●	*	●	*
12			*	*	●	*	●	*	●	*
13			*	*	*	*	●	*	●	*

X	Y
1.00000	0.00000
.99654	.00023
.98621	.00111
.96923	.00307
.94604	.00654
.91742	.01182
.88428	.01890
.84751	.02757
.80801	.03745
.76666	.04799
.72424	.05830
.68083	.06722
.63593	.07442
.58958	.08025
.54234	.08482
.49464	.08805
.44690	.08996
.39957	.09057
.35312	.08992
.30808	.08804
.26485	.08486
.22375	.08044
.18512	.07496
.14938	.06857
.11693	.06137
.08808	.05342
.06297	.04484
.04177	.03594
.02474	.02697
.01209	.01814
.00392	.00965
.00018	.00185
.00127	-.00429
.00801	-.00894
.02053	-.01294
.03845	-.01613
.06167	-.01849
.09001	-.02012
.12317	-.02113
.16075	-.02160
.20226	-.02159
.24730	-.02109
.29534	-.02018
.34590	-.01888
.39838	-.01735
.45218	-.01565
.50667	-.01385
.56120	-.01202
.61511	-.01022
.66775	-.00852
.71846	-.00696
.76666	-.00556
.81168	-.00437
.85297	-.00337
.88999	-.00257
.92225	-.00193
.94931	-.00140
.97063	-.00087
.98666	-.00036
.99659	-.00005
1.00000	.00000

S4158-109-84 COORDINATES

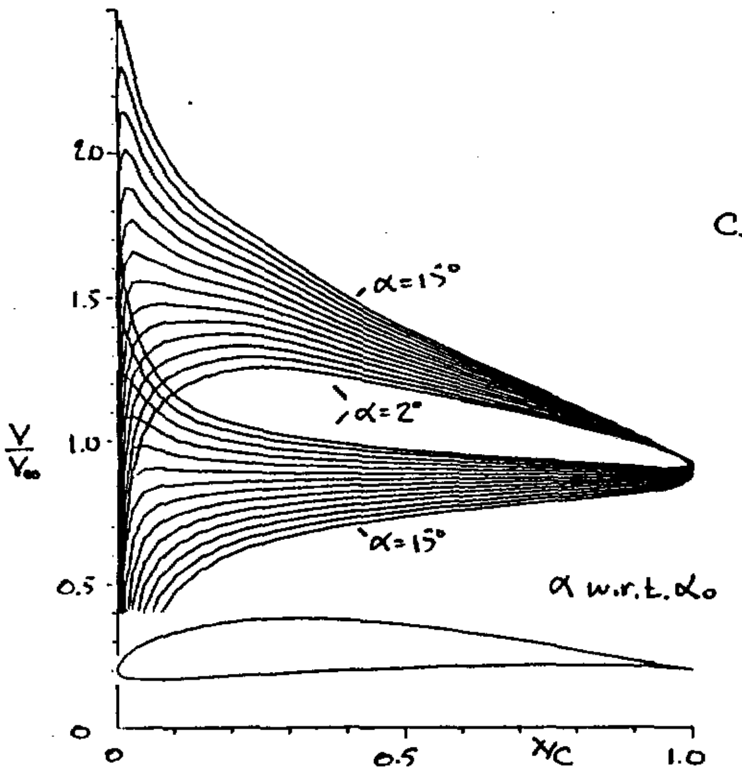

FIG. 42 - VELOCITY DISTRIBUTIONS FOR THE S4180-098-84.

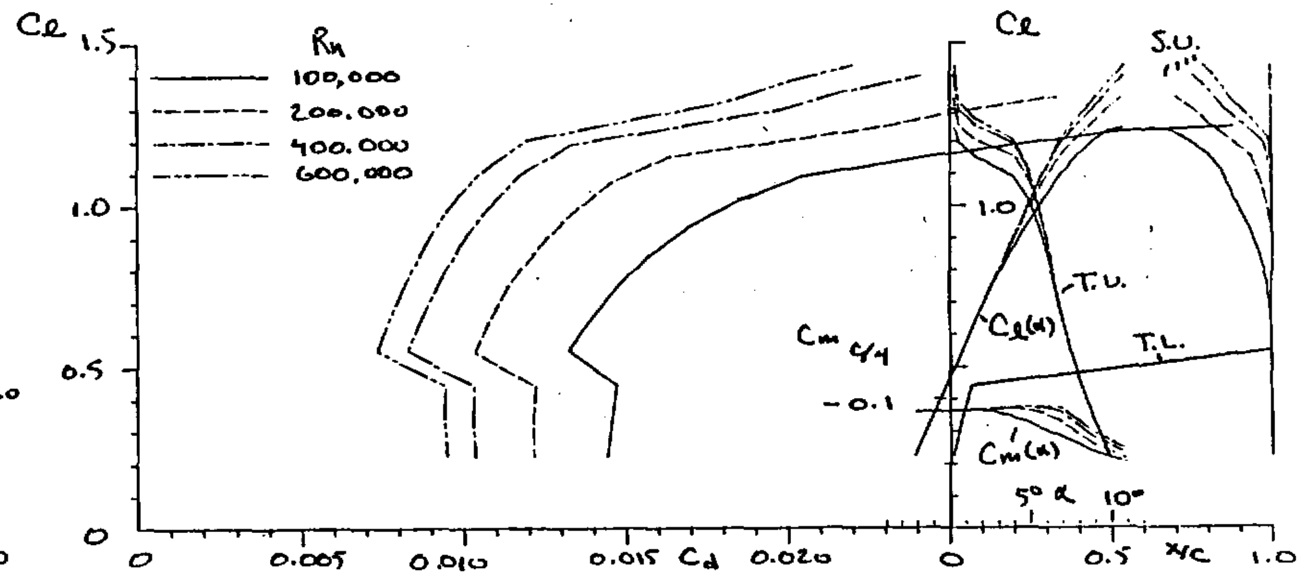

FIG. 43 - THEORETICAL SECTION CHARACTERISTICS FOR THE S4180-098-84.

THEORETICAL BOUNDARY-LAYER SUMMARY TABLE

AIRFOIL 4180-098-84
*-LAMINAR SEPARATION BUBBLE WARNING
O-NO SEPARATION BUBBLE WARNING
●-NO BUBBLE, TRANSITION BEFORE 0.05C
--SEPARATION AT LEADING EDGE (STALL)
+-ANGLE OF ATTACK WITHIN DRAG BUCKET

ALPHA (deg)			REYNOLDS NUMBER 100000		200000		400000		600000	
	us	ls	us	ls	us	ls	us	ls	us	ls
2			*	*	*	●	*	●	*	●
3			*	*	*	*	*	●	O	●
+ 4			*	*	*	O	*	●	O	O
+ 5			*	O	*	O	*	O	O	O
+ 6			*	O	*	O	*	O	O	O
+ 7			*	O	*	O	*	O	O	O
+ 8			*	O	*	O	*	O	O	O
+ 9			*	O	*	O	*	O	O	O
+10			*	O	*	O	*	O	O	O
+11			*	O	*	O	O	O	O	O
+12			*	O	O	O	O	O	O	O
13			*	O	●	O	●	O	●	O
14			*	O	●	O	●	O	●	O
15			*	O	●	O	●	O	●	O

1.00000	0.00000
.99684	.00036
.98746	.00156
.97208	.00376
.95106	.00702
.92463	.01132
.89384	.01661
.85861	.02279
.81971	.02971
.77766	.03718
.73313	.04497
.68661	.05280
.63859	.06042
.58961	.06752
.54019	.07420
.49083	.07997
.44204	.08472
.39427	.08829
.34798	.09050
.30355	.09118
.26126	.09018
.22127	.08751
.18383	.08329
.14916	.07770
.11757	.07095
.08935	.06323
.06476	.05468
.04398	.04553
.02726	.03596
.01467	.02606
.00607	.01606
.00129	.00643
.00016	-.00200
.00377	-.00814
.01306	-.01234
.02779	-.01523
.04791	-.01670
.07351	-.01660
.10453	-.01584
.14065	-.01417
.18140	-.01202
.22624	-.00957
.27459	-.00696
.32585	-.00433
.37936	-.00178
.43445	.00060
.49043	.00273
.54658	.00455
.60221	.00601
.65660	.00708
.70906	.00774
.75897	.00800
.80564	.00786
.84847	.00735
.88692	.00652
.92046	.00540
.94862	.00407
.97093	.00262
.98703	.00131
.99674	.00035
1.00000	.00000

S4180-098-84 COORDINATES

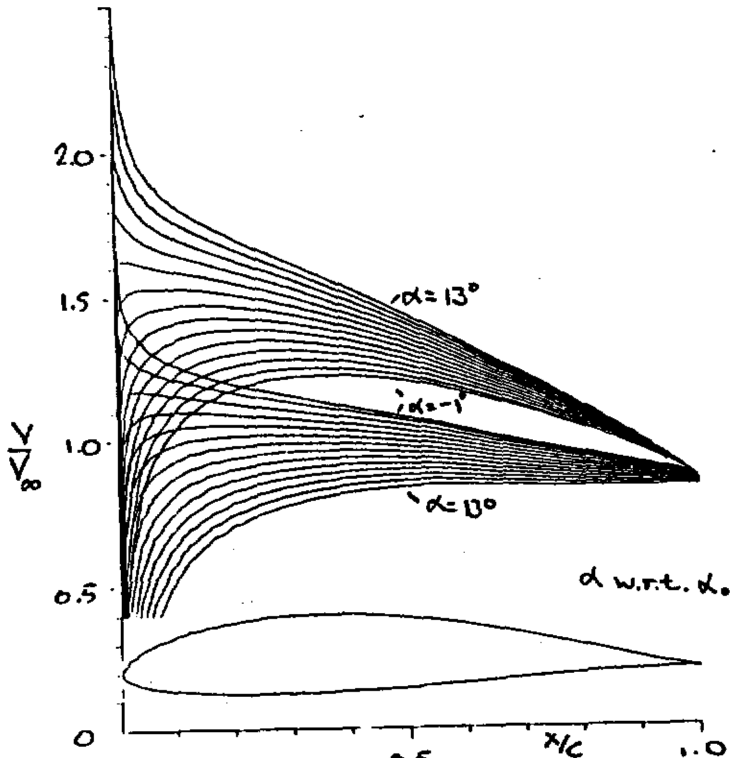

FIG. 44 - VELOCITY DISTRIBUTIONS FOR THE S4233-136-84.

THEORETICAL BOUNDARY-LAYER SUMMARY TABLE										
AIRFOIL 4233-136-84	*-LAMINAR SEPARATION BUBBLE WARNING O-NO SEPARATION BUBBLE WARNING ●-NO BUBBLE, TRANSITION BEFORE 0.05C --SEPARATION AT LEADING EDGE (STALL) +-ANGLE OF ATTACK WITHIN DRAG BUCKET									
ALPHA (deg)	REYNOLDS NUMBER									
			100000		200000		400000		600000	
	us	ls	us	ls	us	ls	us	ls	us	ls
-1			*	-	*	-	*	●	*	●
0			*	●	*	●	*	●	*	●
+ 1			*	*	*	*	*	*	*	*
+ 2			*	*	*	*	*	*	*	*
+ 3			*	*	*	*	*	*	*	*
+ 4			*	*	*	*	*	*	*	*
+ 5			*	*	*	*	*	*	*	*
+ 6			*	*	*	*	*	*	O	*
+ 7			*	*	*	*	*	*	O	*
+ 8			*	*	*	*	*	*	O	*
+ 9			*	*	*	*	*	*	O	*
+10			*	*	*	*	*	*	O	*
+11			*	O	*	O	*	O	O	O
+12			*	O	*	O	O	O	O	O
13			*	O	●	O	●	O	●	O

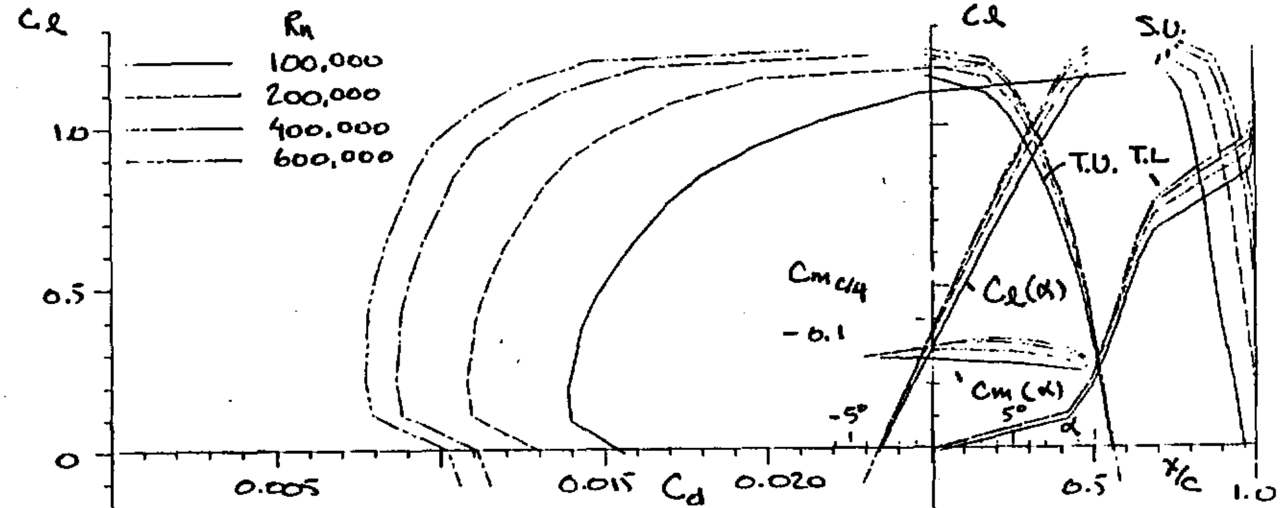

FIG. 45 - THEORETICAL SECTION CHARACTERISTICS FOR THE S4233-136-84.

X	Y
1.00000	0.00000
.99650	.00042
.98618	.00186
.96949	.00461
.94697	.00881
.91927	.01444
.88703	.02138
.85088	.02939
.81146	.03817
.76933	.04740
.72503	.05674
.67907	.06586
.63196	.07443
.58414	.08218
.53609	.08881
.48820	.09406
.44078	.09770
.39411	.09969
.34857	.10001
.30450	.09867
.26227	.09571
.22219	.09119
.18457	.08523
.14971	.07798
.11788	.06983
.08935	.06040
.06437	.05056
.04320	.04033
.02602	.03000
.01301	.01987
.00433	.01032
.00017	.00183
.00156	-.00488
.00916	-.01058
.02237	-.01621
.04069	-.02144
.06388	-.02609
.09171	-.03004
.12392	-.03322
.16018	-.03559
.20012	-.03714
.24337	-.03782
.28950	-.03768
.33802	-.03672
.38846	-.03497
.44031	-.03249
.49306	-.02934
.54625	-.02558
.59939	-.02139
.65199	-.01703
.70341	-.01286
.75289	-.00910
.79966	-.00591
.84299	-.00337
.88219	-.00149
.91664	-.00026
.94576	.00040
.96905	.00058
.98608	.00043
.99649	.00014
1.00000	.00000

S4233 - 136-84 COORDINATES

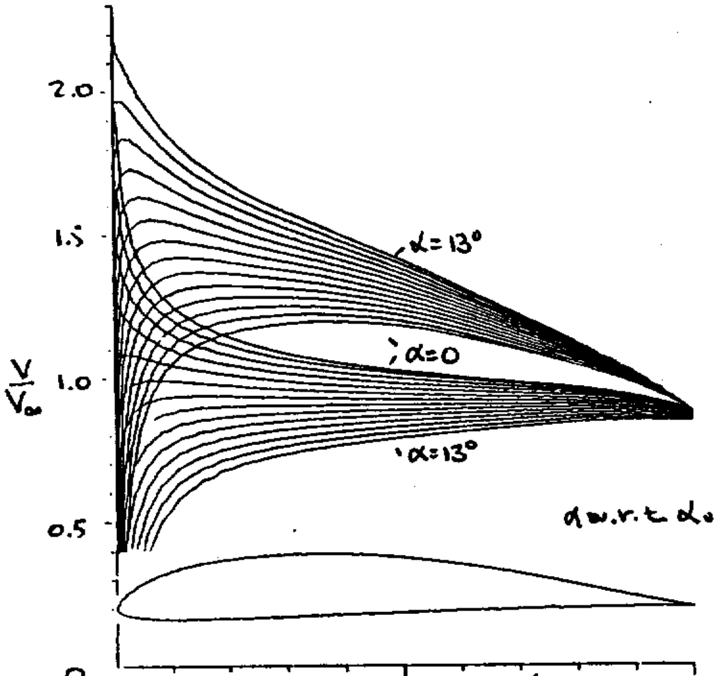

FIG. 46 - VELOCITY DISTRIBUTIONS FOR THE S4310-109-84.

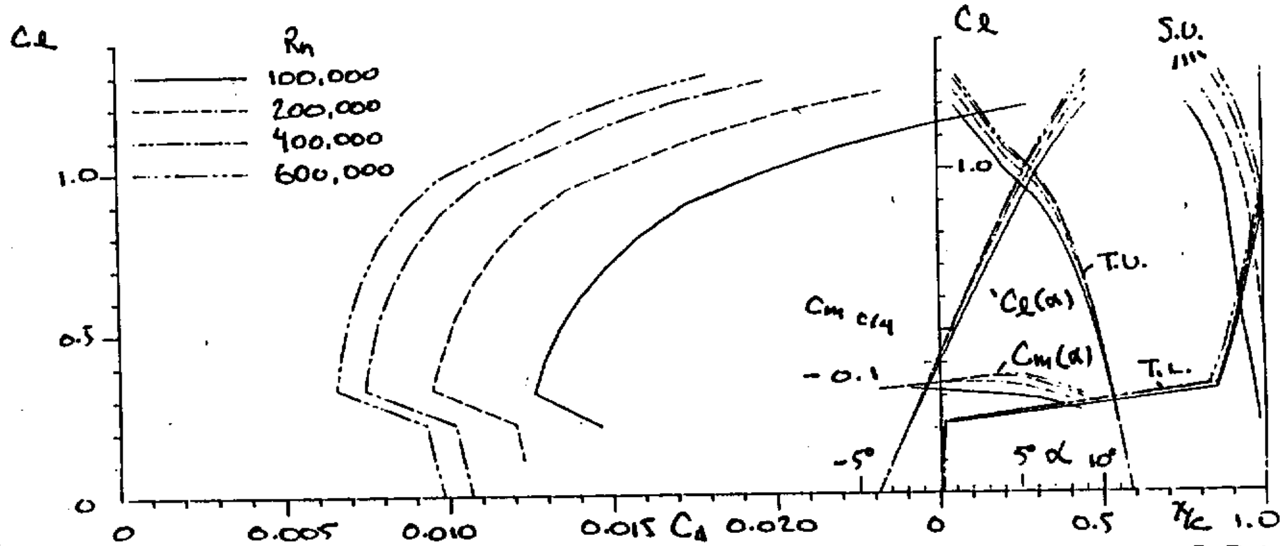

FIG. 47- THEORETICAL SECTION CHARACTERISTICS FOR THE S4310-109-84

THEORETICAL BOUNDARY-LAYER SUMMARY TABLE										
AIRFOIL 4310-109-84	*-LAMINAR SEPARATION BUBBLE WARNING O-NO SEPARATION BUBBLE WARNING ●-NO BUBBLE, TRANSITION BEFORE 0.05C --SEPARATION AT LEADING EDGE (STALL) +-ANGLE OF ATTACK WITHIN DRAG BUCKET									
ALPHA (deg)	REYNOLDS NUMBER									
			100000		200000		400000		600000	
	us	ls	us	ls	us	ls	us	ls	us	ls
1			*	-	*	*	*	●	*	●
2			*	*	*	●	*	●	*	●
+ 3			*	*	*	*	*	*	*	*
+ 4			*	*	*	*	*	*	O	*
+ 5			*	*	*	*	*	*	*	*
+ 6			*	*	*	*	*	*	O	*
+ 7			*	*	*	*	*	*	O	*
+ 8			*	*	*	*	*	*	O	*
+ 9			*	O	*	O	O	O	O	O
+10			*	O	*	O	O	O	O	O
+11			*	O	*	O	O	O	O	O
+12			*	O	O	O	O	O	O	O
+13			*	O	O	O	O	O	O	O

x	y
1.00000	0.00000
.99665	.00043
.98675	.00184
.97069	.00444
.94893	.00834
.92202	.01351
.89054	.01984
.85507	.02714
.81616	.03516
.77439	.04365
.73029	.05230
.68439	.06084
.63721	.06896
.58923	.07640
.54091	.08285
.49265	.08806
.44477	.09187
.39761	.09421
.35154	.09504
.30694	.09439
.26416	.09231
.22361	.08889
.18569	.08418
.15073	.07822
.11898	.07113
.09072	.06303
.06611	.05406
.04530	.04443
.02840	.03437
.01546	.02416
.00643	.01419
.00130	.00509
.00030	-.00210
.00498	-.00721
.01603	-.01117
.03260	-.01434
.05451	-.01664
.08156	-.01807
.11352	-.01869
.15011	-.01857
.19095	-.01784
.23562	-.01661
.28362	-.01503
.33437	-.01323
.38726	-.01133
.44162	-.00942
.49677	-.00758
.55203	-.00585
.60671	-.00428
.66013	-.00291
.71162	-.00175
.76053	-.00079
.80627	.00001
.84833	.00067
.88622	.00114
.91946	.00139
.94757	.00137
.97008	.00110
.98655	.00065
.99661	.00020
1.00000	.00000

S4310-109-84 COORDINATES

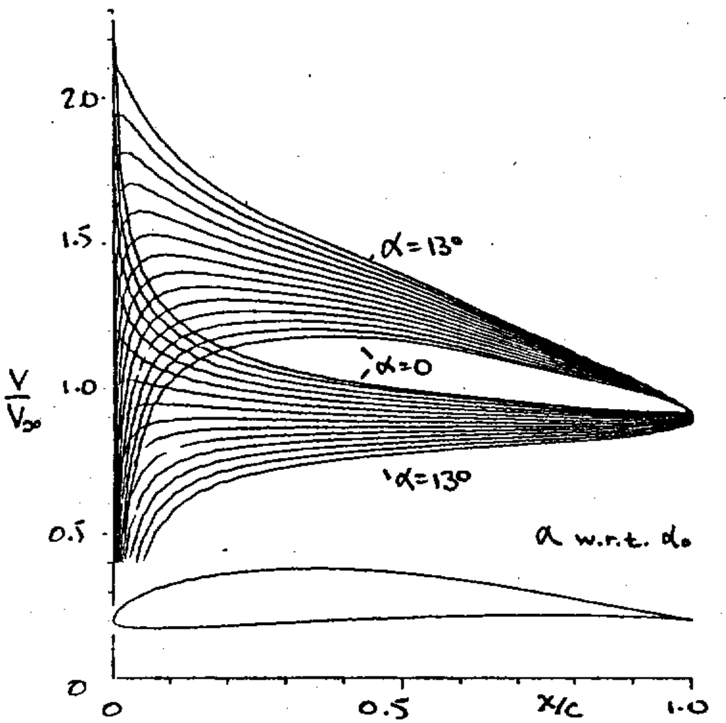

FIG. 48- VELOCITY DISTRIBUTIONS FOR THE S4320-094-84.

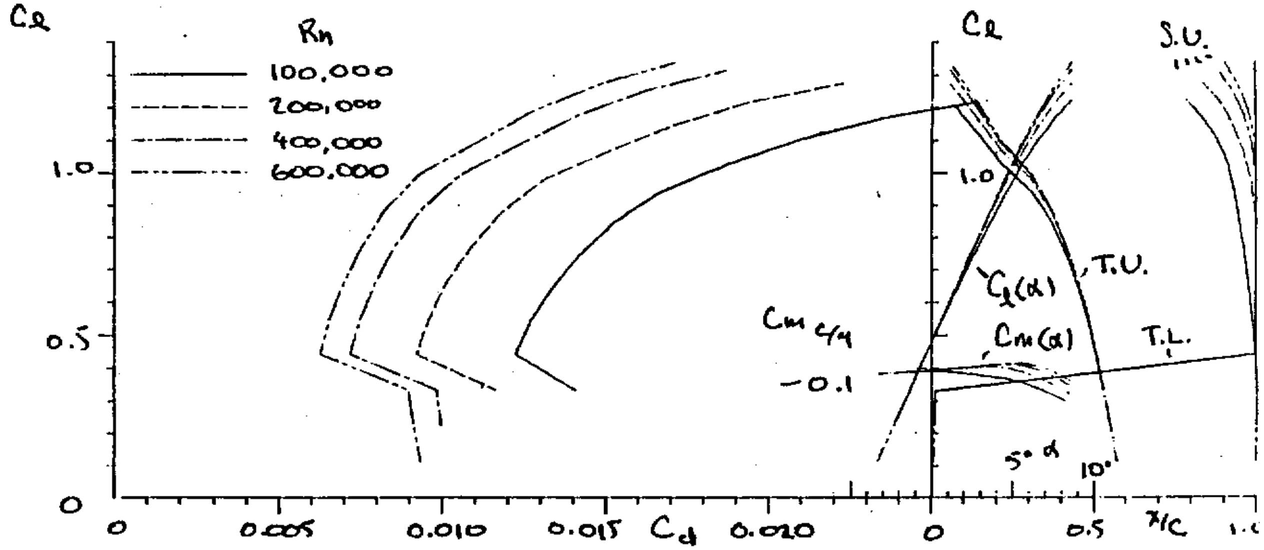

FIG. 49 - THEORETICAL SECTION CHARACTERISTICS FOR THE S4320-094-84

THEORETICAL BOUNDARY-LAYER SUMMARY TABLE										
AIRPOIL	*-LAMINAR SEPARATION BUBBLE WARNING O-NO SEPARATION BUBBLE WARNING ●-NO BUBBLE, TRANSITION BEFORE 0.05C --SEPARATION AT LEADING EDGE (STALL) +-ANGLE OF ATTACK WITHIN DRAG BUCKET									
4320-094-84										
ALPHA (deg)	REYNOLDS NUMBER									
			100000		200000		400000		600000	
	us	ls	us	ls	us	ls	us	ls	us	ls
2			*	-	*	-	*	●	*	●
3			*	●	*	●	*	●	*	●
+ 4			*	O	*	O	*	O	*	O
+ 5			*	O	*	O	*	O	*	O
+ 6			*	O	*	O	*	O	*	O
+ 7			*	O	*	O	*	O	O	O
+ 8			*	O	*	O	*	O	O	O
+ 9			*	O	*	O	O	O	O	O
+10			*	O	*	O	O	O	O	O
+11			*	O	*	O	O	O	O	O
+12			*	O	O	O	O	O	O	O
+13			*	O	O	O	O	O	O	O

X	Y
1.00000	0.00000
.99682	.00044
.98739	.00182
.97202	.00426
.95108	.00780
.92500	.01242
.89426	.01804
.85937	.02454
.82088	.03175
.77933	.03946
.73529	.04746
.68931	.05550
.64196	.06333
.59384	.07063
.54538	.07709
.49698	.08242
.44898	.08642
.40169	.08902
.35549	.09018
.31076	.08991
.26783	.08826
.22712	.08530
.18903	.08108
.15387	.07563
.12192	.06906
.09342	.06147
.06855	.05300
.04745	.04385
.03022	.03425
.01690	.02445
.00744	.01483
.00179	.00598
.00009	-.00116
.00380	-.00601
.01372	-.00931
.02926	-.01168
.05023	-.01305
.07648	-.01348
.10780	-.01304
.14390	-.01186
.18445	-.01009
.22900	-.00788
.27707	-.00540
.32807	-.00283
.38137	-.00031
.43629	.00206
.49213	.00417
.54818	.00596
.60374	.00738
.65811	.00838
.71057	.00894
.76047	.00906
.80716	.00871
.85000	.00791
.88833	.00671
.92161	.00528
.94939	.00373
.97133	.00229
.98719	.00110
.99678	.00029
1.00000	.00000

S4320-094-84 COORDINATES

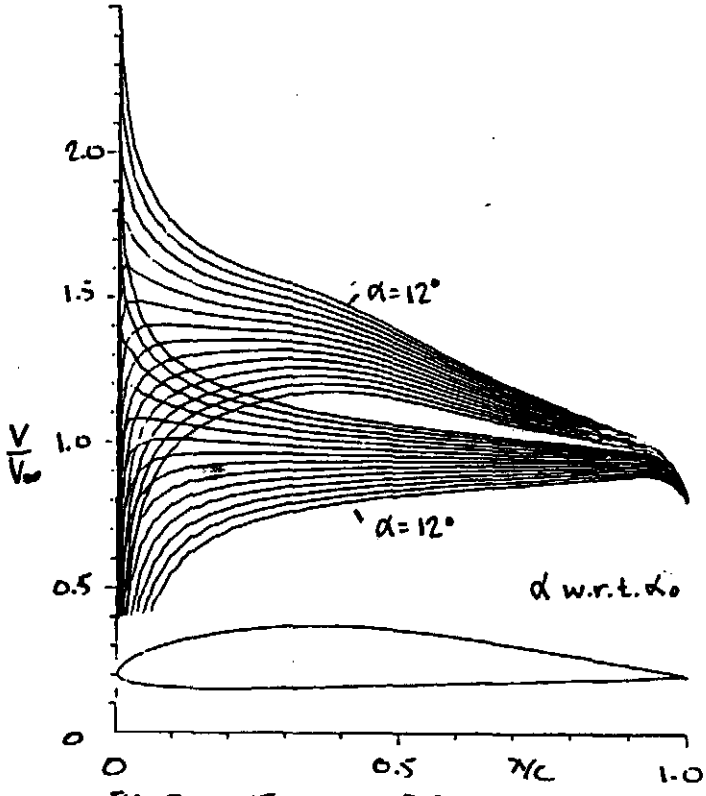

FIG. 50- VELOCITY DISTRIBUTIONS FOR THE ANTARES AIRFOIL.

THEORETICAL BOUNDARY-LAYER SUMMARY TABLE

AIRFOIL: ANTARES

*-LAMINAR SEPARATION BUBBLE WARNING
O-NO SEPARATION BUBBLE WARNING
●-NO BUBBLE, TRANSITION BEFORE 0.05C
--SEPARATION AT LEADING EDGE (STALL)
+-ANGLE OF ATTACK WITHIN DRAG BUCKET

ALPHA (deg)	REYNOLDS NUMBER									
			100000		200000		400000		600000	
	us	ls	us	ls	us	ls	us	ls	us	ls
-1			*	-	*	-	*	●	*	●
0			*	*	*	●	*	●	*	●
+ 1			*	*	*	*	*	*	*	*
+ 2			*	*	*	*	*	*	*	*
+ 3			*	*	*	*	*	*	*	*
+ 4			*	*	*	*	*	*	*	*
+ 5			*	*	*	*	*	*	*	*
+ 6			*	*	*	*	*	*	*	*
+ 7			*	*	*	*	*	*	O	*
+ 8			*	*	*	*	*	*	*	*
+ 9			*	*	*	*	*	*	O	*
+10			*	*	*	*	*	*	O	*
11			●	*	●	*	●	*	●	*
12			*	*	●	*	●	*	●	*

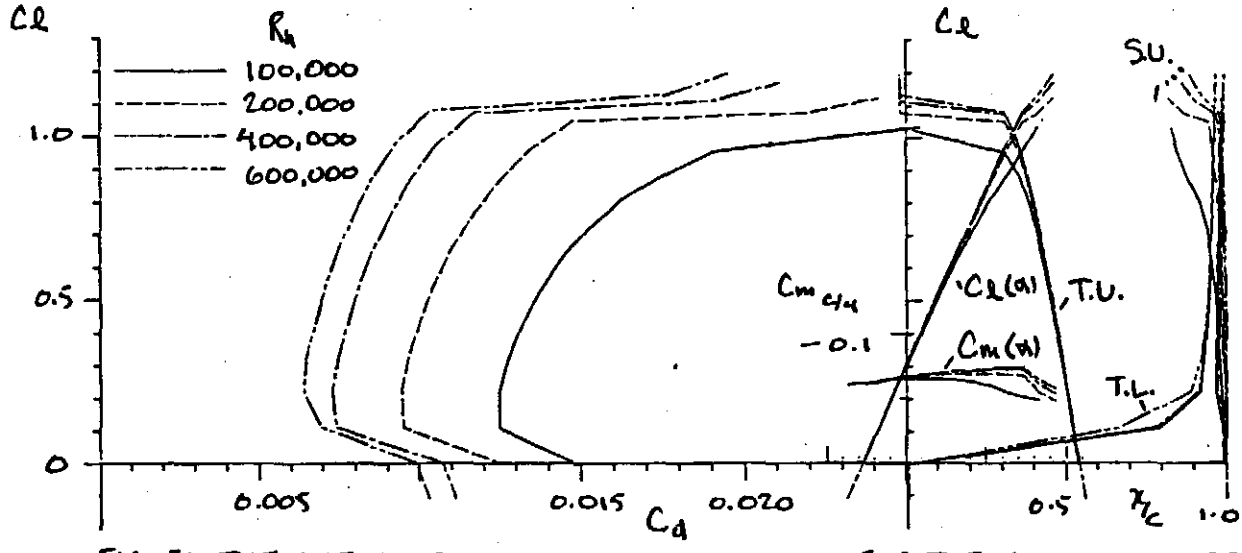

FIG. 51- THEORETICAL SECTION CHARACTERISTICS FOR THE ANTARES AIRFOIL.

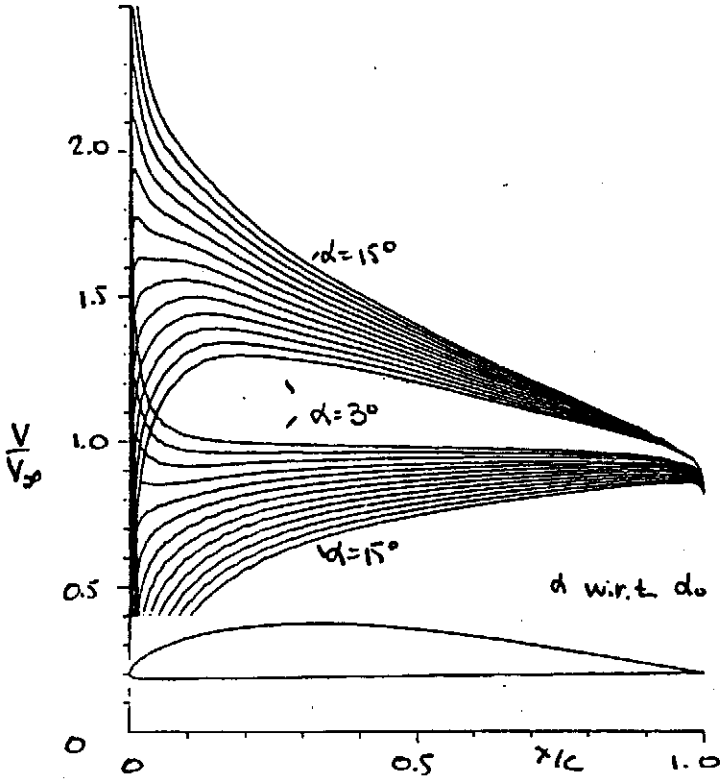

FIG. 52 - VELOCITY DISTRIBUTIONS FOR THE AQUILA AIRFOIL.

THEORETICAL BOUNDARY-LAYER SUMMARY TABLE										
AIRFOIL	*-LAMINAR SEPARATION BUBBLE WARNING O-NO SEPARATION BUBBLE WARNING ●-NO BUBBLE, TRANSITION BEFORE 0.05C --SEPARATION AT LEADING EDGE (STALL)									
AQUILA	+-ANGLE OF ATTACK WITHIN DRAG BUCKET									
ALPHA (deg)	REYNOLDS NUMBER									
	us	ls	100000 us	100000 ls	200000 us	200000 ls	400000 us	400000 ls	600000 us	600000 ls
4			*	*	*	●	*	●	*	●
+ 5			*	*	*	*	*	*	O	*
+ 6			*	*	*	*	*	*	O	*
+ 7			*	*	*	*	*	*	O	*
+ 8			*	*	*	*	O	*	O	*
+ 9			*	*	*	*	O	*	O	*
+10			*	*	*	*	O	*	O	*
+11			*	*	*	*	O	*	O	*
+12			*	*	O	*	O	*	O	*
13			●	*	●	*	●	*	●	*
14			●	*	●	*	●	*	●	*
15			*	*	●	*	●	*	●	*

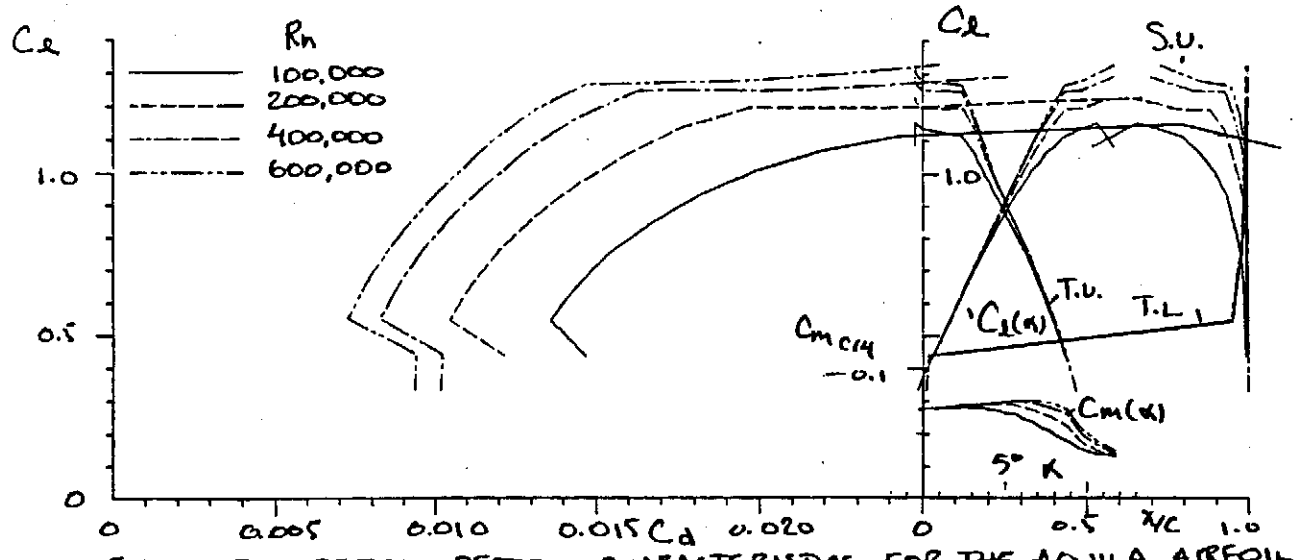

FIG. 53- THEORETICAL SECTION CHARACTERISTICS FOR THE AQUILA AIRFOIL

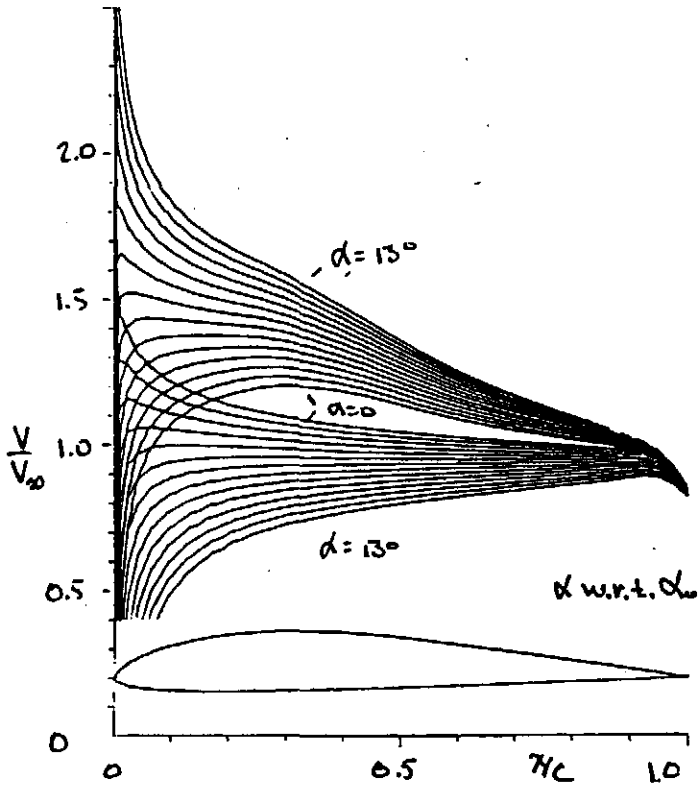

FIG. 54 - VELOCITY DISTRIBUTIONS FOR THE E205.

THEORETICAL BOUNDARY-LAYER SUMMARY TABLE

AIRFOIL E 205

*-LAMINAR SEPARATION BUBBLE WARNING
O-NO SEPARATION BUBBLE WARNING
●-NO BUBBLE, TRANSITION BEFORE 0.05C
--SEPARATION AT LEADING EDGE (STALL)
+-ANGLE OF ATTACK WITHIN DRAG BUCKET

ALPHA (deg)	REYNOLDS NUMBER 100000 us	100000 ls	200000 us	200000 ls	400000 us	400000 ls	600000 us	600000 ls
-1	*	●	*	●	*	●	*	●
0	*	●	*	●	*	●	*	●
+ 1	*	*	*	*	*	*	*	*
+ 2	*	*	*	*	*	*	O	*
+ 3	*	*	*	*	*	*	*	*
+ 4	*	*	*	*	*	*	O	*
+ 5	*	*	*	*	*	*	*	*
+ 6	*	*	*	*	*	*	O	*
+ 7	*	*	*	*	*	*	O	*
+ 8	*	*	*	*	*	*	O	*
+ 9	*	*	*	*	*	*	O	*
10	*	*	●	*	●	*	●	*
11	●	*	●	*	●	*	●	*
12	*	*	*	*	●	*	●	*

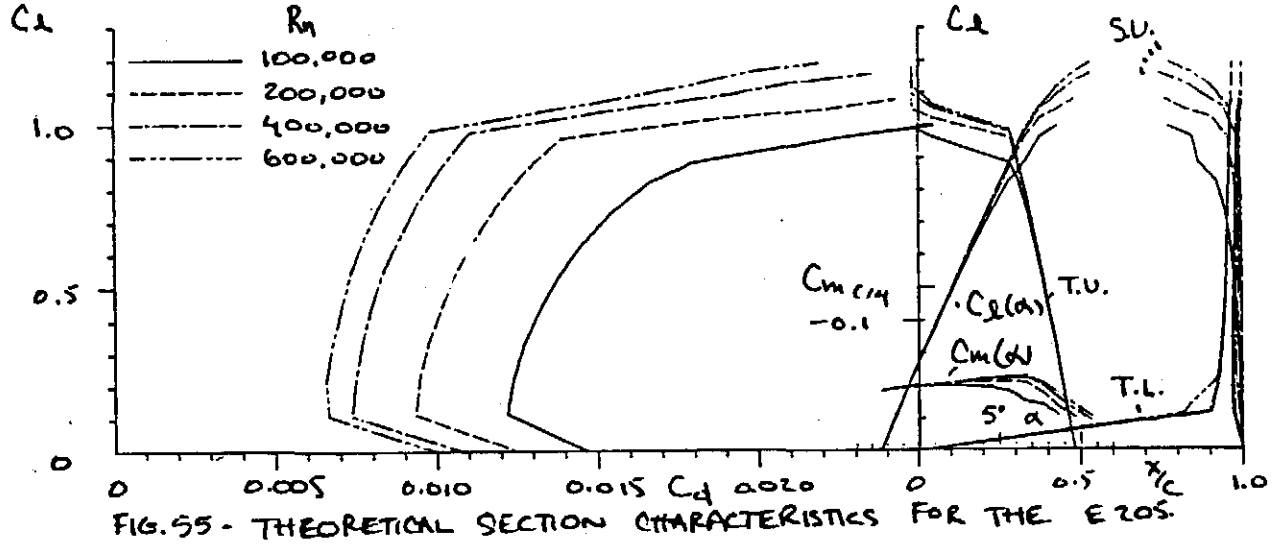

FIG. 55 - THEORETICAL SECTION CHARACTERISTICS FOR THE E205.

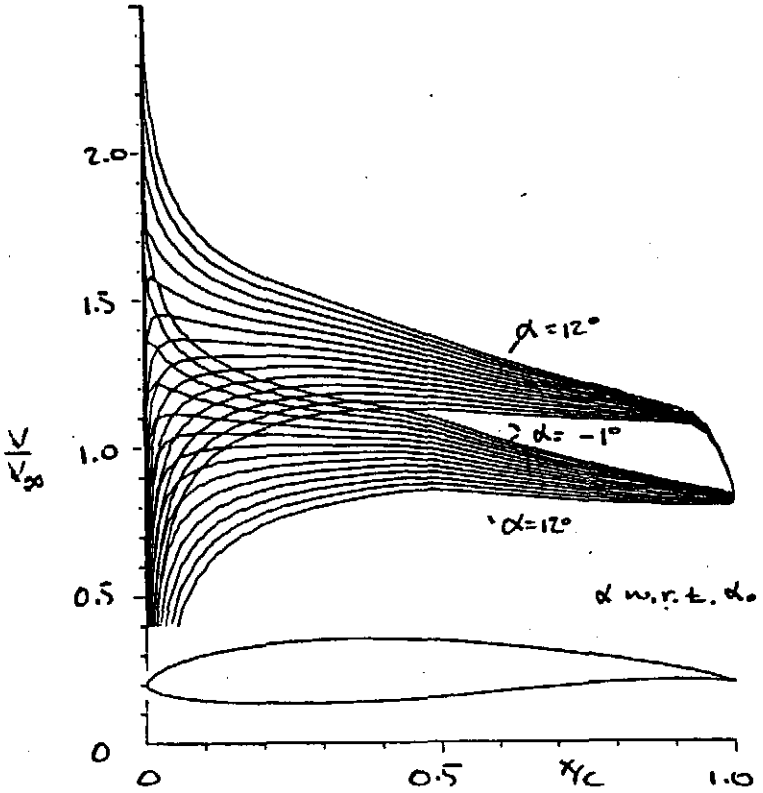

FIG. 56 - VELOCITY DISTRIBUTIONS FOR THE E211.

THEORETICAL BOUNDARY-LAYER SUMMARY TABLE

AIRFOIL E211

*-LAMINAR SEPARATION BUBBLE WARNING
O-NO SEPARATION BUBBLE WARNING
●-NO BUBBLE, TRANSITION BEFORE 0.05C
--SEPARATION AT LEADING EDGE (STALL)
←ANGLE OF ATTACK WITHIN DRAG BUCKET

ALPHA (deg)	REYNOLDS NUMBER									
			100000		200000		400000		600000	
	us	ls	us	ls	us	ls	us	ls	us	ls
-1			-	-	*	●	*	●	*	●
0			*	*	*	●	*	●	*	●
+ 1			*	*	*	*	*	*	*	*
+ 2			*	*	*	*	*	*	*	*
+ 3			*	*	*	*	*	*	*	*
+ 4			*	*	*	*	*	*	*	*
+ 5			*	*	*	*	*	*	*	*
+ 6			*	*	*	*	*	*	O	*
+ 7			*	*	*	*	*	*	*	*
+ 8			*	*	*	*	*	*	O	*
+ 9			*	*	*	*	*	*	O	*
+10			*	*	O	*	O	*	O	*
12			*	O	*	O	●	O	●	O
13			*	O	*	O	●	O	●	O

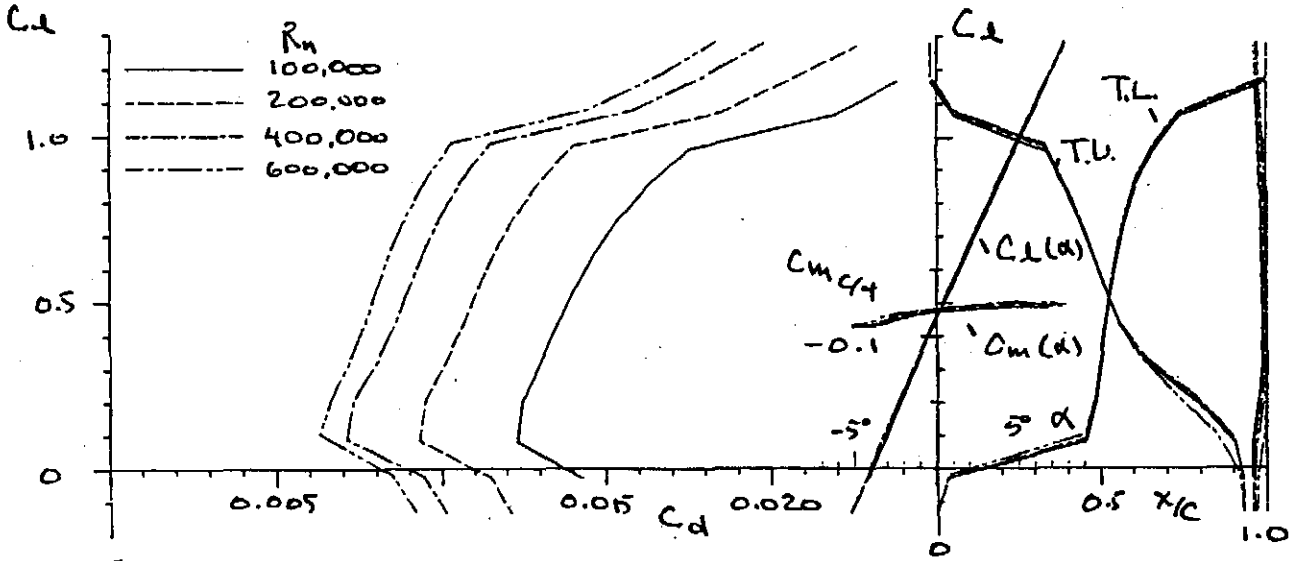

FIG. 57 - THEORETICAL SECTION CHARACTERISTICS FOR THE E211.

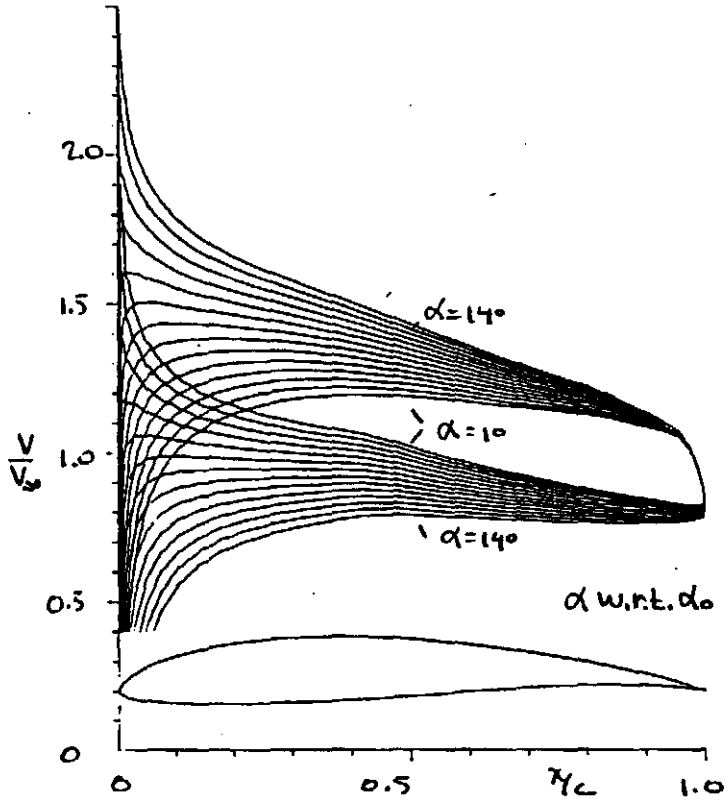

FIG. 58- VELOCITY DISTRIBUTIONS FOR THE E214.

THEORETICAL BOUNDARY-LAYER SUMMARY TABLE										
AIRFOIL	*-LAMINAR SEPARATION BUBBLE WARNING O-NO SEPARATION BUBBLE WARNING ●-NO BUBBLE, TRANSITION BEFORE 0.05C --SEPARATION AT LEADING EDGE (STALL) +-ANGLE OF ATTACK WITHIN DRAG BUCKET									
E214										
ALPHA (deg)	REYNOLDS NUMBER									
			100000		200000		400000		600000	
	us	ls	us	ls	us	ls	us	ls	us	ls
1			*	●	*	●	*	●	*	●
2			*	*	*	●	*	●	*	●
+ 3			*	*	*	*	*	*	*	*
+ 4			*	*	*	*	*	*	*	*
+ 5			*	*	*	*	*	*	*	*
+ 6			*	*	*	*	*	*	*	*
+ 7			*	*	*	*	*	*	*	*
+ 8			*	*	*	*	*	*	*	*
+ 9			*	*	*	*	*	*	O	*
+10			*	*	*	*	*	*	O	*
+11			*	O	*	O	*	O	O	O
+12			*	O	*	O	O	O	O	O
13			●	O	●	O	●	O	●	O
14			●	O	●	O	●	O	●	O

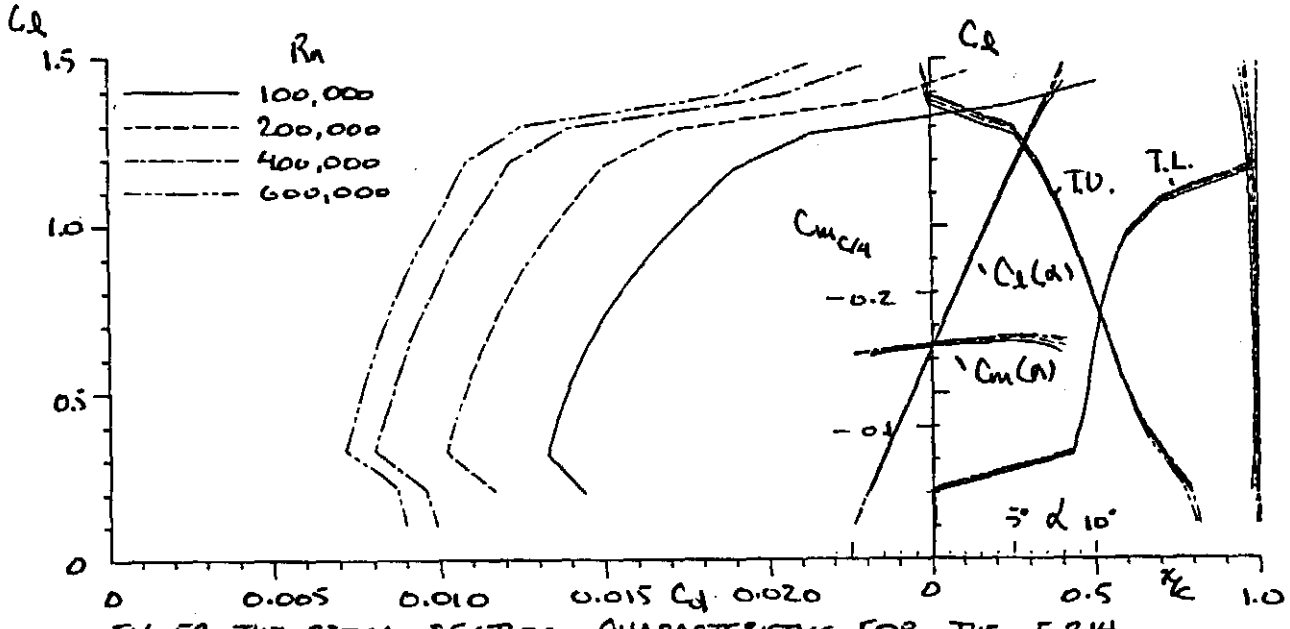

FIG. 59- THEORETICAL SECTION CHARACTERISTICS FOR THE E214.

4

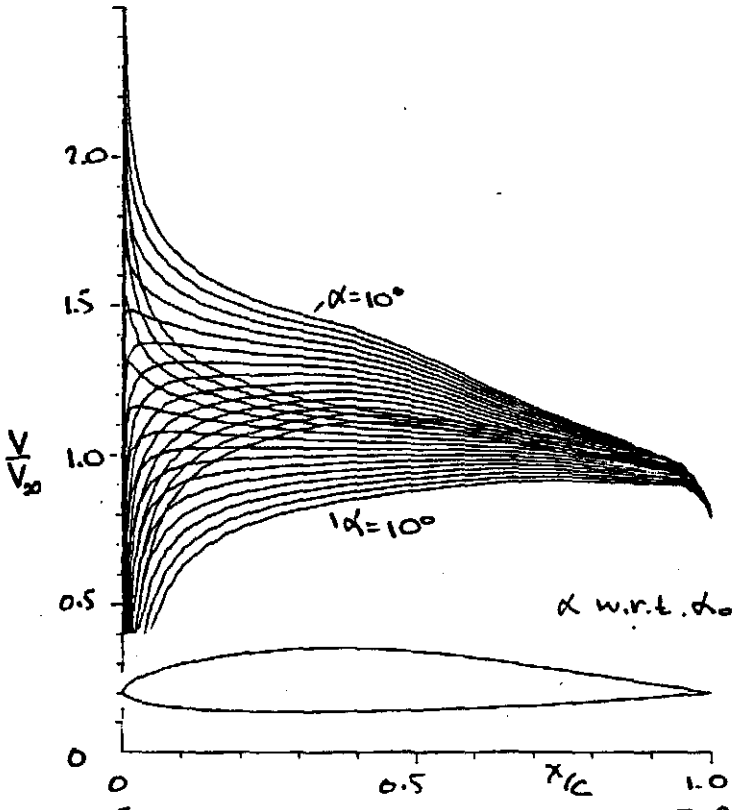

FIG. 60 - VELOCITY DISTRIBUTIONS FOR THE E374.

THEORETICAL BOUNDARY-LAYER SUMMARY TABLE										
AIRFOIL	*-LAMINAR SEPARATION BUBBLE WARNING O-NO SEPARATION BUBBLE WARNING ●-NO BUBBLE, TRANSITION BEFORE 0.05C --SEPARATION AT LEADING EDGE (STALL)									
E374	+-ANGLE OF ATTACK WITHIN DRAG BUCKET									
ALPHA (deg)	REYNOLDS NUMBER									
	us	ls	100000 us	100000 ls	200000 us	200000 ls	400000 us	400000 ls	600000 us	600000 ls
-3			*	-	*	*	*	●	*	●
-2			*	*	*	●	*	●	*	●
+-1			*	*	*	*	*	*	*	*
+ 0			*	*	*	*	*	*	*	*
+ 1			*	*	*	*	*	*	*	*
+ 2			*	*	*	*	*	*	*	*
+ 3			*	*	*	*	*	*	*	*
+ 4			*	*	*	*	*	*	*	*
+ 5			*	*	*	*	*	*	*	*
+ 6			*	*	*	*	*	*	*	*
+ 7			*	*	*	*	*	*	O	*
8			●	*	●	*	●	*	●	*

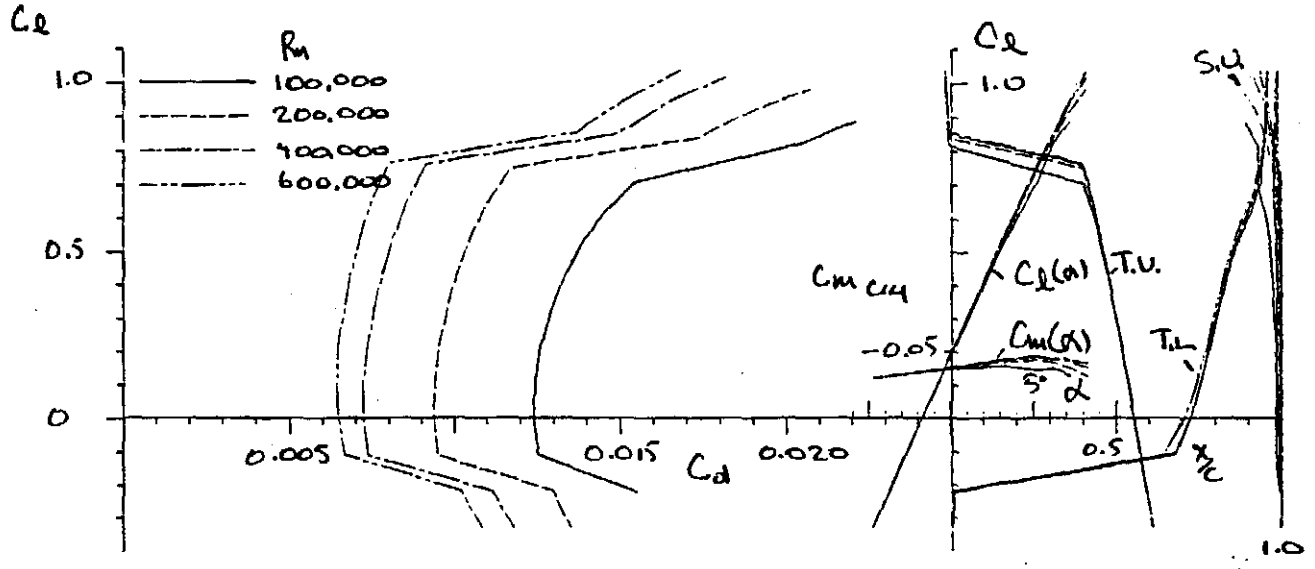

FIG. 61 - THEORETICAL SECTION CHARACTERISTICS FOR THE E374.

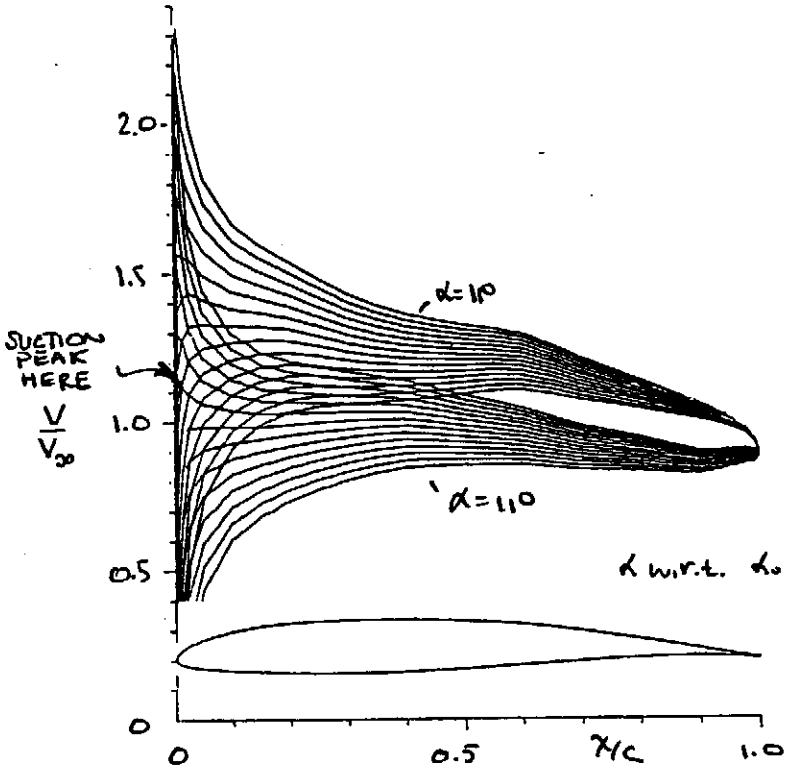

FIG. 62 - VELOCITY DISTRIBUTIONS FOR THE HQ 2.5 19.

THEORETICAL BOUNDARY-LAYER SUMMARY TABLE										
AIRFOIL	*-LAMINAR SEPARATION BUBBLE WARNING O-NO SEPARATION BUBBLE WARNING ●-NO BUBBLE, TRANSITION BEFORE 0.05C --SEPARATION AT LEADING EDGE (STALL) +-ANGLE OF ATTACK WITHIN DRAG BUCKET									
HQ 2.5/9										
ALPHA (deg)	REYNOLDS NUMBER									
	60000		100000		200000		400000		600000	
	us	ls	us	ls	us	ls	us	ls	us	ls
1	*	*	*	*	*	●	*	●	*	●
+ 2	*	*	*	*	*	*	*	*	*	*
+ 3	*	*	*	*	*	*	*	*	*	*
+ 4	*	*	*	*	*	*	*	*	*	*
+ 5	*	*	*	*	*	*	*	*	*	*
+ 6	*	*	*	*	*	*	*	*	*	*
+ 7	*	*	*	*	*	*	O	*	O	*
+ 8	*	*	*	*	*	*	O	*	O	*
+ 9	*	O	*	O	O	O	O	O	O	O
10	*	O	*	O	●	O	●	O	●	O
11	-	-	*	O	●	O	●	O	●	O

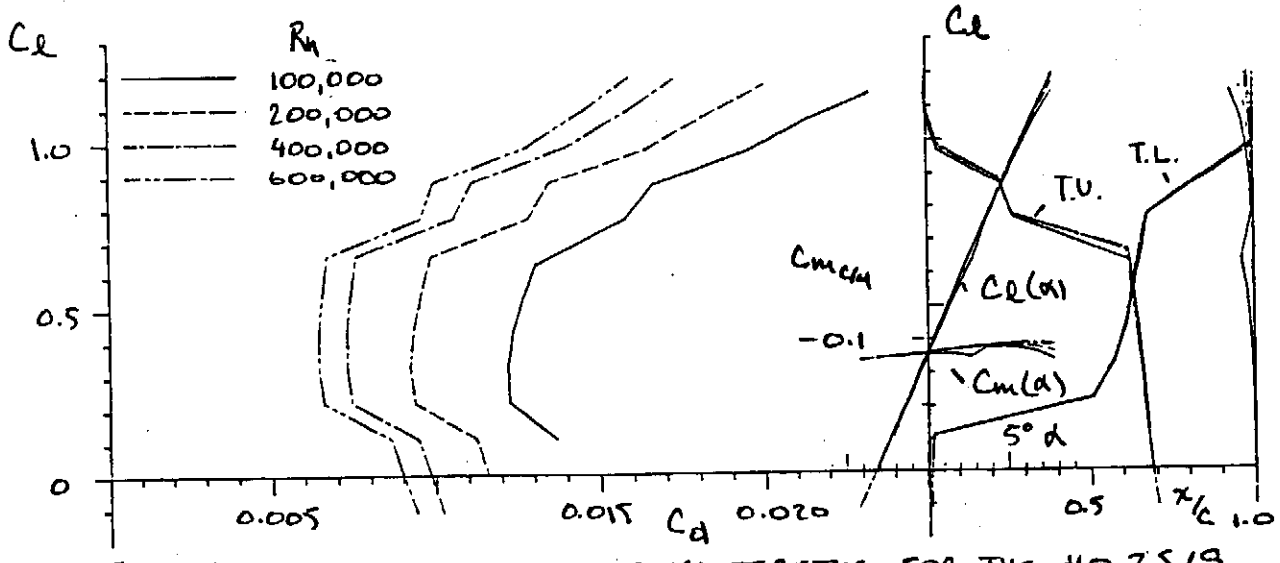

FIG. 63 - THEORETICAL SECTION CHARACTERISTICS FOR THE HQ 2.5 19.

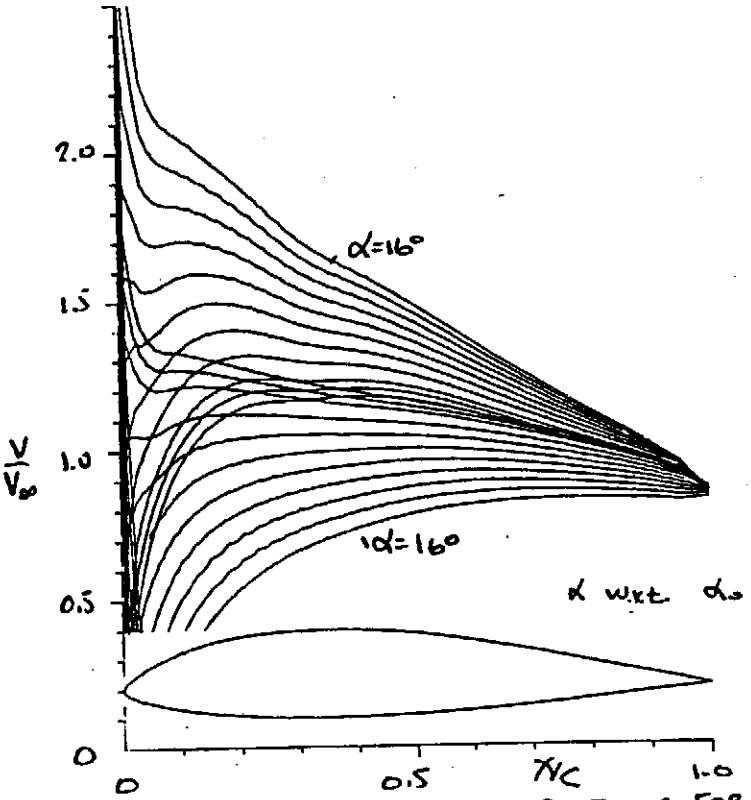

FIG. 64 - VELOCITY DISTRIBUTIONS FOR THE MB253515.

THEORETICAL BOUNDARY-LAYER SUMMARY TABLE										
AIRFOIL	*-LAMINAR SEPARATION BUBBLE WARNING O-NO SEPARATION BUBBLE WARNING ●-NO BUBBLE, TRANSITION BEFORE 0.05C --SEPARATION AT LEADING EDGE (STALL)									
MB 253515	+-ANGLE OF ATTACK WITHIN DRAG BUCKET									
ALPHA (deg)	REYNOLDS NUMBER									
			100000		200000		400000		600000	
	us	ls	us	ls	us	ls	us	ls	us	ls
-2			-	-	*	●	*	●	*	●
-1			*	*	*	●	*	●	*	●
+ 0			*	*	*	*	*	*	*	*
+ 1			*	*	*	*	*	*	*	*
+ 2			*	*	*	*	*	*	*	*
+ 4			*	*	*	*	*	*	O	*
+ 5			*	*	*	*	*	*	*	*
+ 6			*	*	*	*	*	*	O	*
+ 7			*	*	*	*	O	*	O	*
+ 8			*	*	*	*	O	*	O	*
+ 9			*	*	*	*	O	*	O	*
10			●	*	●	*	●	*	●	*
11			●	*	●	*	●	*	●	*
12			*	*	●	*	●	*	●	*

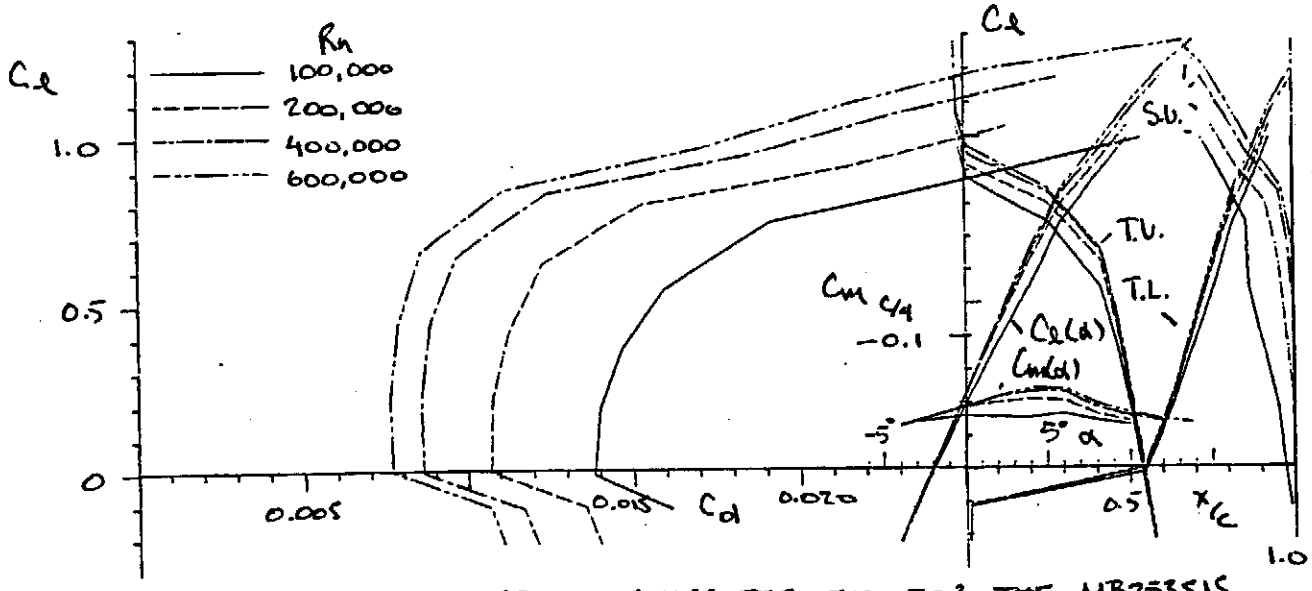

FIG. 65 - THEORETICAL SECTION CHARACTERISTICS FOR THE MB253515.